UNIVERSITY OF OKLAHOMA

GRADUATE COLLEGE

ACOUSTIC VELOCITY STUDY IN TIGHT ANHYDRITIC DOLOMITE OF THE LATE PERMIAN KHUFF FORMATION

A THESIS

SUBMITTED TO THE GRADUATE FACULTY

in partial fulfillment of the requirements for the

Degree of

MASTER OF SCIENCE

By

MOHAMMED ALMUZEL
Norman, Oklahoma
2016

ACOUSTIC VELOCITY STUDY IN TIGHT ANHYDRITIC DOLOMITE OF THE LATE PERMIAN KHUFF FORMATION

A THESIS APPROVED FOR THE
MEWBOURNE SCHOOL OF PETROLEUM AND GEOLOGICAL ENGINEERING

BY

_____
Dr. Chandra Rai, Chair

_____
Dr. Carl Sondergeld

_____
Dr. Siddharth Misra

I dedicate this work to the memory of my Brother

Ali Hassan Almuzel (1981-2016)

Acknowledgements

I would like to express my very great appreciation to Dr. Chandra Rai for his continues support and guidance during the long journey of this research work. Despite his busy schedule and duties, his willingness to spare time and give constructive feedback has been very appreciated. He helped me think critically and directed me to find a solution whenever I get stuck with a dead end. He believed in me and supported me until the end.

I would like to offer my special thanks to Dr. Carl Sondergeld and Dr. Siddharth Misra for their useful comments, guidance and time during this research. Their support in explaining the complicated petrophysical and physical rock concepts helped me understand the rock behavior and their responses.

My special thanks are extended to Saudi Aramco representatives Dr. Ed Clerke, Mr. Mohammed Faqira and Mr. Abdulfattah Bakhait for their effort and support by providing the plug samples for the study. Without their help, such study would not have been conducted.

I am very thankful for the assistance and help that I received from Mr. Gary Stowe, Ms. Mikki Langevin, Dr. Ali Tinni and Mr. Bruce Spears in the IC3 lab during my extensive set of measurements. They provided their valuable experience and time to help me understand the lab equipment and their technical aspects.

I’m particularly grateful for the assistance given by Mr. Jeremy Jernigen in running the QEMSCAN measurements. I’m really thankful for his time and effort in explaining these difficult measurements and clarifying all my doubts.

I also would like to thank Dr. Dick Larese for the detailed petrographic analysis that he provided to the study. I’m glad that the analysis has been done by an experienced consultant like him. He identified and explained many of the complicated texture and features within the samples.

My great appreciation and thanks extend to my family for their support, patience and encouragement during the difficult time of my study.

Table of Contents

List of Tables

List of Figures

Abstract

Carbonate reservoirs are usually associated with diagenesis processes which result in complex mineralogy and pore structure. As a result, rock physics models that predict the petrophsyical properties using seismic based geophysical parameters become more complicated. Most rock physics models studies relate the effect of pore structure and mineralogy to acoustic velocity over a wide range of porosity and mineralogy.

In this study, we are trying to investigate the acoustic velocity response over a narrow range of porosity and mineralogy. Extensive petrophysical and velocity measurements have been conducted on 38 carbonate plug samples. In addition, detailed petrographic and SEM analysis have been done on part of the samples. Results from this investigation highlight the importance of the petrographic analysis to explain the various velocity response. QEMSCAN and FTIR mineralogy quantification techniques provided consistent results over the studied section despite some minor differences. When there is a limited change in pore structure and mineralogy, the carbonate texture and fabric have a major control over velocity.

Biot-Gassmann rock physics model does not provide good estimations in the studied low porosity carbonate rocks. Due to the complicated microstructure, at ultrasonic velocity, these rocks show velocity dispersion effect that leads to underestimated P- and S-wave velocities using the model.

Chapter 1: Introduction

Reservoir petrophysical parameters are essential for many disciplines within the oil and gas industry. They are used by geologist, geophysicists, drilling engineers, production engineers and others for both exploration and development purposes. Rock physics models are used to help predict these petrophysical parameters using seismic and other geophysical variables. However, limited studies have been done on carbonates because of their complex nature. Unlike sandstones, carbonates are usually affected by diagenetic processes that alter their porosity, lithology and petrography. Several studies have shown that porosity type and lithology directly affect the velocity response in carbonates (Gomez et al., 2007; Weger et al., 2009; Anselmetti and Eberli, 2012; Kittridge, 2014).

Clastic rocks in general received higher attention compare to carbonates. They are not associated with any diagenetic potential and they revealed early success utilizing seismic techniques like amplitude versus offset (AVO). Sandstone hydrocarbon potential is usually associated with sand bodies within non reservoir rocks. These sand bodies are not always associated with structure. Therefore, reservoir detection using AVO found a ready application in sandstone (Fuller et al., 1989).

Because of the diagenetic complexity in carbonate, most rock physics studies have focused on pore type, lithology and rock-fluids interactions. Pure carbonate minerals have narrow velocity values and several studies concluded minor control of acoustic velocity by mineralogy (Rafavich et al., 1984; Sayers,

2008). On the other hand, porosity and pore type have always been considered the major controller of velocity. Weger et al., (2009) suggested that porosity and pore type are the main factors that affect acoustic velocity. However other studies argue that without the proper evaluation and estimation of carbonates mineralogy, interpreting the elastic properties as a function of porosity and pore type will be inadequate (Kittridge, 2014). Gomez et al., (2007) illustrated the effect of pore types on acoustic velocity using petrographic analysis. Spherical pores have been associated with high velocity while thinner and more complex pores resulted in low velocity response.

Several rock physics models are available in the literature that tries to relate the various carbonate petrophysical parameters to velocity. Biot-Gassmann theory is one of the widely used and well justified theoretical models. It takes into account three major parameters that affect the velocity response: porosity, mineralogy and fluids. However, it does not include a pore type parameter, like aspect ratio, which has been found significantly helpful for better velocity estimation (Weger et al., 2009). Besides, rock-fluid interaction is another concern that should be avoided for better velocity estimation using the model. Bhagat et al., (2012) investigated the saturation effect of various fluids in carbonates. Brine or dodecane helped in minimizing the chemical or dissolution effect in these rocks compare to water. Such studies confirmed that water should be avoided when saturating carbonate samples to eliminate any possible rock-fluid interactions.

Because of the complexity of the carbonate lithology, extra care should be considered when estimating their mineralogy. Several mineralogy estimation techniques are available in the industry (XRD, FTIR, QEMSCAN etc.) and they all have some limitations and strengths. Not to mention that the heterogeneity of the carbonates makes the sample orientation and scale very important. Therefore, the required amount of sample could be different based on the complexity of the lithology and the measurement technique. Mineralogy studies over the complex carbonate formation (Khuff) recommended fairly large samples of about 15cc when using XRD in order to get accurate results. However, QEMSCAN analysis when done on samples of 0.2cc were sufficient to provide enough details about the mineralogy distribution of the system (Ardila and Clerke, 2014).

Investigating the carbonates deposition and diagenetic history may provide good explanation for the rock physical response. For example, it has been seen that early compaction decreases porosity and increases velocity linearly. Leaching or dissolution of metastable minerals increases porosity with minor decrease in velocity (Anselmetti and Eberli, 2012). Nevertheless, it is usually hard to trace or quantify the diagenetic history that the rock went through. Therefore, it is preferable to incorporate petrographic analysis in order to understand the physical behavior of carbonates (Gomez et al., 2007).

Chapter 2: Geological Background

The focus of this study is on the Khuff reservoir within the giant Ghawar field in Saudi Arabia. Powers et al., (1963) suggested that Khuff is a late Permian age formation and it is considered to be the earliest known carbonate section in the region. The Khuff formation is divided into four major units named as Khuff-A, B, C and D. The unit Khuff-D is the oldest and Khuff-A is the youngest in the section. These units represent cycles within a tidal flat environment ranging from a subtidal marine transgressive to a supratidal regressive phase on top acting as a reservoir seal. Khuff-B and Khuff-C unites are usually well developed with major transgressive carbonate phases while Khuff-A and Khuff-D are generally less developed consisting of muddy carbonates and few zones of grainstones (Al-Jallal, 1987).

Khuff-C reservoir is our main focus in this study and it is generally dolomite with calcite and streaks of anhydrite. Besides depositional facies discontinuity, reservoir quality within the Khuff formation is affected greatly by diagenesis. Leaching and destructive dolomite usually increase porosity while dolomite and anhydrite cement usually deteriorate reservoir quality (Al-Jallal, 1987). This may result in porosity occlusion, complex pore type and complex mineralogy (Ardila and Clerke, 2014). The porosity in our study section is generally low with an average of 2.7% and a maximum of 6.9%.

According to Al-Jallal (1987), there are two diagenetic processes that could decrease the porosity within the Khuff section: extensive dolomitization with no leaching and formation of anhydrite cement. Dolomitization usually

preserves the primary interparticle porosity but as it continues further, if it is not associated with dissolution of unstable aragonitic grains, it progresses into interlocking dolomite crystals with very little porosity. Anhydrite cement is very common in Khuff reservoirs because of the tidal flat deposition cycles. Anhydrite precipitates during arid supratidal regressive time and works as cement plugging most of the primary porosity.

The lithology of the Khuff section is mainly fine to medium crystalline dolomite. Calcite was the primary lithology however, the extensive dolomitization replaced almost all the primary limestone matrix. It is estimated that only 2-3% of the primary matrix remained as calcite (Fathalla, 1985). Anhydrite is another mineral that is often present within the Khuff formation, both as anhydrite nodules and cement. Disseminated pyrite has also been associated with the lithology of this section.

Development of reservoir quality is one of the primary challenges in the Khuff reservoirs. It is usually controlled by the lateral continuity of the deposition of the reservoir facies. Therefore, reservoir development in this section is not always associated with the current structural position (Al-Jallal, 1987). Wells drilled on current structural highs will not always be better developed compare to wells drilled on the flanks. In such complex reservoir conditions, accurate prediction of the acoustic properties is required to differentiate between the reservoir and the non-reservoir rocks.

The Khuff reservoirs contain excellent hydrocarbon potential and therefore have received a lot of attention in the last years (Ehrenberg et al., 2007). Extensive high quality seismic data has been acquired over the Khuff section that needs to be properly tied to the petrophysical reservoir parameters. Studies over the Khuff complex reservoirs are ongoing and focusing on mineralogy, petrography, electrofacies and acoustic velocity (Clerke, 2009). Additional studies related to acoustic velocity modeling and rock physics over the Khuff section are needed in order to understand and predict the rock behavior and the reservoir potential.

Chapter 3: Motivation and Objective

Carbonate rocks hold a significant amount of oil and gas reserves especially in the Middle East. Schlumberger estimated that more than 60% of the world's oil and more than 40% of world's gas reserves are in carbonate reservoirs. These reservoirs are also known for their high degree of heterogeneity and complexity and extra effort is needed in order to predict their behavior (MacDonald et al., 2009).

Most of the carbonates rock physics studies have focused on the effect of porosity on acoustic velocity since they have obvious inverse relationship (Anselmetti and Eberli, 2012; Weger et al., 2009). Moreover, porosity has a strong effect and usually dominate over the effect of mineralogy and fluids. The wider the porosity range in a study set, the easier it is to find meaningful relationship with velocity even if mineralogy and diagenesis are not fully studied.

Other carbonates rock physics studies have incorporated the effect of mineralogy by dividing the samples into two groups in the porosity/velocity plot: dolomite rich or calcite rich. Rafavich et al., (1984) suggested that the influence of mineralogy on velocity is small and porosity is the major factor that affects velocity. However, within a group with the same dominant mineral, velocity variation at a specific porosity value is reduced. This approach gave better relationship but still over a wide range of porosity values with no explanation for the deviation from the general trend.

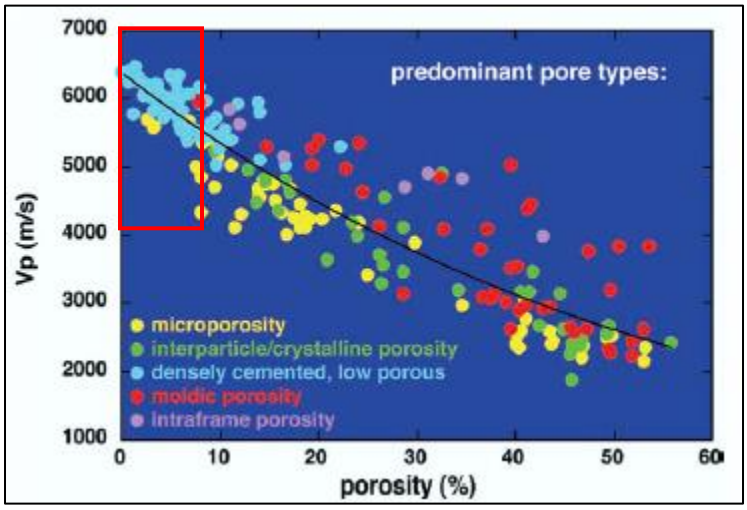

Figure 3-1: Graph of velocity vs. porosity color coded by the type of predominant pore type (Eberli et al., 2003). Red box shows our study range of porosity.

In order to highlight the effect of mineralogy and texture, we will investigate the acoustic velocity behavior using a densely cemented carbonate sample set with limited porosity range of 0 - 7% (Figure 3-1). A large data set of 38 carbonate plug samples will be investigated over this porosity range. We will use extensive analyses of petrophysical laboratory measurements including detailed petrographic analyses in order to capture as much details as possible.

The objective of the study is to investigate the acoustic velocity of the carbonate Khuff formation as a function of mineralogy, mineral morphology and texture over a narrow range of porosity.

Chapter 4: Methodology

In our study, 38 horizontal plug samples representing more than 150ft of the Khuff section in Saudi Arabia will be used. Extensive set of measurements will be acquired including porosity, permeability, density, NMR T_2 relaxation data, mineralogy, velocity and thin section petrographic analyses. Figure 4-1 shows all the measurements that will be done on the samples.

Laboratory Measurements

Before acquiring the dry measurements, we dried the samples in a conventional oven at 100°C for 20 hours. Then, the samples were left in a desiccator to cool down and then their weights were recorded. We selected 6 random samples to clean in an soxhlet extractor using a mixture of 90% toluene and 10% methanol at 75°C and a pressure of a 100 bar. Then we dried them in the oven for 20 hours. The average weight difference between the clean and the unclean samples was about 0.01g which suggested that cleaning is not required.

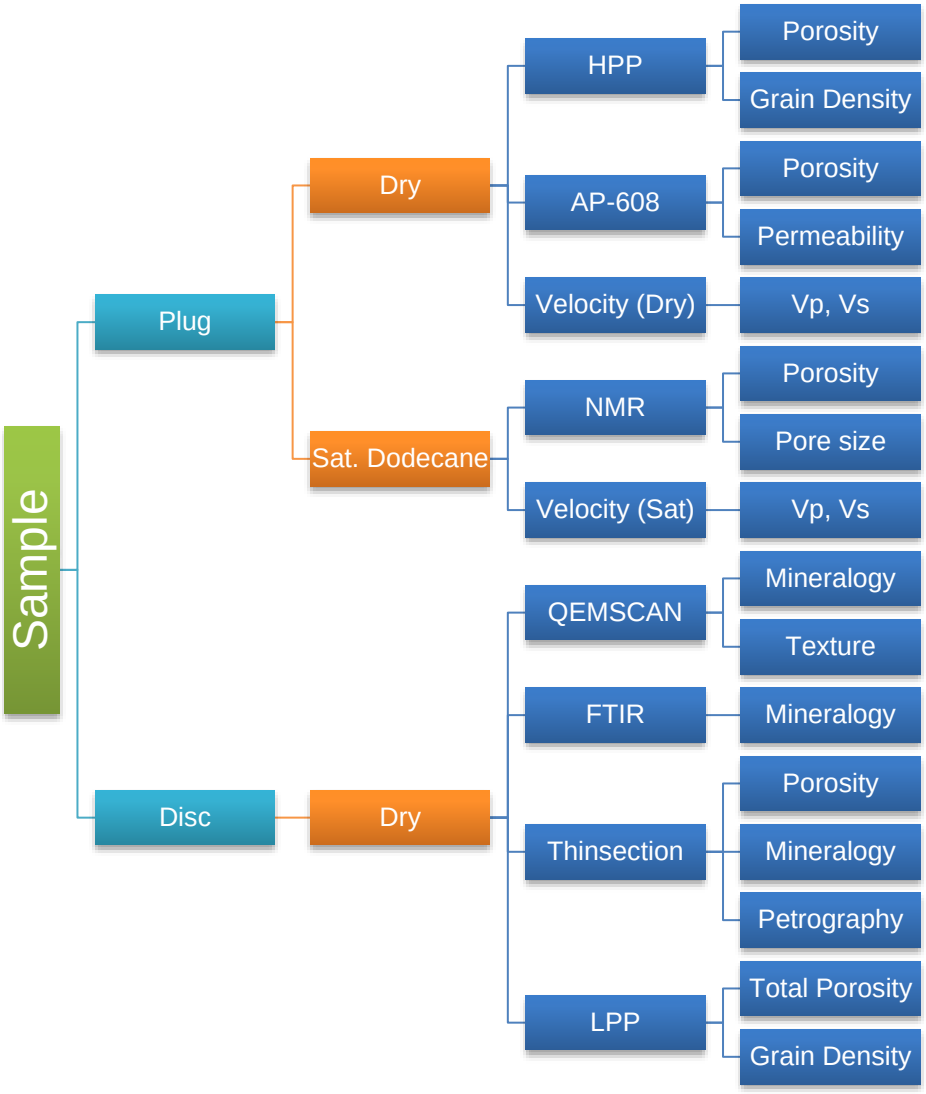

Figure 4-1: Chart showing all the lab measurements that were done on the plug samples in the study

Dry Measurements

The core plug sample is cut into two specimens, a disc with a length of about 0.2 inches and a plug of about 1 ½ inches. The disc was used to perform QEMSCAN mineralogy analysis which is an elemental detection tool using x-ray counts (see Chapter 5 for more details). After QEMSCAN, the same disc was

cut in half perpendicular to bedding. One half was used for mineralogy quantification using Transmission Fourier Transform Infrared Spectroscopy-FTIR (see Sondergeld and Rai (1993) for more details about the procedure). The other half was used to prepare thin section for visual porosity and mineralogy analysis using point count and detailed petrographic analysis. A total of 8 disc samples were selected for the FTIR and thin section analysis.

On the plug samples, we obtained porosity and permeability measurements at a confining pressure of 800psi using the Automated Permeameter Porosimeter (AP608). Also, we used the High Pressure Pycnometer (HPP) to acquire grain density and grain volume. Then, the pore volume was calculated by subtracting the grain volume (HPP) from the bulk volume (plug diameter and length).

Next, we obtained the dry velocity measurements on the plug samples. We used a pressure vessel that contains mineral oil which is used to provide uniform confining pressure around the sample. The samples were placed between two piezoelectric transducers and wrapped with a rubber jacket which is used to provide a seal between the confining pressure and the pore pressure. In order to maximize contact between the samples and the piezoelectric transducers, the samples were machined polished to be as close to a perfect cylinder as possible. The velocity measurements were run using confining pressure ranging from 250psi to 5000psi while keeping the pore pressure constant (atmospheric pressure). During each pressure step, 5 minutes soaking

time was allowed for pressure equilibrium then a compressional (V_p) and two perpendicular shear (V_{s1}, V_{s2}) velocity measurements were acquired.

After the dry velocity measurements, the samples were cleaned in an soxhlet extractor using a mixture of toluene and methanol at 75°C and a pressure of a 100 bar. Then, they were placed in a conventional oven for 24 hours at 100°C. Then, they were placed in a desiccator to cool down.

Saturated Measurements

We used dodecane to saturate our samples to minimize any rock-fluid interaction that could results in shear weakening/strengthening which could affect the velocity measurements (Baechle et al., 2009). In addition, using dodecane will provide measurements that follow Biot-Gassmann behavior and minimize any possible chemical or dissolution effect that might result from saturating the samples with water (Bhagat et al., 2012). The plug samples were saturated over three pressure steps to minimize induced cracks. First, the pressure was set at 500psi for an hour, then the pressure was raised to a 1000psi for another hour and then it was raised to 2000psi for a period of 24 hours.

NMR measurements were done on the dodecane saturated samples using 2-MHz Oxford-Maran Spectrometer with an average signal to noise ratio (SNR) of 50. Finally, saturated velocity measurements were acquired using the same procedure that we used for acquiring the dry velocity measurements.

Chapter 5: QEMSCAN Technology

Introduction

QEMSCAN is a fully automated system that evaluate mineralogy and petrography. It provides non-destructive and reliable quantitative analysis of the rock minerals. QEMSCAN (Quantitative Evaluation of Minerals by Scanning Electron Microscopy) integrates an electron beam source from scanning electron microscopy and an energy dispersive x-ray spectrometer (EDS) to measure elemental abundances (Ayling et al., 2012). It is an elemental detection method that depends on x-ray (EDS) counts and it drives mineralogy from overlapping elemental composition (Figure 5-1). The x-ray (EDS) count is acquired at each measurement point (pixel). The measured electron-induced x-ray spectra is input to an inversion software to analyze the mineralogy data based on known minerals' chemical compositions (Wood, 2013).

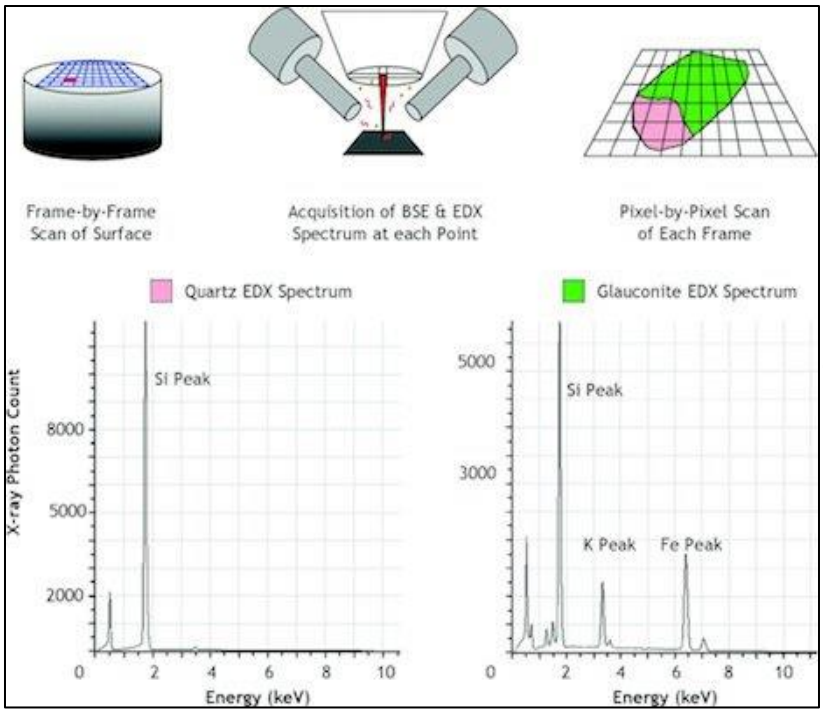

Figure 5-1: Schematic showing the process of acquiring the x-ray spectrum and analyzing the mineralogy data using QEMSCAN (Wood, 2013)

The software provides mineral maps of different resolutions based on the desired outcome. High resolution images utilize 2.5-micron pixel while low resolution images use 10-micron pixel with significant difference in acquisition time based on the area. Commonly, the low resolution images are more efficient. They provide enough details about the mineralogy, texture, grains and fractures in relatively few hours compared to the high resolution images. However, small minerals like clay tend to have little x-ray emissions and they may require higher resolution in order to be captured correctly.

History

In the 1970s, Commonwealth Scientific and Industrial Research Organization (CSIRO) patented the first QEMSCAN technology in Australia. It was called QEM*SEM, referring to the two platforms that the technology uses: The Quantitative Evaluation of Minerals using x-ray spectroscopy and the scanning electron microscopy. The main use of the technology was in the mining industry for mineral identification and ore characterization (Gottlieb et al., 2000). With the development and the automation of the QEMSCAN measurements, more fields became applicable for it like the oil and gas field. The oil and gas industry prefer technologies that provide fast, reliable and non-destructive results. In this industry, it is always better to use the same exact sample for multiple tests to reduce uncertainty. Therefore, the thriving capabilities of QEMSCAN started to be used in the oil and gas industry (Goergen et al., 2014; Ardila and Clerke, 2014).

Sample Preparation

In order to run a sample in QEMSCAN, the sample must be a ~1-inch in diameter and about 0.15 inches thick. It should be flat and machined polished as fine as possible. We used a fine saw to cut an end trim (disc) of about 0.2 inches from each plug to prepare the QEMSCAN samples. These discs were mounted using crystal bound to 1-inch diameter aluminum stubs (Figure 5-2).

Figure 5-2: QEMSCAN Samples mounted to 1-inch aluminum stubs

In order to finely polish the samples, we used the Alied Multi-prep polisher. This polisher insures that the sample is evenly polished using the selected grit size and load force. It also uses a water source to wash the polished-off particles away from the sample surface to minimize scratches that could affect the QEMSCAN x-ray spectra. The samples were polished in stages starting with 400 grit size to level out the sample and going up to 800 grit size to obtain a very high polished surface. Polishing the samples in stages insure maximum efficiency and minimize water interaction. After precise polishing, the

samples were ion milled using the Fischione model 1060 SEM mill at low angle for 3 hours at 5kV. Finally, they were coated with carbon using the Denton Vacuum Desk V Carbon coater. At this stage, the samples were ready for QEMSCAN analysis. Extra care should be considered when touching or mobilizing the samples. Finger prints, hair and/or fine particles could affect the sample surface and ultimately affect the QEMSCAN results.

Measurements

Our QEMSCAN measurements have been done using the automated FEI system. The electron beam was run at 15 kV and 7 nA. We ran all 38 carbonate samples using this system at two different resolutions and areas:

1. Low resolution at 10-micron pixel over an area of 1cm square.
2. High resolution at 2.5-micron pixel over an area of 1mm square.

We found that all the samples consist mainly of calcite, dolomite, anhydrite and traces of other minerals like quartz. Figure 5-3 shows a list of the minerals that were observed within the sample set. The images that we get out of the QEMSCAN system is color coded based on the distribution of the minerals within the sample. They also give an idea about the texture and fractures if they exist (Figure 5-4).

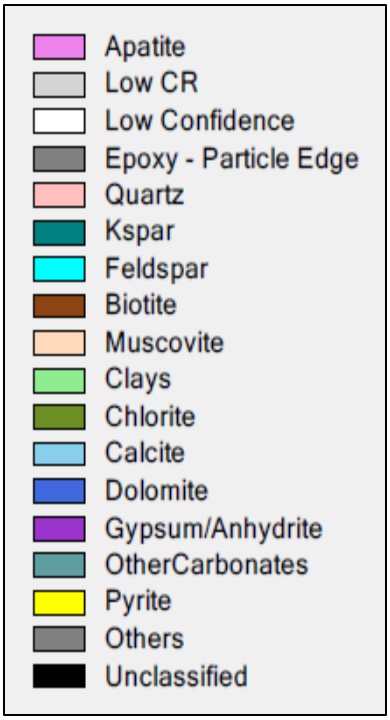

Figure 5-3: list of the minerals and their color code in the system.

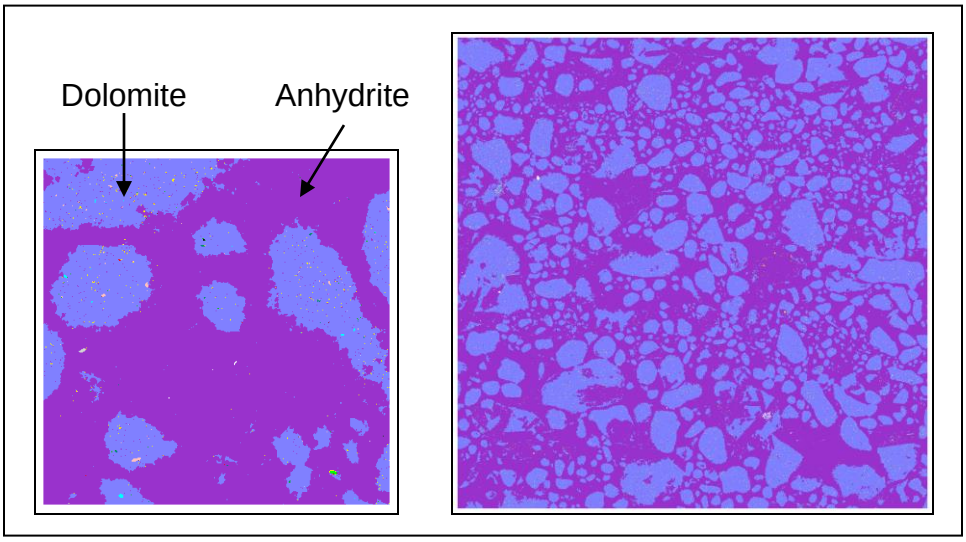

Figure 5-4: QEMSCAN images: High resolution over 1mm square area and low resolution over 1cm square area. Notice the mineral distribution and the type of texture that could be recognized in these images.

Chapter 6: Experimental Results and Discussion

During our extensive lab measurements, several petrophysical properties have been acquired. Based on distinctive petrophysical properties, the study section will be divided into two zones: Zone 1 (shallow) and Zone 2 (deep). Because of the complexity of the carbonate's section that we are studying, some of the properties were measured using two or more different techniques. Carbonate rocks usually undergo different periods of compaction, dissolution and cementation which would have a major influence on mineralogy and pore space. As a result, almost all petrophysical properties will be affected. Comparing the results of different techniques that measure the same petrophysical property could help explain complex rock behavior. In this chapter we will illustrate our experimental results sorted by measured properties.

Porosity

Porosity is one of the major petrophysical properties that could significantly be affected by diagenesis and has a direct effect on the elastic properties (Raymer et al., 1980). Because of the importance of this property, it has been measured using five different techniques:

1. HPP (High pressure pycnometer)
2. LPP (Low pressure pycnometer)
3. AP-608 (Automated permeameter porosimeter @ 800psi confining pressure)
4. NMR (T_2 relaxation time)
5. Point count (Thin section)

Table 6-1 below shows a summary of all the porosity data that were measured using the various lab techniques:

Table 6-1: Summary of the Porosity Data in Percent

Method	Lowest	Highest	Average	# of Samples
HPP	0.1	5.3	1.3	38
LPP	1.9	6.8	3.2	6
AP-608	0.1	5.4	1.4	38
NMR	1.2	6.9	2.7	38
Point count	0.3	5.3	1.9	8

The overall porosity of the section is very low. HPP, AP-608 and point count porosities usually measure the connected porosity. These three methods show similar porosity values with an average of about 1.5% (Table 6-1). NMR measures the volume of pore space by detecting the total volume of fluids in the sample. Fluids could be in connected pores and/or in isolated pores. LPP porosity is a measure of the crushed total porosity and their values were close to the porosities from NMR (See Bocangel et al., 2013 for details on LPP porosity measurements). Figure 6-1 illustrate the relationship between NMR versus HPP and LPP porosities.

We can conclude that the study section has an average connected porosity of 1.5%. NMR and LPP porosities has an average of 3.0%. Suggesting the presence of an average isolated or occluded porosity of 1.5%. When the

porosity is very low, any uncertainty would lead to significant error. The higher porosity that was measured by NMR has been confirmed as valid porosity with the measurements of LPP (crushed porosity). The relationship between these two type of measurements provided excellent correlation with and R^2 of 0.94 with almost 1 to 1 response.

Carbonate porosity and pore structure is one of the major building blocks that affect the velocity data (Weger et al., 2009). Hence, extensive attention was given to the porosity measurements of the section to reduce uncertainty. Any possible doubt within the porosity measurement should be avoided. Since both measurements are valid with enough confidence, both types of porosity will be investigated in the study. The HPP porosity will be considered the connected porosity and NMR porosity will be considered the total porosity.

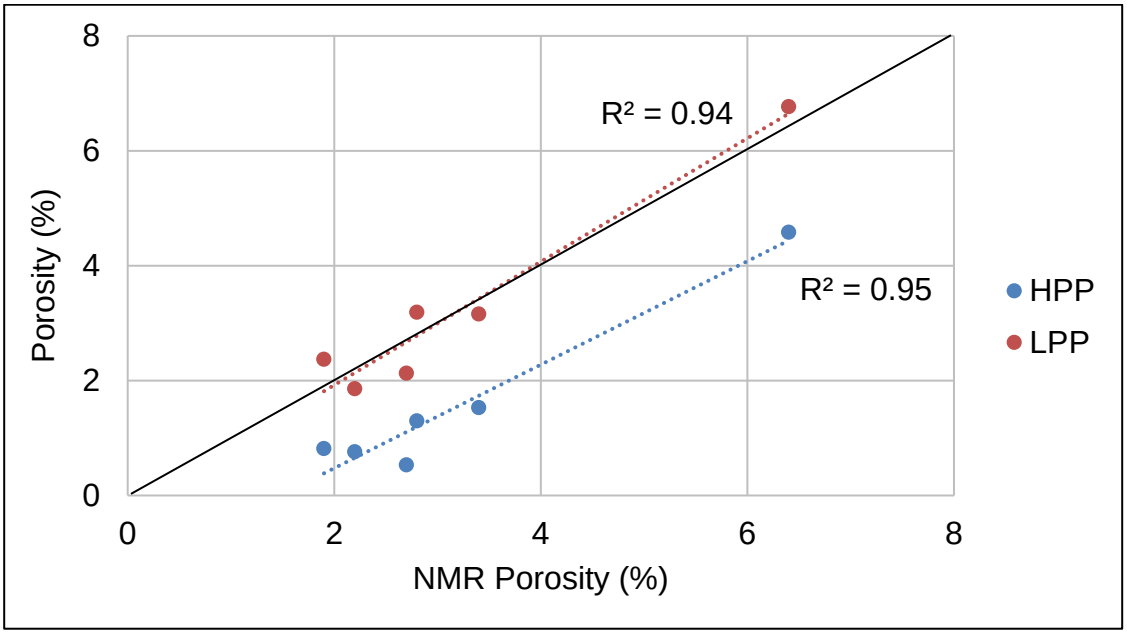

Figure 6-1: The relationship between NMR vs. LPP (in red) and NMR vs. HPP (in blue). Black line is the one to one line.

Mineralogy

Carbonates mineralogy usually seems simple with three major minerals (calcite, dolomite and anhydrite). However, the various diagenesis effects add complexity and make the mineralogy hard to predict. In order to understand the complex mineralogy in the study section, three mineralogy quantification techniques were used:

1. QEMSCAN
2. FTIR
3. Thin section

QEMSCAN Mineralogy

QEMSCAN is one of the leading techniques for minerals quantification. Besides, it has the capability to provide mineralogy images to better understand the rock fabric and texture (see chapter 5 for more details). All 38 samples were run using QEMSCAN. Figure 6-2 and Figure 6-3 show the mineralogy distribution based on the low resolution 1cm square (10 micron pixel) and the high resolution 1mm square (2.5 micron pixel) respectively.

QEMSCAN mineralogy shows that dolomite occurs over the whole section, ranging from 6% to 98%. Calcite only appears on the top section and it ranges up to 89%. Anhydrite is more prominent on the bottom section and it ranges from 0% to 60%. Both the low and high resolution QEMSCAN acquisitions gave very similar mineralogy. Minor differences were noticed which could be related to the difference in the scanned area.

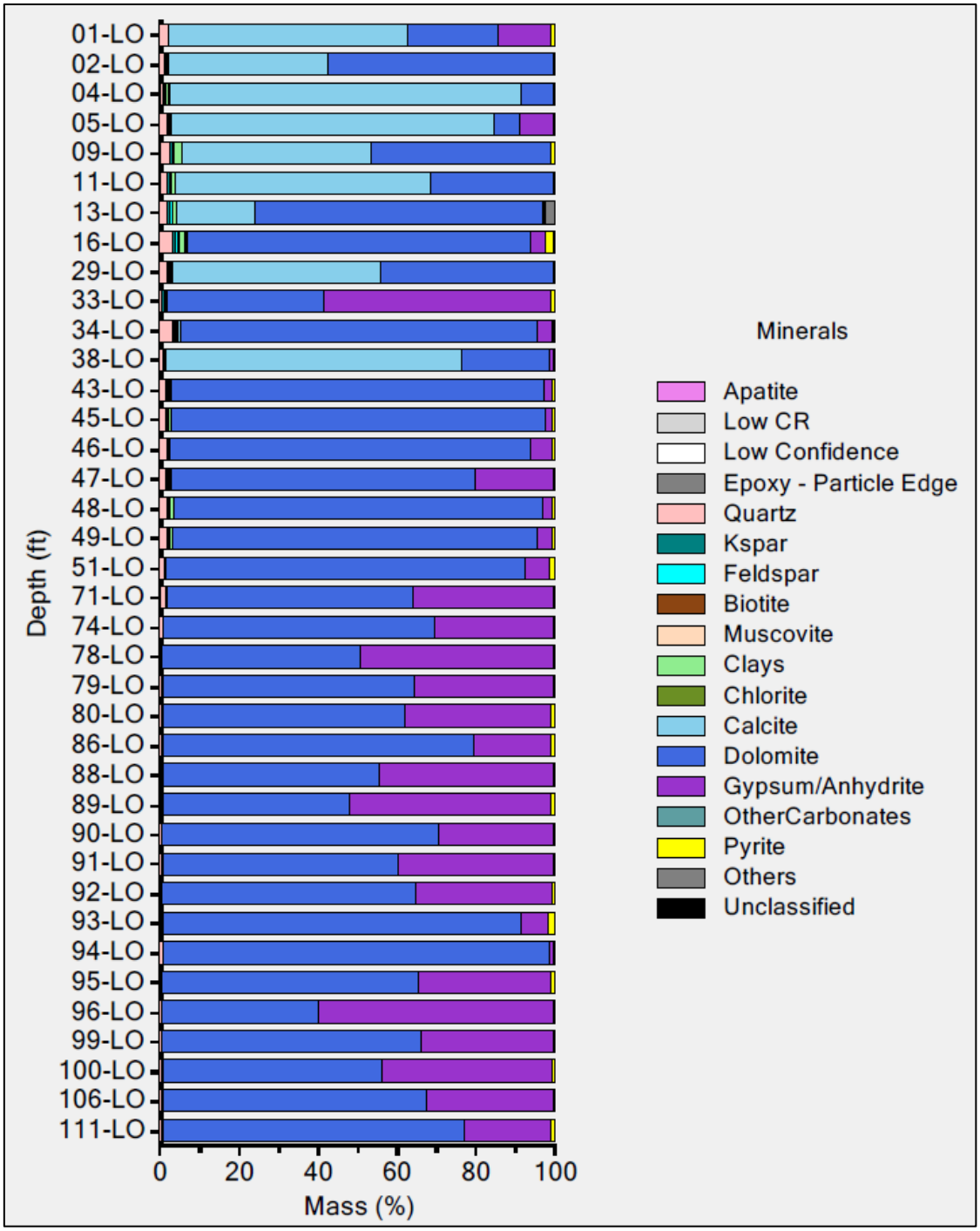

Figure 6-2: Mineralogy quantification using QEMSCAN based on 1cm square and 10 micron pixel resolution

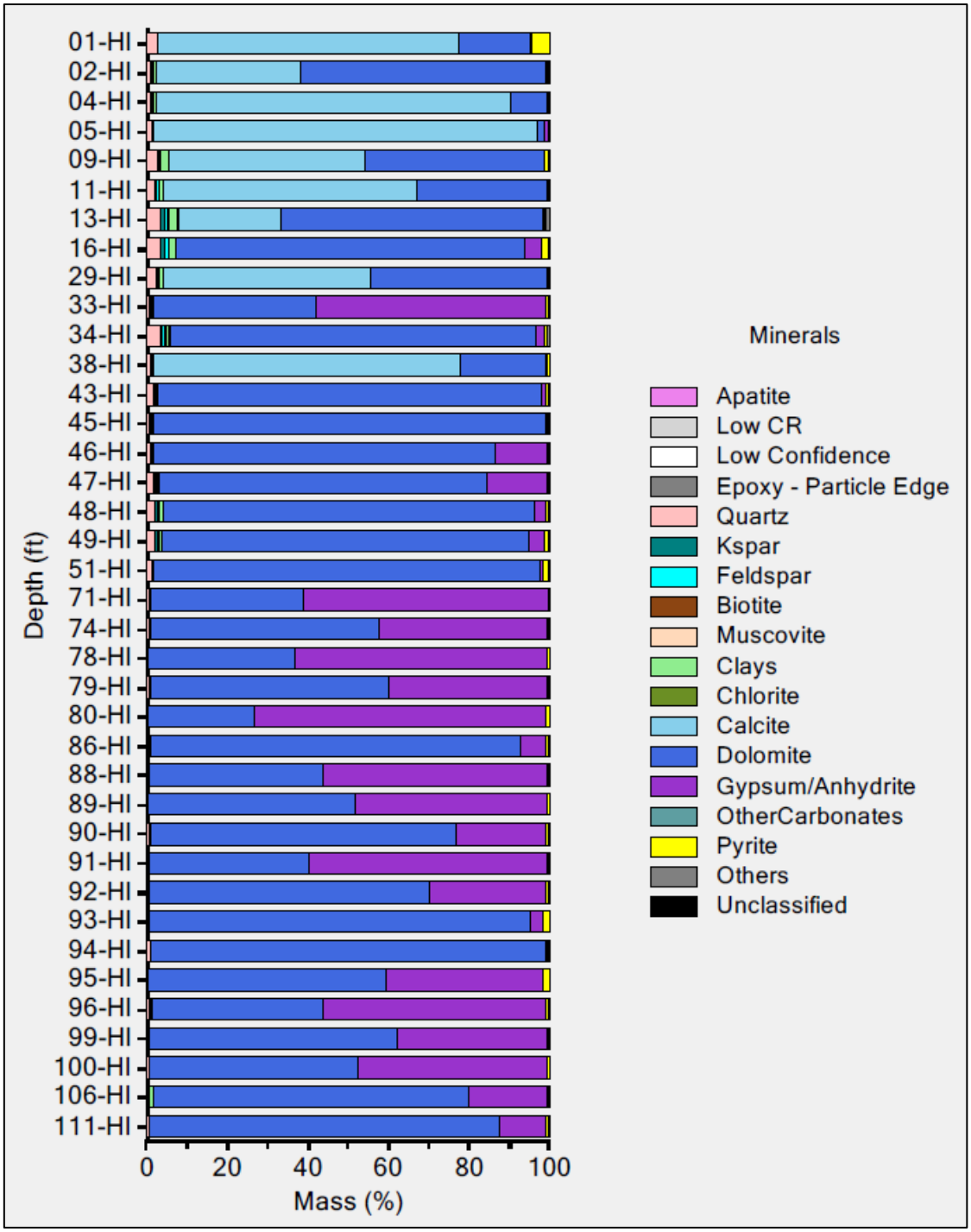

Figure 6-3: Mineralogy quantification using QEMSCAN based on 1mm square and 2.5 micron pixel resolution

In addition to the minerals quantification, Figure 6-4 and Figure 6-5 show eight sample images that were acquired using QEMSCAN. The images illustrate the complexity of the carbonate texture and the distribution of their mineralogy. Figure 6-6 shows a summary of the main minerals within these eight samples.

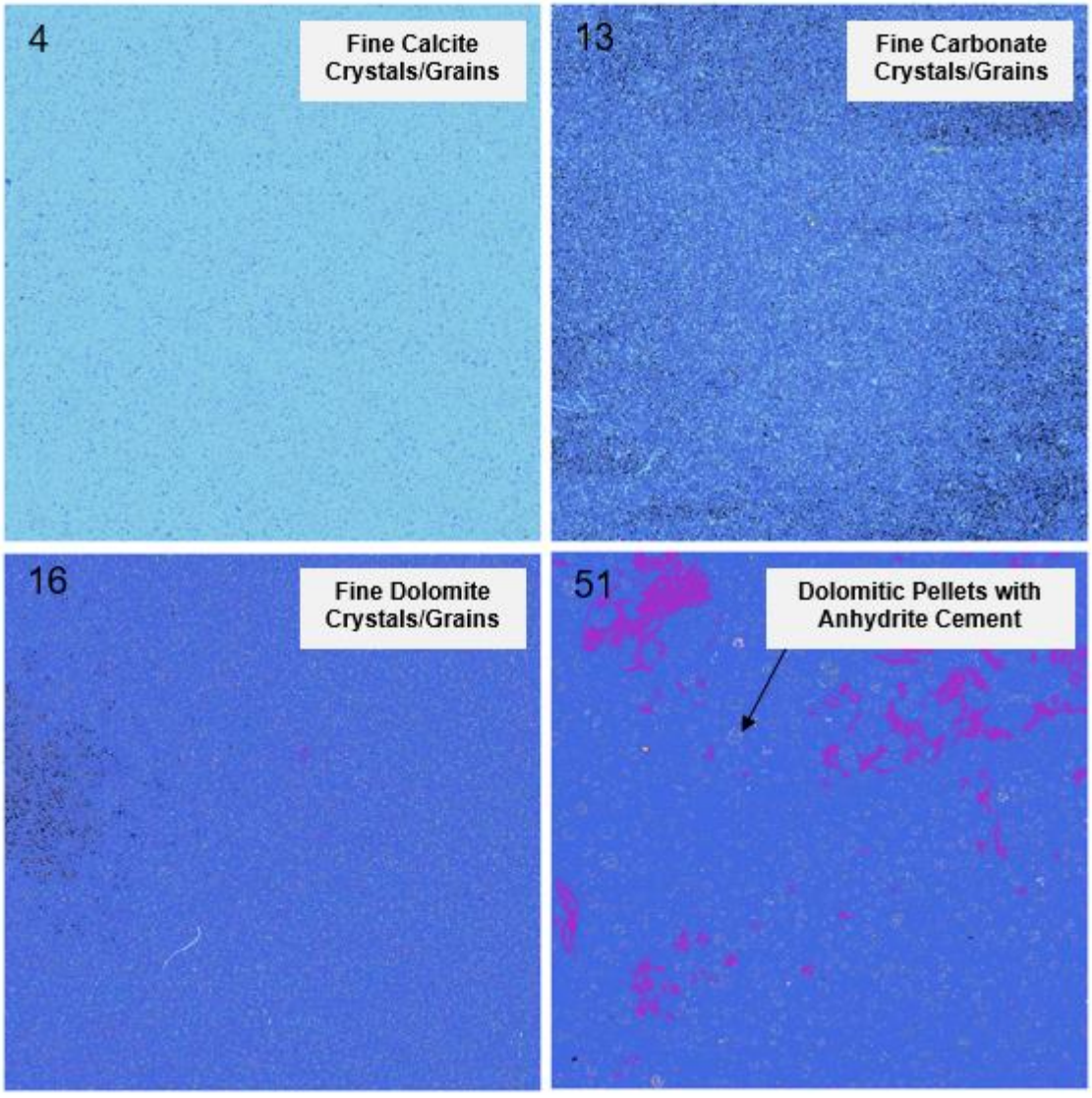

Figure 6-4: QEMSCAN low resolution images (1cm square each). Sample numbers are on the top left corner. Notice the difference in texture and the distribution of the minerals. Color code can be seen in the QEMSCAN mineralogy chart (Figure 6-2).

The images show a considerable amount of details about the grain size, grain shapes, fractures, fabric, sorting and compaction. However, no porosity can be seen because QEMSCAN can only recognizes minerals. It usually sees the minerals inside the pores and doesn't identify the pore space itself. Especially when the pores are very small like the section we are studying.

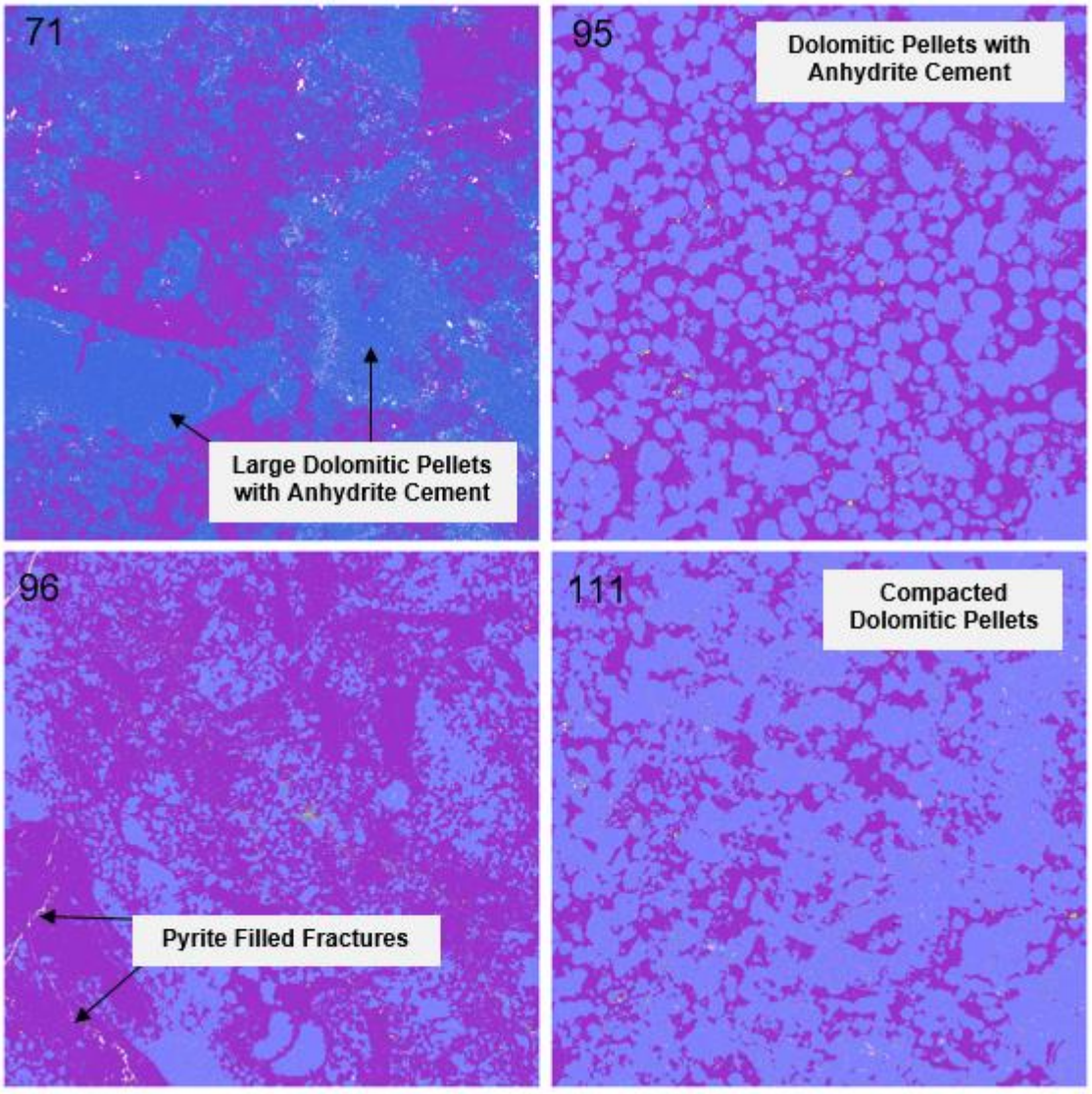

Figure 6-5: QEMSCAN low resolution images (1cm square each). Sample numbers are on the top left corner. Notice the difference in texture and the distribution of the minerals. Color code can be seen in the QEMSCAN mineralogy chart (Figure 6-2).

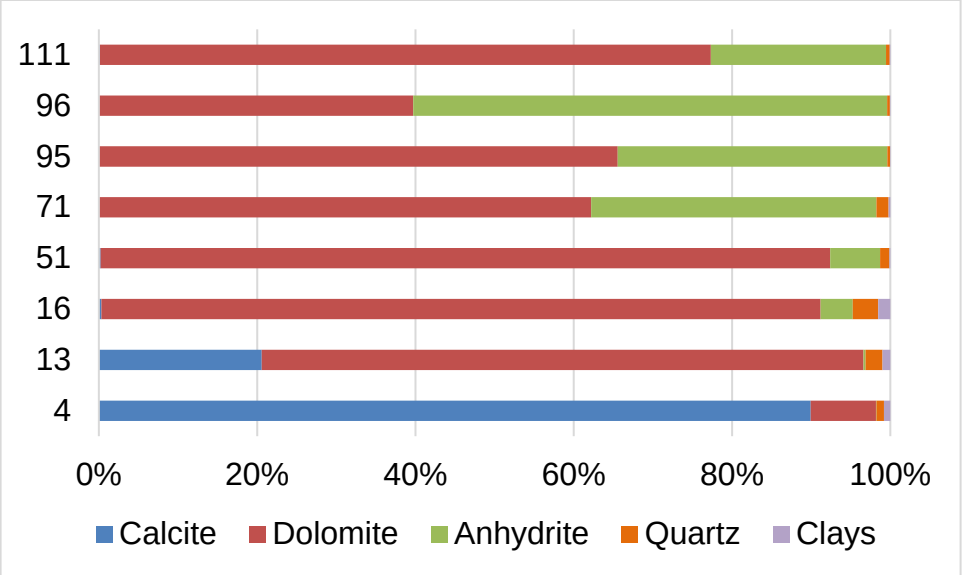

Figure 6-6: QEMSCAN mineralogy quantification

FTIR Mineralogy

FTIR is another widely used mineralogy quantification technique. It is known for its efficiency and ability to detect 16 different minerals in relatively short time (Sondergeld and Rai, 1993; Ballard, 2007). It mainly depends on the detection of the vibrational energy of molecular bonds in order to quantify mineralogy. Studies have seen that in more than 90% of the time, FTIR gives mineralogy quantification that is within +/-5 wt% of the actual mineralogy (Ruessink and Harville, 1992; Ballard, 2007). Eight samples were selected for FTIR and thin section analysis. Sample selection was made based on porosity, velocity, pore size (NMR) and mineralogy.

FTIR mineralogy results were in very good agreement with QEMSCAN. In addition, it was able to detect small amount of illite (up to 10 wt%) and

siderite (up to 7 wt%) which were around 1 wt% in QEMSCAN (Figure 6-6 and Figure 6-7).

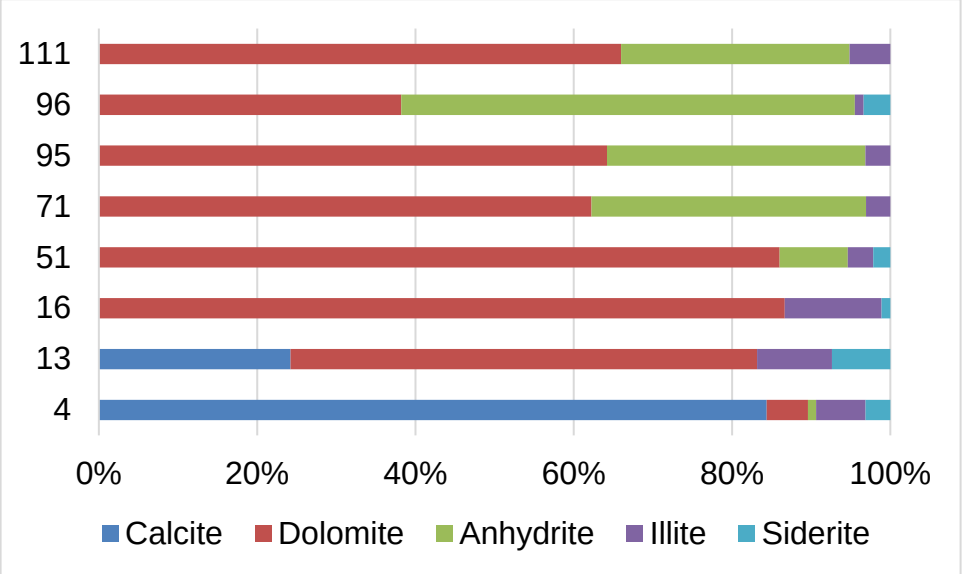

Figure 6-7: FTIR mineralogy quantification

Thin Section Mineralogy

The same eight samples that were used for FTIR analysis, were also used for thin section mineralogy, porosity and texture analysis. Mineralogy using this method is more of a qualitative and it does not carry a lot of details as FTIR and QEMSCAN, however enormous details can be obtained about the rock deposition history, fabric, texture, grains, diagenesis, pore size and pore shape. Figure 6-8 gives a summary of the mineralogy obtained from the thin section analysis.

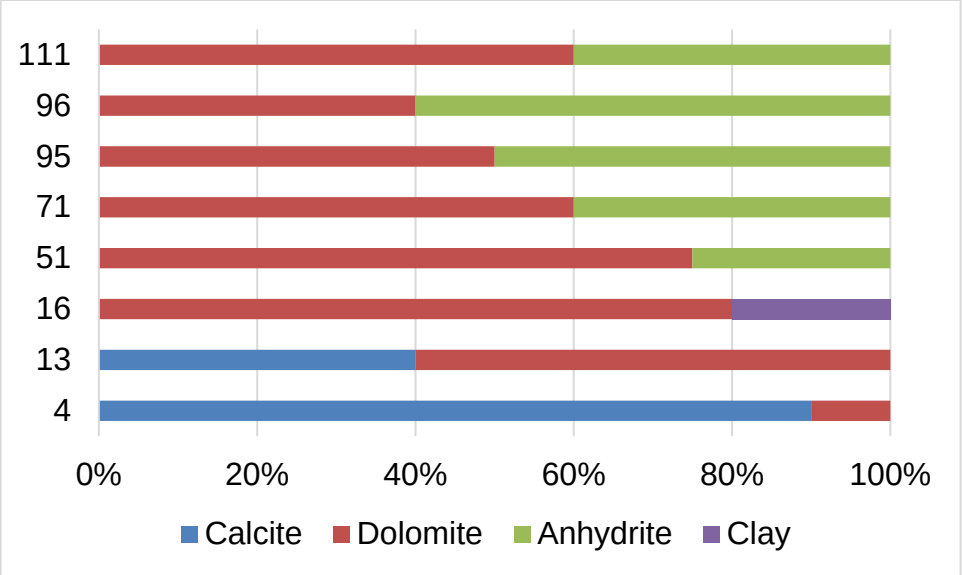

Figure 6-8: Thin section mineralogy estimation

The eight rock samples that were evaluated using thin sections suggest that we are dealing with the following carbonate categories:

I. Finely crystalline calcite.

II. Finely crystalline calcareous dolostone.

III. Finely crystalline argillaceous dolostone.

IV. Anhydritic pelletal dolostone

The analyzed samples are expected to be deposited with calcite lithology that subsequently dolomitized and replaced the original fabric with burial. Both original pellets and ooids have been dolomitized and negligible internal fabric can be seen.

Texture

Two major groups of textures can be recognized within the samples. Samples 4, 13 and 16 can be referred to as microcrystalline carbonate lithology

with uniform distribution of calcite and dolomite crystals (10-40 micrometer in size). Minor argillaceous material can be seen within this group ranging up to a moderate amount in sample 16. The second group (samples 51, 71, 95, 96 and 111) is texturally characterized by dolomite pelletal crystals bounded by anhydrite/dolomite cement. The pelletal grain size within the group has a range of 0.15-4.9mm with an average of 0.4mm in diameter. The dolomite crystals that fill the pelletal grains range in size from 10-20 micrometer. The porosity is mainly intercrystalline micropores and it is uniformly distributed.

Cement

Two types of cement have been seen in the samples. Most of the samples show anhydritic cement (Sample 71, 95, 96, 111), while sample 51 exhibits some dolomitic cement. Anhydrite shows up mainly as diagenetic interparticle cement or chemical replacement material replacing parts of the dolomite pellets. Coarsely crystalline dolomite sometimes acts as a cement agent between the fine crystalline dolomite pellets.

Porosity

Field emission scanning electron microscope was used to analyze porosity and pore type. The main type of porosity that was seen within all samples was intercrystalline pores. They occur either between micritic finely crystalline dolomite and calcite crystals or within pellet-like grain components. Most of these pores range in size from 0.5 to 2 micrometer with uniform

distribution. Some samples (sample 71) exhibit porosity of linear form between diagenetic anhydrite cleavage planes (Figure 6-9). Most of the pore walls were associated with diagenetic illite clays.

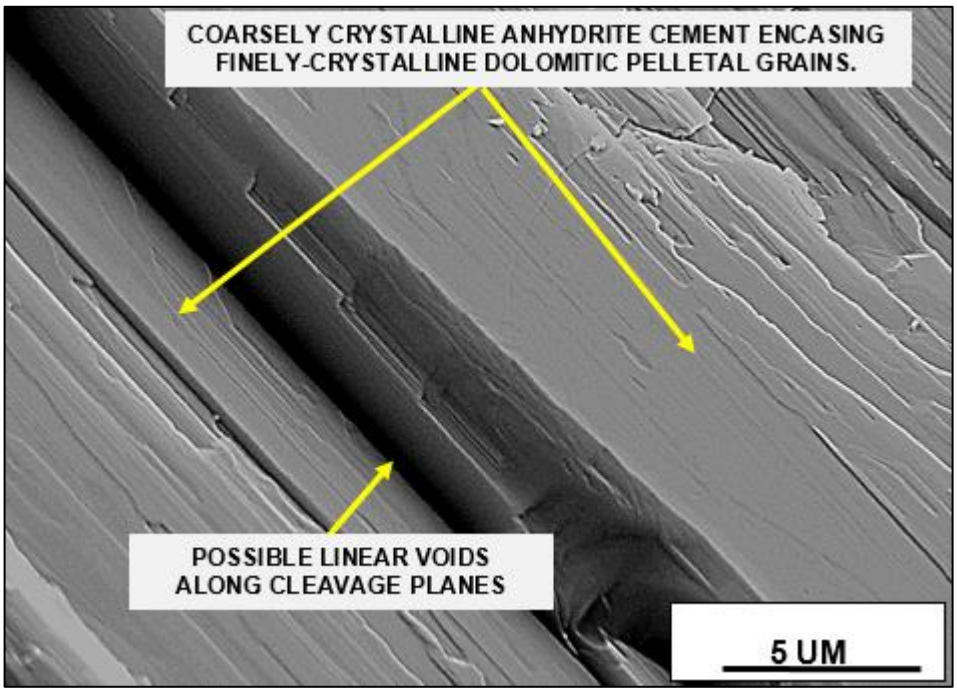

Figure 6-9: SEM image (Sample 71) showing anhydritic cement and possible linear porosity between cleavage planes

Fractures were seen in sample 95 cutting across anhydrite cement and dolomitic pelletal grains but completely healed by cement and possible organic material (Figure 6-10). The fact that these fractures cut though anhydrite cement suggest that the fractures are younger than the major anhydrite cement pulse. Bigger fractures have been seen in sample 96 and they are more likely artifacts of the sampling process than being naturally occurred. More details about each specific sample can be found in Appendix A.

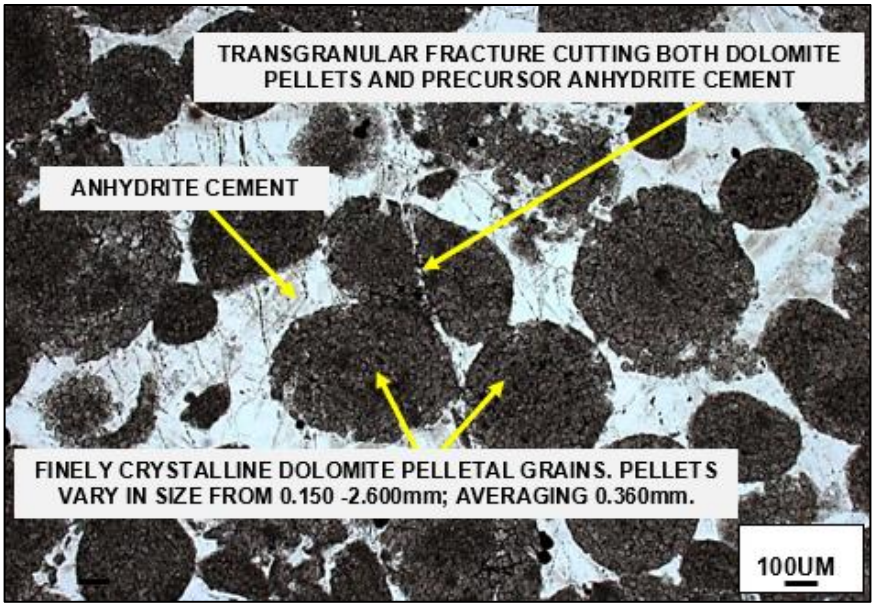

Figure 6-10: Thin section image (Sample 95) showing dolomitic pelletal grains texture and transgranular fracture

QEMSCAN vs. FTIR Mineralogy

QEMSCAN and FTIR are excellent mineralogy quantification techniques with some advantages and disadvantages. Table 6-2 below summaries the major differences between the two techniques.

Table 6-2: Comparison Between FTIR and QEMSCAN Techniques

	FTIR	QEMSCAN
Measurement	Molecular bonds	Simple X-ray count
Time	Fast but requires precision	Slow but automated
Condition	Destructive	None destructive
Quality	Better recognition for small minerals	Underestimate small minerals
Sample Size	~0.0005g fine particles	~0.2 cc disc

Both techniques were tested on the carbonate samples in the study and they were in good agreement for the major minerals (dolomite, calcite and anhydrite). Comparing the content of dolomite given by both techniques provide an excellent correlation with R^2 of 0.97 and values very close to the 1 to1 line (Figure 6-11). The major difference between the results was the detection of illite and siderite by FTIR. Considerable amount of illite up to 10 wt% was reported. Thin section petrographic analysis confirmed the presence of illite in association with the walls of the pores. Even though illite is usually known for decreasing porosity and plugging pore space, a plot of porosity vs. illite content shows positive correlation (Figure 6-12).

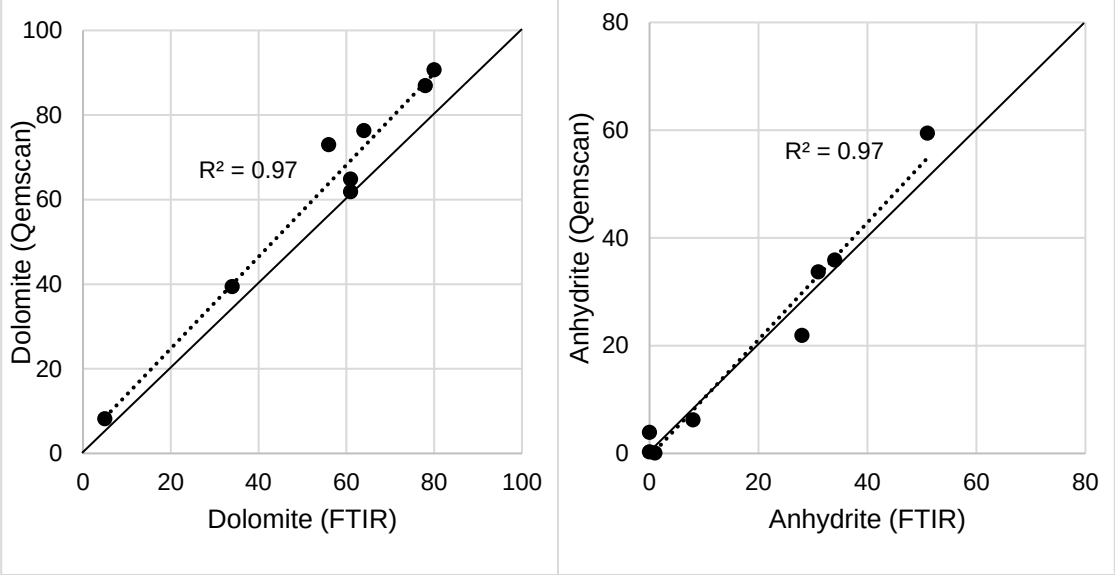

Figure 6-11: Cross plot of the dolomite content by QEMSCAN vs. FTIR (left). Anhydrite content by QEMSCAN vs. FTIR (right). Black lines are the 1 to 1 lines.

Thin section analysis confirms the detected illite by FTIR which was not detected by QEMSCAN. If we compare the science behind each technique, we notice that QEMSCAN is based on simple x-ray counts. Mineralogy

quantification is derived from overlapping elemental composition. Since clay fraction is small, clay tend to give very little x-ray emissions that get overshadowed by more abundant minerals like dolomite/calcite. Not to mention that many clays have similar elemental composition. On the other hand, FTIR is based on vibrational energy of chemical bonds. Thus, it is a much more reliable method for quantifying small quantity of minerals like clays because it can detect their molecular bonds.

Despite the poor detection of clays and other accessory minerals, QEMSCAN is still an excellent tool that could accurately quantify the overall mineralogy of the rock (Figure 6-11). Besides, it is a fully automated and non-destructive technique that can be repeated multiple times. Also, QEMSCAN samples of 0.2cc provided consistent mineralogy with XRD data of different sample sizes (Ardila and Clerke, 2014). In addition to the quantitative mineralogy, QEMSCAN will also provide excellent mineralogy maps where texture and fabric could be recognized (Figure 6-4, Figure 6-5).

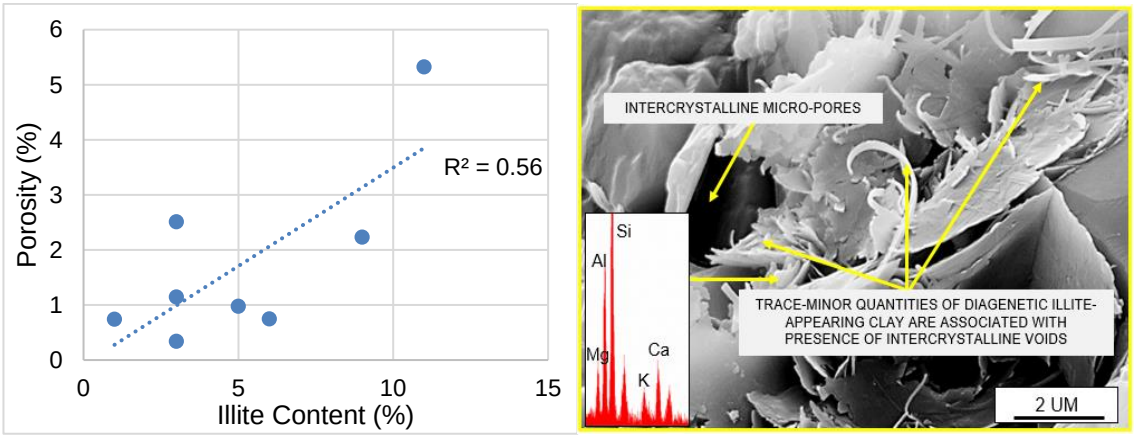

Figure 6-12: Left-Cross plot of illite content vs. porosity. Right-SEM image showing illite in association with the pore space

Carbonate rocks are known for their heterogeneity where the larger the sample used, the better representation of mineralogy. Nevertheless, the very small amount of samples (0.0005g) that were used for FTIR measurements were in excellent agreement with QEMSCAN entire disc evaluation. FTIR samples were prepared from half the disc samples that were used in QEMSCAN. Yet, they provided excellent representation of the mineralogy.

In summary, both techniques are excellent mineralogy quantification techniques. Depending on the desired details and available time and samples, one technique might be preferable over the other.

Grain Density

The grain density has been measured using two methods:

1. HPP (High pressure pycnometer)
2. LPP (Low pressure pycnometer)

HPP grain density data (Figure 6-13) shows that the top part of the section (samples 1-51) has a range of 2.711 to 2.888 g/cc. This section is mainly characterized by calcite and dolomite mineralogy with little anhydrite occurring. On the other hand, the bottom part of the section (samples 71-111) is showing a range of grain density between 2.853 and 2.906 g/cc. The samples in this section comprise mainly dolomite and anhydrite. They range from nearly pure dolomite to almost 60 wt% anhydrite and 40 wt% dolomite.

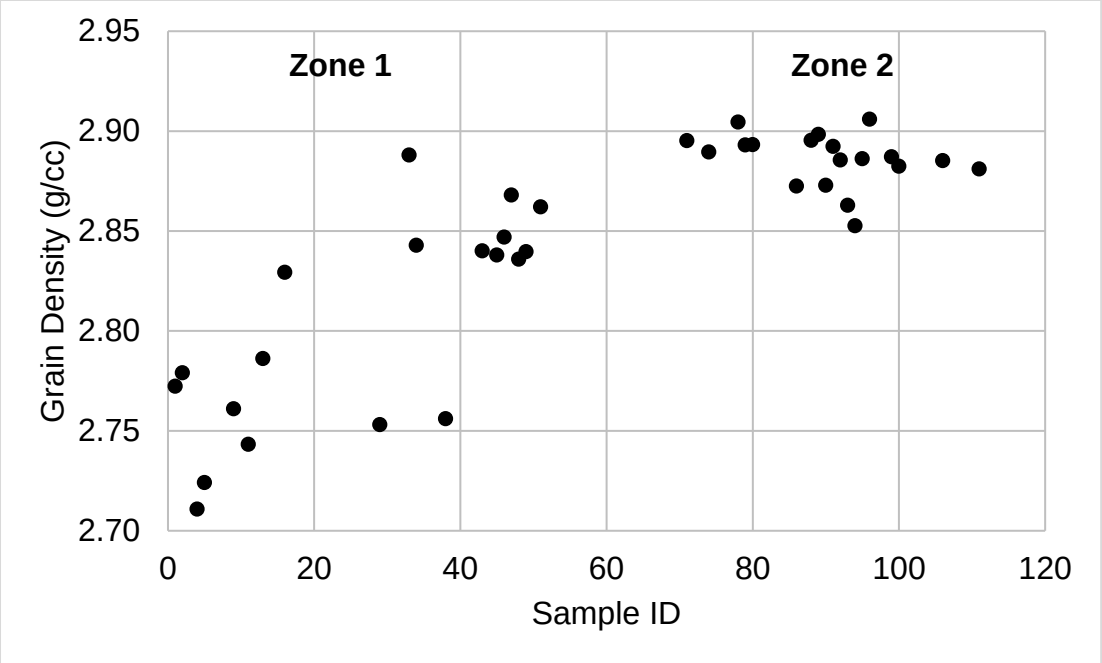

Figure 6-13: HPP grain density data plotted against sample ID

LPP grain density were measured for six samples to cross correlate the results with the results from HPP measurements (Figure 6-14). LPP grain density is consistently higher than HPP measurement. It has an average increase of 0.021 g/cc compare to the HPP grain densities. The increase of density using LPP compare to HPP is more likely the result of crushing the rock and opening the occluded pores. This allowed the occluded fluids to dry out and resulted in an increase in the grain density. This difference in density support the presence of occluded pores and explain the higher porosities that were measured by NMR.

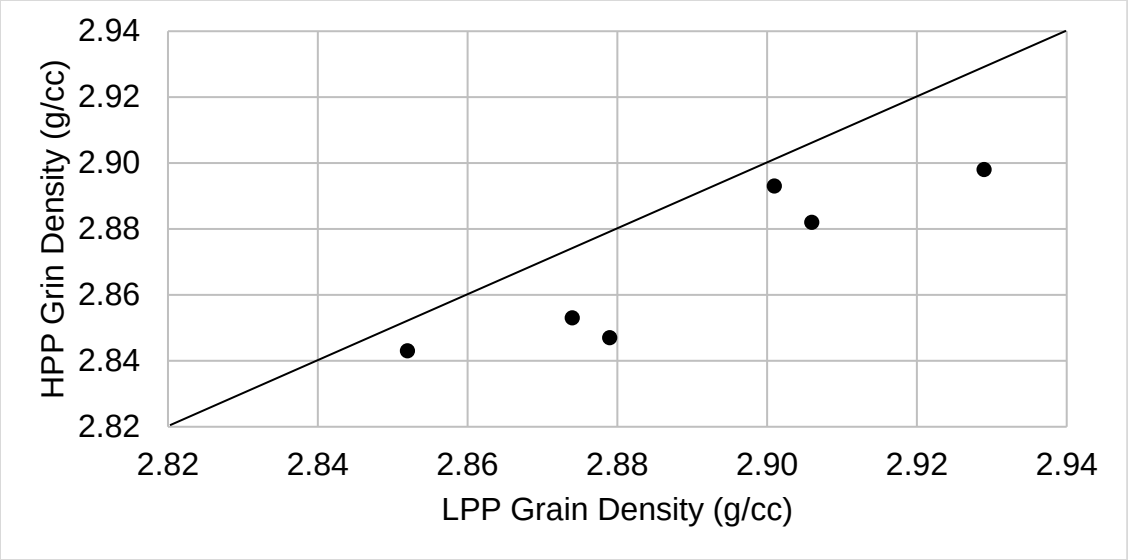

Figure 6-14: Cross plot of HPP grain density and LPP grain density. Black line is the one to one line.

Permeability

Permeability was measured using the AP-608 Automated Permeameter Porosimeter @ 800psi confining pressure. Just like porosity, the permeability of the entire section was very low and ranges between 0.002 to 0.189 mD with an arithmetic average of 0.019 mD. Plotting the porosity and permeability data on a chart of Winland plot suggests that the top section (Zone 1) has mainly a pore throat radius of 0.2 micrometer. The bottom section (Zone 2) is more dispersed and the pore throat radius ranges between 0.2 and 2 micrometers (Figure 6-15).

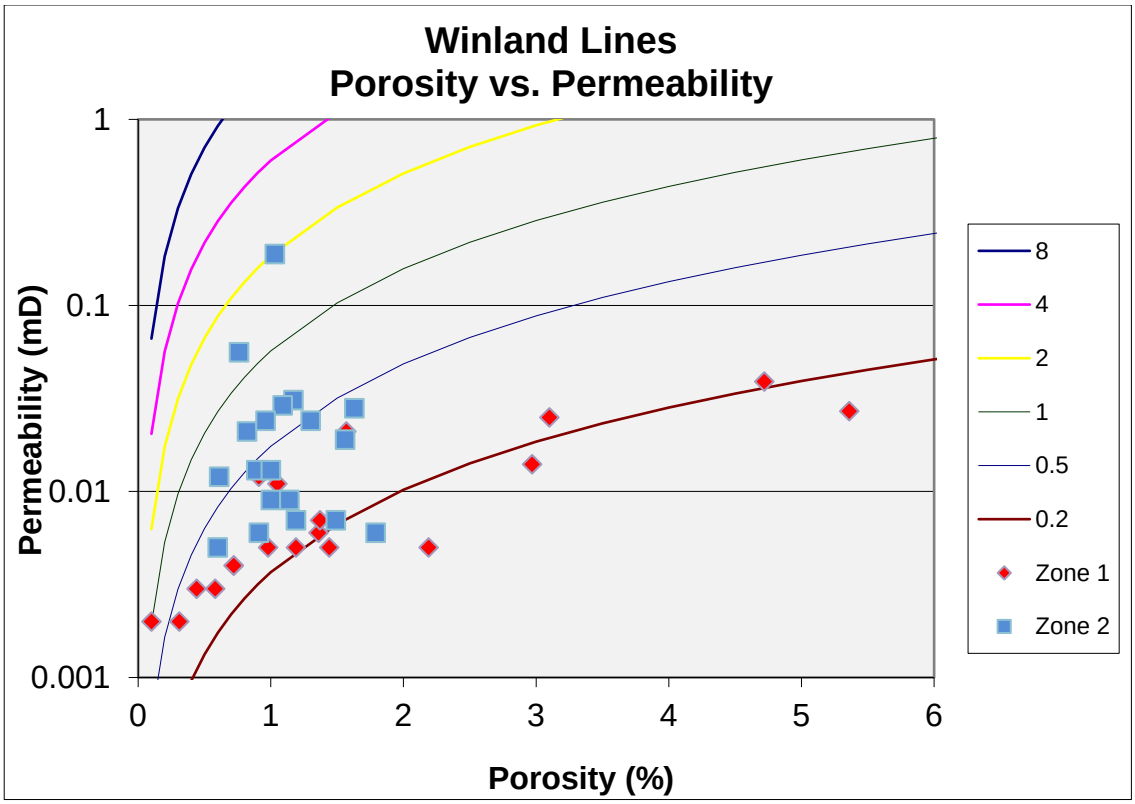

Figure 6-15: Winland plot of porosity and permeability. Colored lines represent the pore throat radius (in micron) at 35% mercury saturation

NMR Pore Size

NMR was measured on the dodecane saturated plugs and the NMR porosity was reported in the porosity section above. However, in order to fully characterize the pore space, NMR T_2 incremental relaxation time could help distinguish the samples with single, dual or triple porosity systems. Also, it could help provide insight about the pore sizes that we are dealing with.

Based on NMR, almost all of the samples in Zone 1 consist of a single pore system. Zone 2 is more complex than Zone 1 and shows very little porosity in general. NMR relaxation time can be converted to pore size knowing the

surface relaxivity and the shape of the pores. If we assume that we are dealing with spherical pores, we get the below relationship (Kenyon, 1992):

$$\frac{1}{T_2} = \rho \frac{3}{r} \qquad 6\text{-}1$$

Where: ρ is the surface relaxivity (um/s)

r is the pore radius (mm)

From equation 6-1 we can notice that if we keep the surface relaxivity constant, the T_2 relaxation time is directly proportional to the pore radius. Therefore, the T_2 relaxation time scale can be considered as a relative pore size scale. The bigger the T_2 relaxation time, the bigger the pore size. Nevertheless, assuming surface relaxivity of 5um/s for carbonates (Chang et al., 1994), Figure 6-16 to Figure 6-19 show the estimated pore sizes for Zone 1 and Zone 2 samples respectively.

Zone 1 and Zone 2 can be divided based on the NMR estimated pore system to four sub groups: Zone 1-A, Zone 1-B, Zone 2-A and Zone 2-B. Zone 1-A samples (Figure 6-16) have relatively bigger pores compare to Zone 1-B (Figure 6-17). Zone 2-A samples exhibit single pore system around 1um of size (Figure 6-18). Zone 2-B samples (Figure 6-19) are showing dual porosity systems with wider distribution in pore sizes (1-5um). The pore sizes that we get using NMR are comparable to the pore sizes that were analyzed using SEM images. This indicate that a surface relaxivity of 5um/s is applicable to this formation. Combining NMR and mercury injection data may help predicting the best surface relaxivity value for the formation (Sulucarnain et al., 2012).

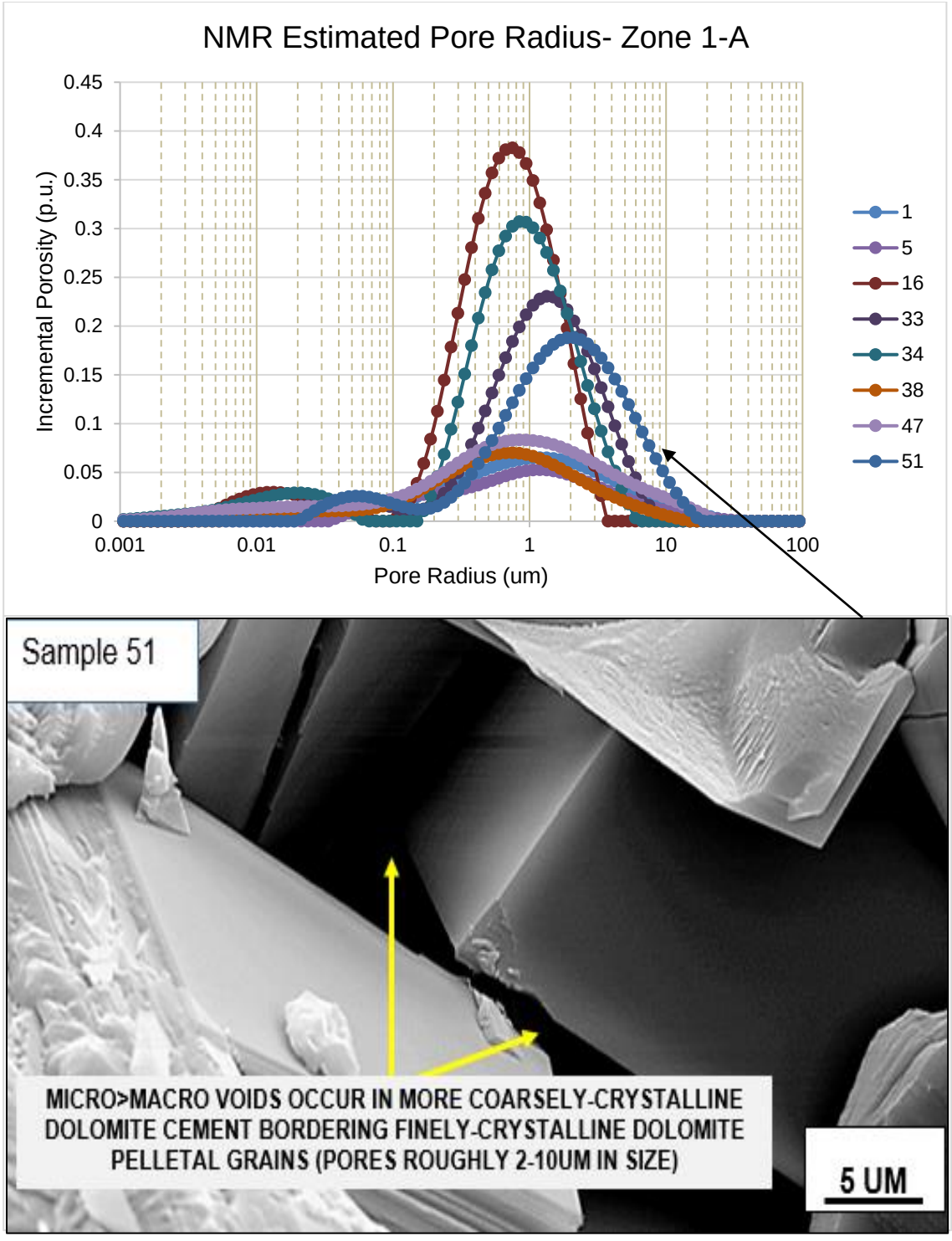

Figure 6-16: Pore body sizes distribution for Zone 1-A samples with an SEM image example.

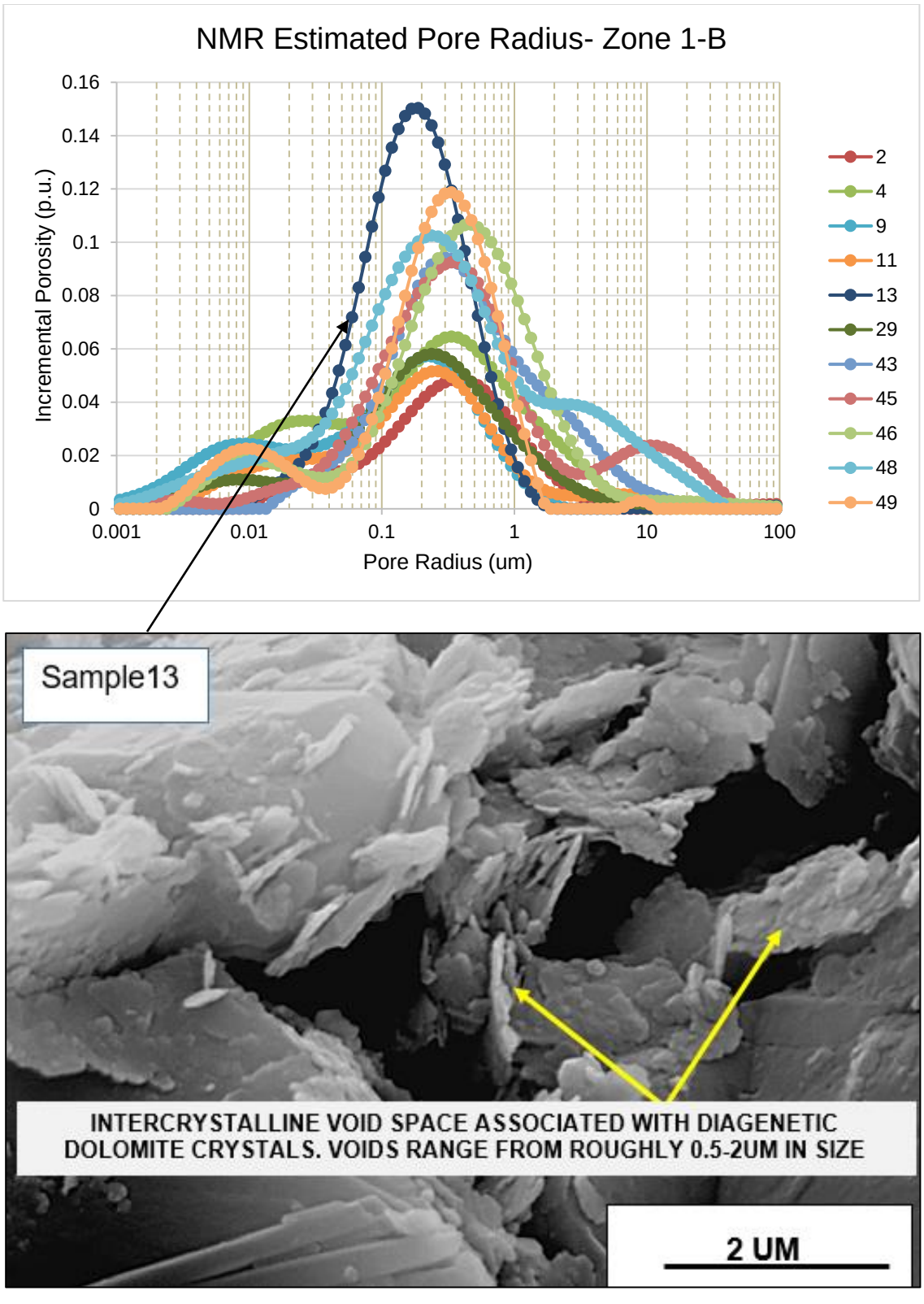

Figure 6-17: Pore body sizes distribution for Zone 1-B samples with an SEM image example.

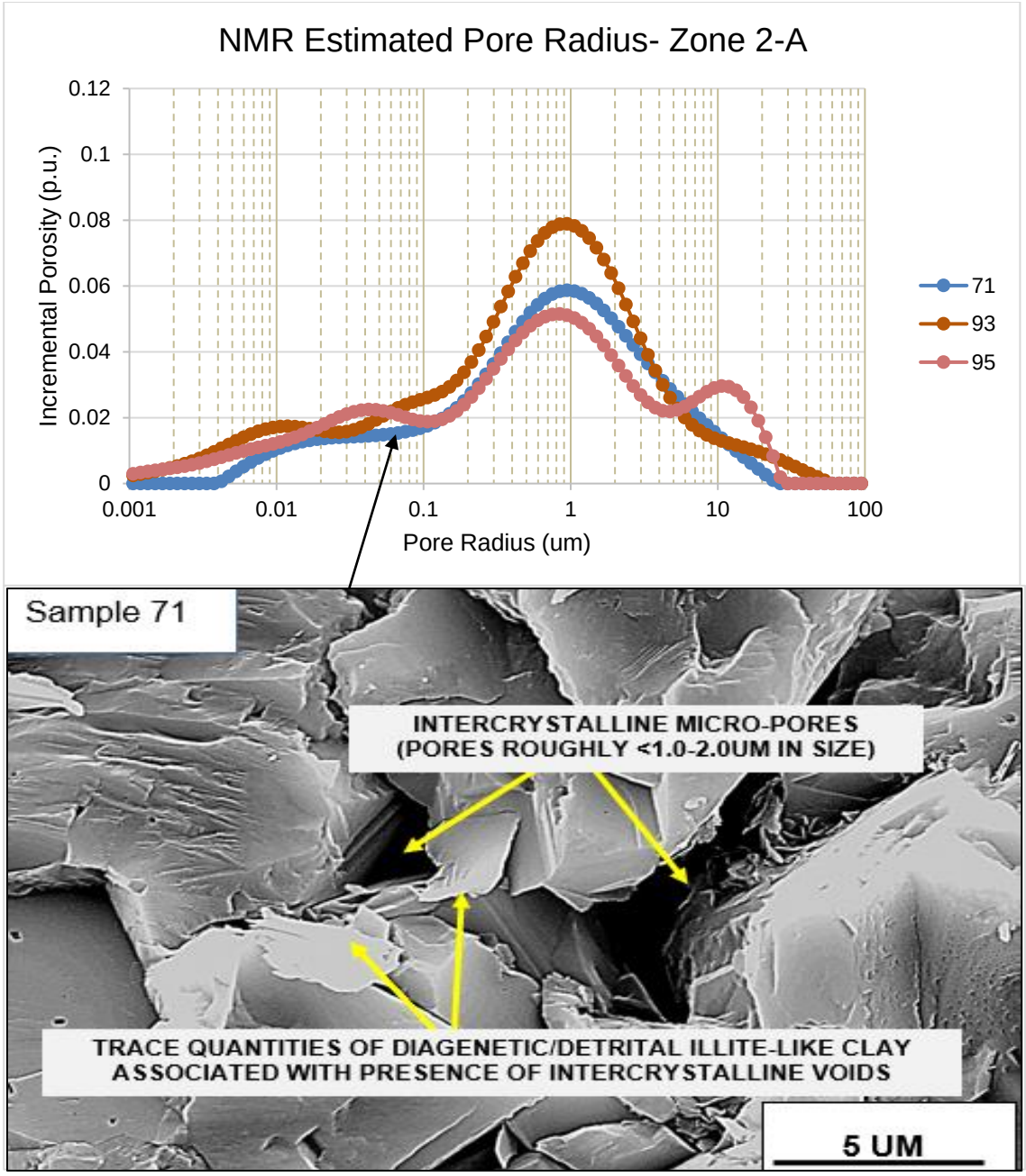

Figure 6-18: Pore body sizes distribution for Zone 2-A samples with an SEM image example.

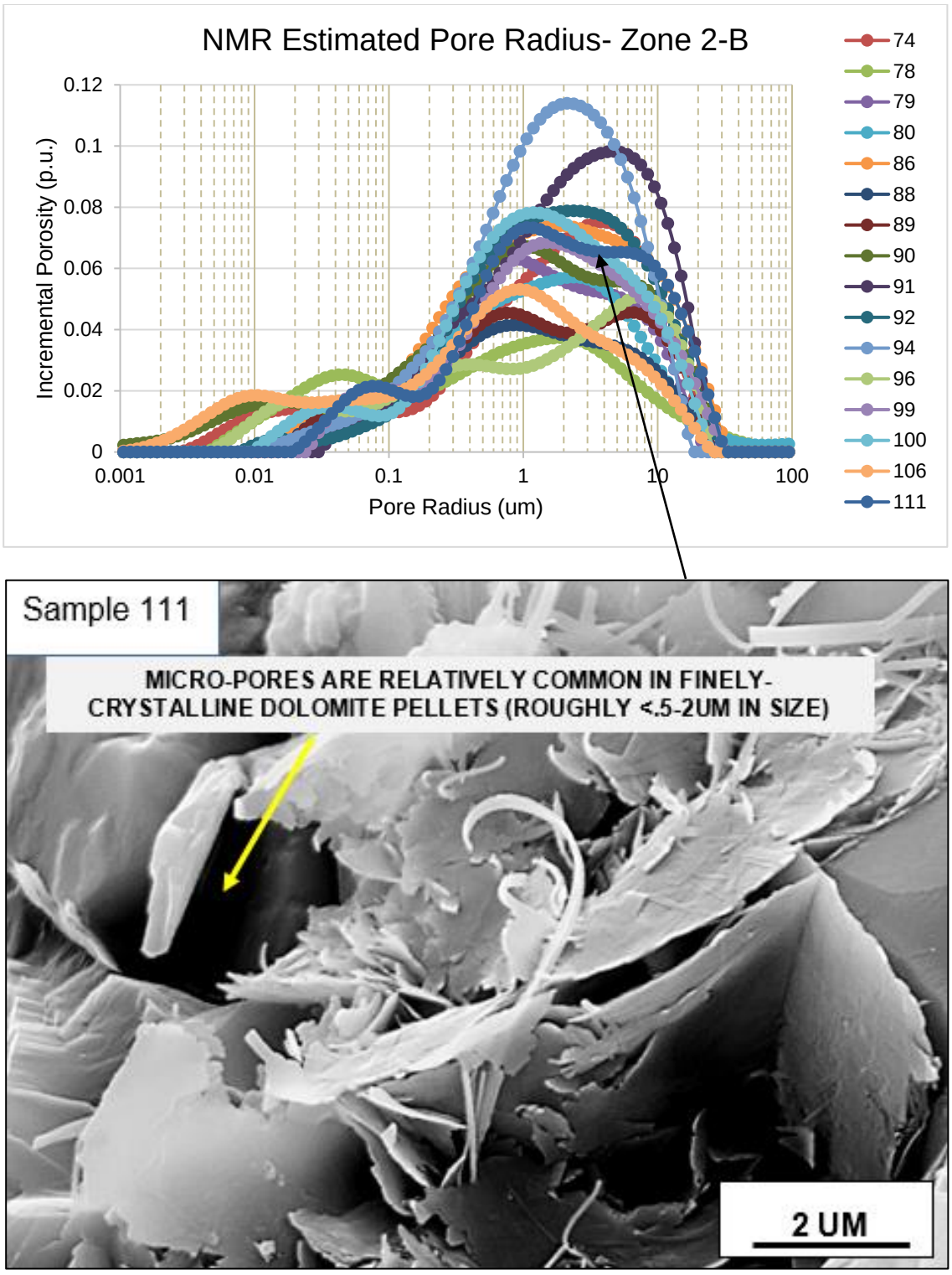

Figure 6-19: Pore body sizes distribution for Zone 2-B samples with an SEM image example.

Compressional and Shear Velocity

The compressional V_p and shear V_s velocities have been measured on dry and dodecane saturated samples over a range of differential pressure (250-5000 psi). The table below summaries the velocity data for all samples:

Table 6-3: Summary of the Dry and Saturated Velocity Data in km/s

Velocity	Minimum	Maximum	Average
V_p Dry @ 5000	4.36	6.27	5.33
V_p Saturated @ 5000	5.51	6.75	6.24
V_{s1} Dry @ 5000	2.86	3.37	3.14
V_{s2} Dry @ 5000	2.86	3.60	3.17
V_{s1} Saturated @ 5000	2.99	3.57	3.32
V_{s2} Saturated @ 5000	3.03	3.65	3.34

Plotting the compressional wave velocity (V_p) vs. pressure shows that most of the samples velocity exhibit relatively flat behavior as a function of deferential pressure (Confining pressure – pore pressure). Only a couple of samples show some exceptions (Figure 6-20). The percentage difference between the dry and the saturated V_p is 15.7%. The shear wave velocity from the table above and Figure 6-21 appears to be isotropic as the perpendicular shear velocities V_{s1} and V_{s2} data are within 1% difference. However, percentage difference between the dry and the saturated V_s is 5.8%. In addition, plotting the dry vs. saturated velocity for the P-wave and S-wave velocity show that both V_p and V_s increase with saturation (Figure 6-22, Figure 6-23).

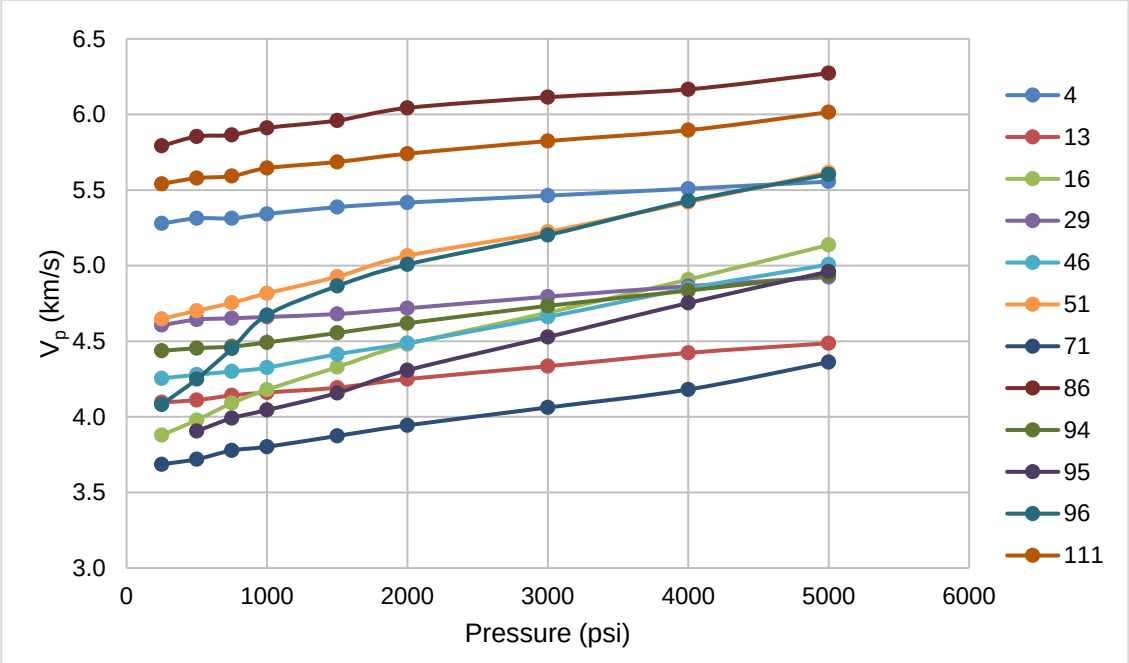

Figure 6-20: Plot of dry compressional velocity data as a function of differential pressure

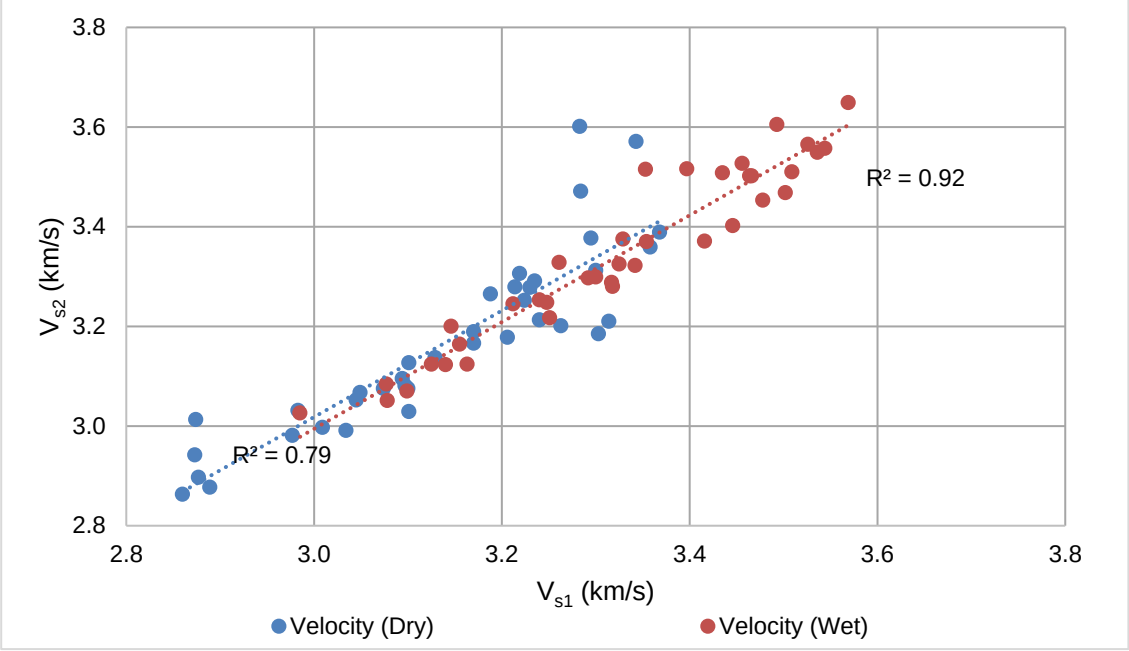

Figure 6-21: Plot of V_{s1} vs. V_{s2} for the dry and saturated shear wave velocity

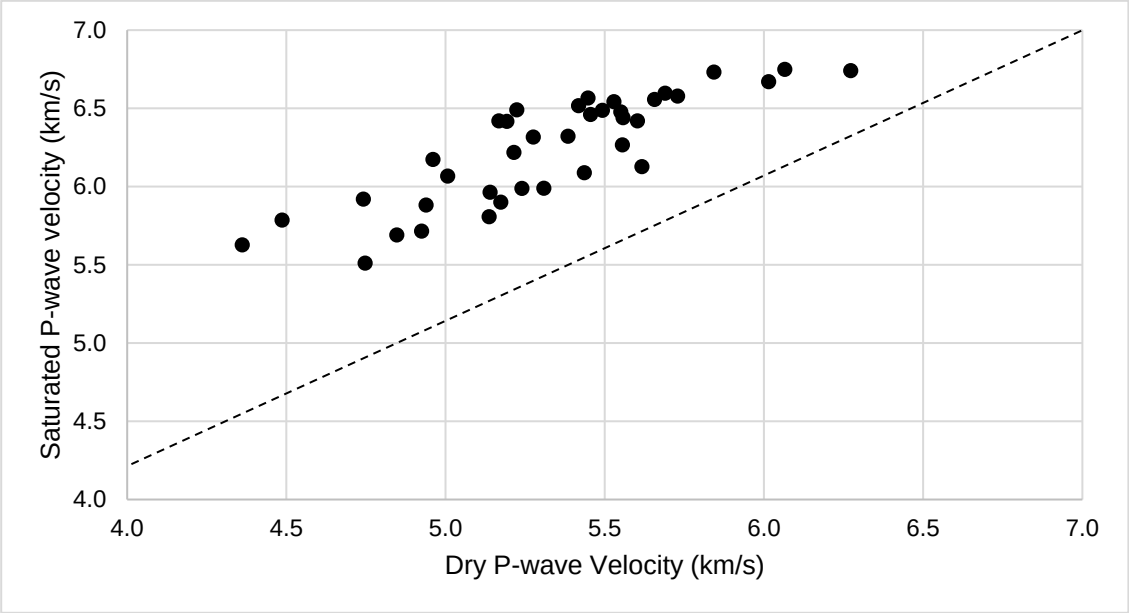

Figure 6-22: Plot of dry vs. saturated P-wave velocity. Dashed line: one to one line.

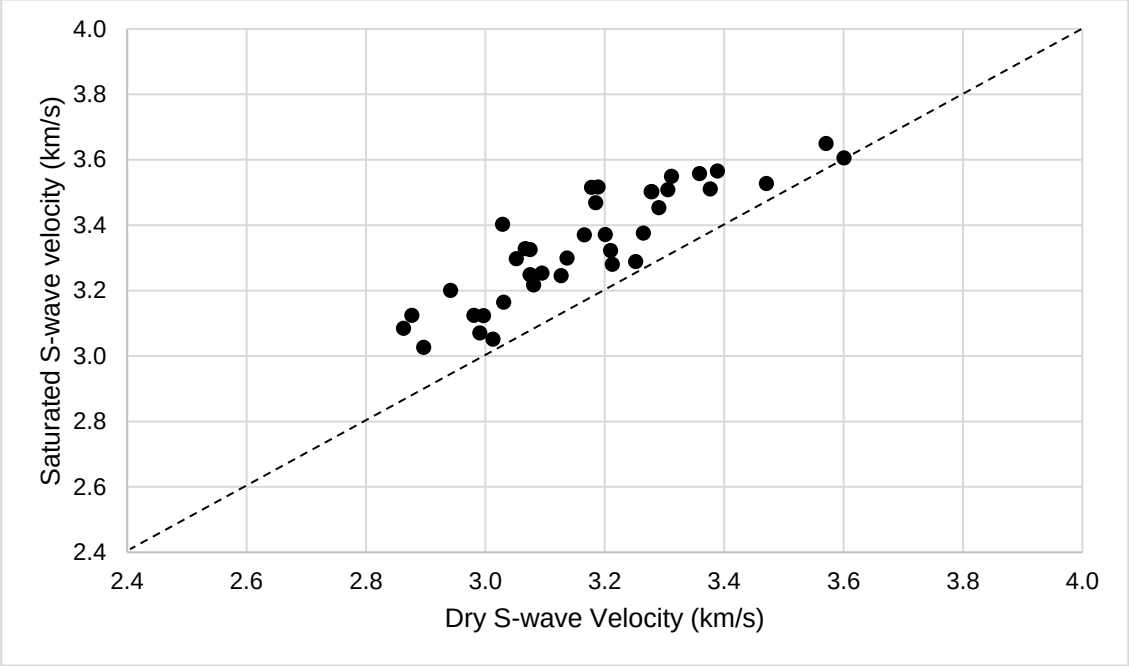

Figure 6-23: Plot of dry vs. saturated S-wave velocity. Dashed line: one to one line.

Fluids Effect: V_p/V_s Ratio

The V_p/V_s ratio has been widely used as one of the strong tools for fluids differentiation (Vanorio, 2006). It takes into account the effect of both the P-wave and S-wave velocities. The P-wave velocity is more sensitive to the pore and fluid compressibility. The bulk modulus (K) changes rapidly depending on the compressibility of the fluids in the pores. The S-wave velocity is only sensitive to the density. Combining these terms in the V_p/V_s ratio help in distinguishing the gas, water or hydrocarbon saturated rocks.

$$V_s = \sqrt{\frac{G}{\rho}} \qquad 6\text{-}2$$

$$V_p = \sqrt{\frac{K+\frac{4}{3}G}{\rho}} \qquad 6\text{-}3$$

In general, the P-wave velocity increases with saturation while the S-wave velocity decreases. Fluids have no effect on the shear modulus (G), therefore, V_s is inversely proportional to density (Equation 6-2). Dry rocks have low density compare to saturated rocks. As a result, V_s dry is larger than V_s saturated. V_p is also inversely proportional to density (Equation 6-3). However, the effect of fluids on the bulk modulus (K) is larger than their effect on density. Fluids greatly reduce the pore compressibility and ultimately reduce the overall rock compressibility. The bulk modulus (K) is the inverse of compressibility. Therefore, V_p saturated is larger than V_p dry which leads to:

$$\left.\frac{V_p}{V_s}\right|_{Dry} < \left.\frac{V_p}{V_s}\right|_{Saturated} \qquad 6\text{-}4$$

The saturated P-wave data for our carbonate samples were higher than the dry data just as expected (Figure 6-22). However, the saturated S-wave data were also higher than the dry data (Figure 6-23). This indicate an increase in the shear modulus (G) with saturation (Figure 6-24). Hence, these rocks do not fit with Biot-Gassmann model assumption which suggests that $G_{Dry} \equiv G_{Sat}$. This phenomenon will be investigated in great details later in this chapter.

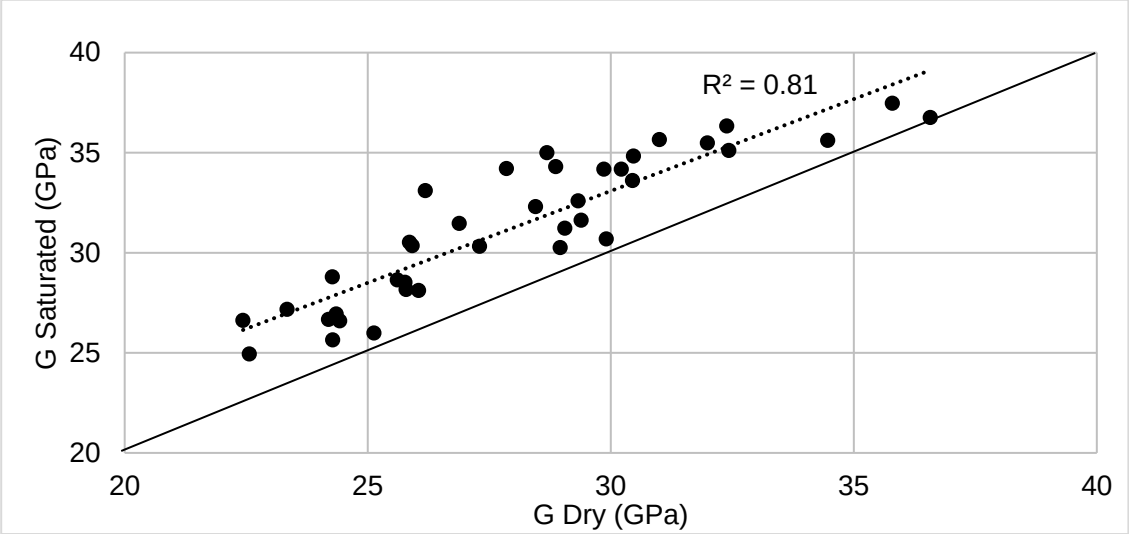

Figure 6-24: Cross plot of dry and saturated shear modulus. Black line is one to one line.

Despite the unexpected increases in V_s with saturation, the overall saturated V_p/V_s is larger than the dry V_p/V_s. In addition, there is a distinctive separation between the dry and the saturated data that could be used for fluid identification. Figure 6-25 illustrate data measured at 5000 psi and it suggests that V_p/V_s ratio of 1.8 can distinguish the fluid's saturated rocks from the dry or gas saturated rocks.

The reservoir condition might have high pore pressure which ultimately decreases the overall differential pressure. Figure 6-25 and Figure 6-26 show

that the separation between the dry and saturated V_p/V_s ratio at low differential pressure is larger than the separation at high differential pressure. Therefore, V_p/V_s ratio can also be used to detect formations with overpressure conditions (low differential pressure).

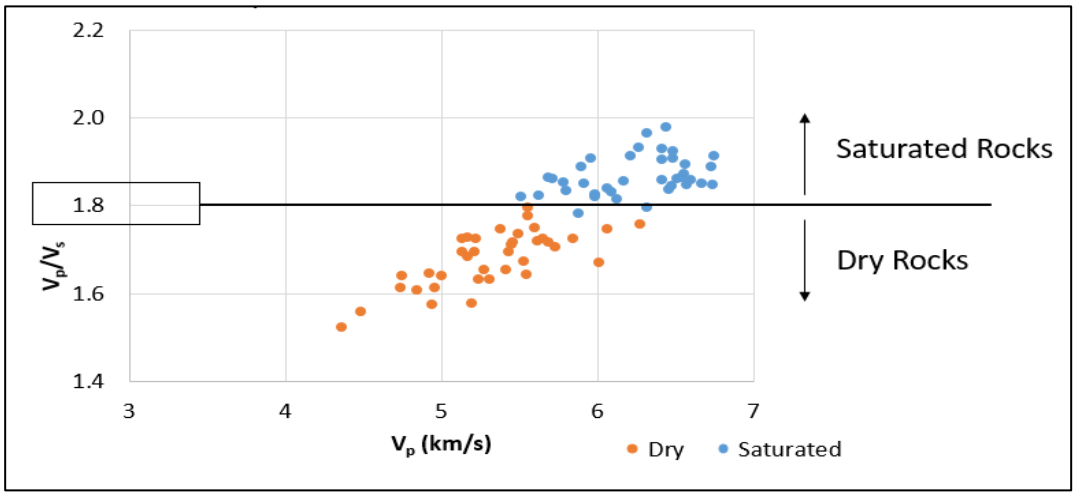

Figure 6-25: V_p/V_s vs. V_p for the dry and saturated samples at 5000psi. Notice the sharp separation between the two groups at a V_p/V_s ratio of 1.8.

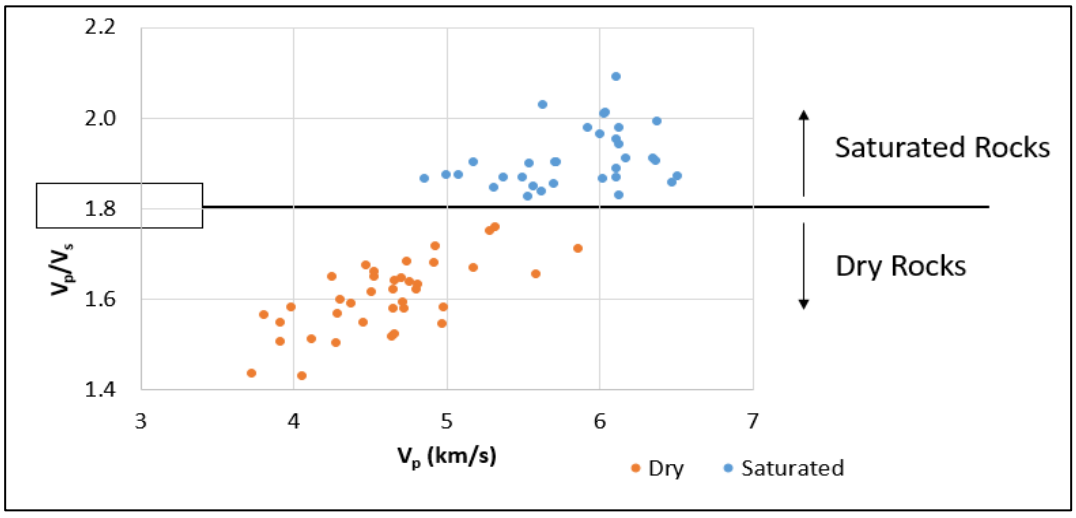

Figure 6-26: V_p/V_s vs. V_p for the dry and saturated samples at 500psi. Notice the sharp separation between the two groups at a V_p/V_s ratio of 1.8.

Looking at the 5000psi and the 500psi data, we can see more clear separation at V_p/V_s of 1.8 at lower differential pressure. Also, as we decrease the differential pressure, we see an increase in the saturated V_p/V_s values and decrease in the dry values. Similar behavior was seen in laboratory and theoretical modeling studies (Vanorio, 2006). Figure 6-27 shows the V_p/V_s laboratory results for oil saturated and dry sandstone rocks from (Siggins and Dewhurst, 2003). As the differential pressure decreases (increasing pore pressure), V_p/V_s increases in the saturated rocks and decreases in the dry rocks (Figure 6-25, Figure 6-26).

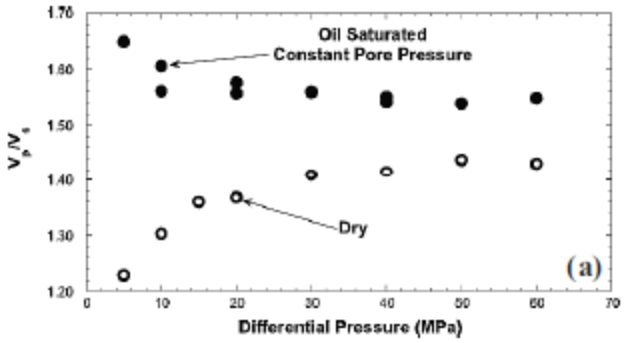

Figure 6-27: Differential pressure effect on V_p/V_s ratio for oil saturated and dry rocks.

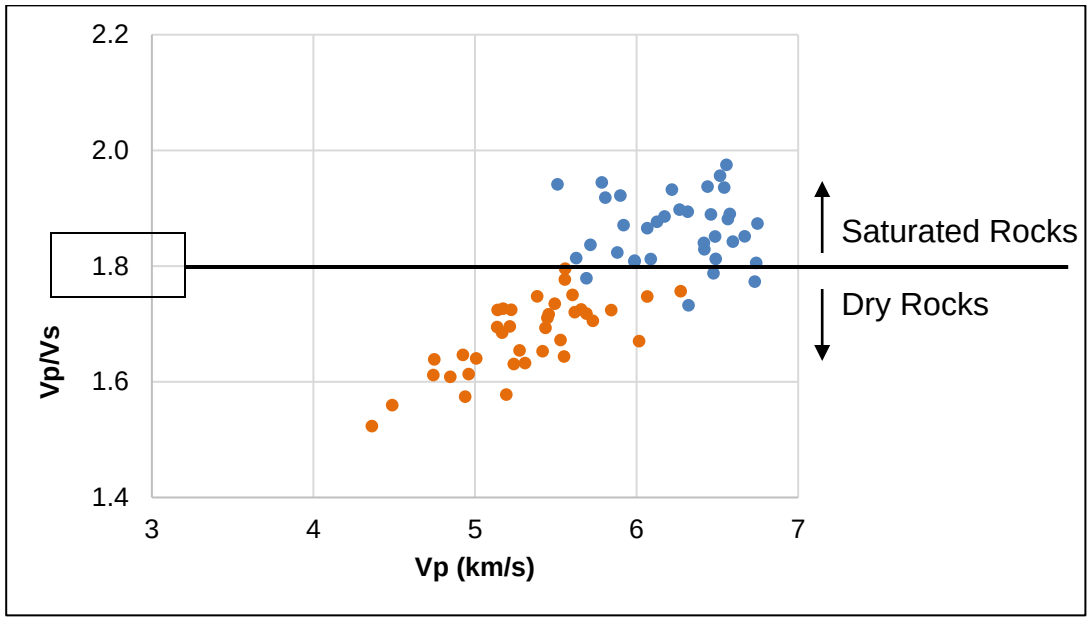

Figure 6-28: V_p/V_s vs. V_p. The saturated values are estimated from the dry values at 5000psi. Separation between the two groups at a V_p/V_s ratio of 1.8 can still be identified.

Since the saturated moduli and velocities measured at ultrasonic velocity can be associated with dispersion, V_p and V_s saturated values have been calculated from the dry values using Biot-Gassmann model. When we use the calculated V_p and V_s saturated values, we can estimate the V_p/V_s ratio that is free of any dispersion effect. Plotting the V_p/V_s ratio for the dry and the saturated dispersion-free values still shows a good separation between the dry and the saturated values (Figure 6-28). Even when we eliminate any dispersion effect, the V_p/V_s ratio can be used to detect gas/fluids in the system.

In addition, it was found that V_p/V_s ratio has no dependence on porosity (Figure 6-29), however, it has a good relationship with mineralogy (Figure 6-30). Rafavich et al., (1984) ilisturated the dependence of the V_p/V_s ratio on mineralogy. They showed that the calcite rich samples are usually associated with higher V_p/V_s ratios compare to the dolomite rich samples. Our data suggest that the dolomite content has an inverse relationship with V_p/V_s while calcite has a direct relationship with V_p/V_s. However, there was no distinctive separation between the calcite and the dolomite rich samples based on their V_p/V_s values. We also found that the correlation coefficient reduces when we use the dry V_p/V_s values in the plots vs. dolomite and calcite content.

Studies have shown that V_p/V_s ratio is a good tool to determine the saturation state of the rocks (Siggins and Dewhurst, 2003; Vanorio, 2006). The lower the differential pressure, the better the differentiation. Our data confirmed this analysis and showed excellent separation (Figure 6-25) even at high pressure. Such finding can be incorporated with seismic data in order to

generate quick and reliable maps showing the possible locations of the gas saturated rocks. This is an excellent tool for exploration, reservoir delineation, reservoir monitoring and identifying possible bypass zones. In addition, it could be used to detect formations with overpressure zones (Rojas et al., 2005).

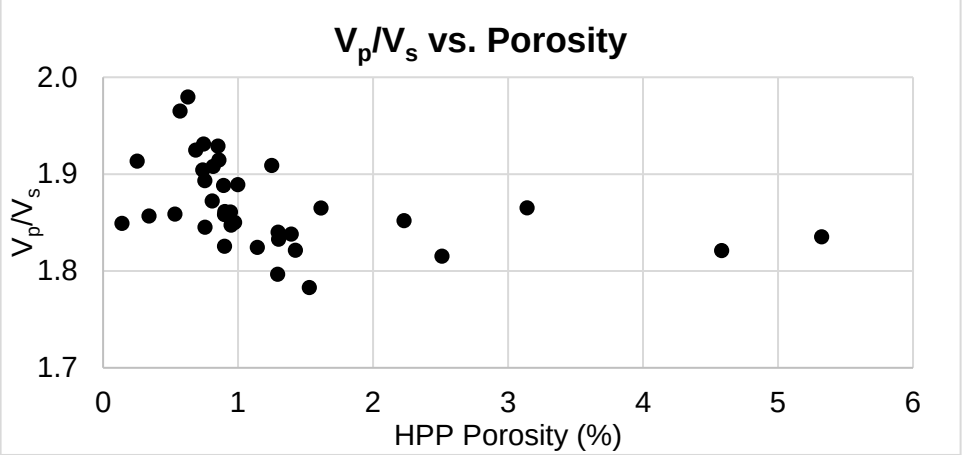

Figure 6-29: Saturated V_p/V_s vs. porosity shows no significant dependence of V_p/V_s on porosity

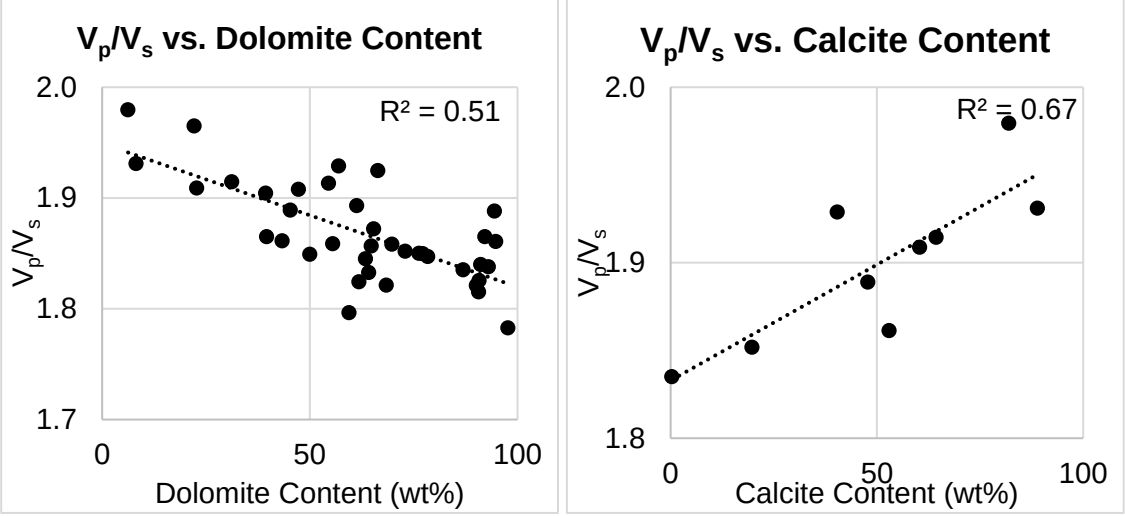

Figure 6-30: Saturated V_p/V_s vs. dolomite content (left). Saturated V_p/V_s vs. calcite content (right). Both show good relationship

Compressional Velocity and Tight Carbonate Petrography

Several studies show that acoustic velocity in carbonates is mainly controlled by porosity, or more precisely, by the pore geometry (Gomez et al., 2007; Eberli et al., 2003; Xu et al., 2007; Weger et al., 2009; Anselmetti and Eberli, 2012). In general, the acoustic velocity is inversely related to porosity. However, these studies show a wide range of velocities at a given porosity values that need to be explained. Classifying or quantifying the pore types worked well in reducing the uncertainty between porosity and velocity.

Weger et al., (2009) introduced a quantitative approach using digital image analysis. Several pore parameters were measured using 2-D images and were incorporated to the porosity/velocity relationship. Perimeter Over Area (PoA), Dominant Pore Size (DomSize), Aspect ratio (AR) and content of microporosity were measured using this technique. Applying these parameters reduced the uncertainty and made the porosity/velocity relationship more meaningful (Figure 6-31). Notice that the range of porosity that was used in the study is 10 to 45%.

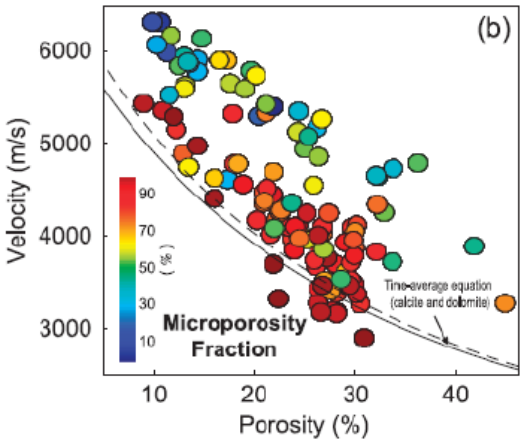

Figure 6-31: Cross plot of porosity vs. velocity. Data points color coded by content of microporosity

Kittridge (2014) after highlighting the importance of accurate mineralogy, illustrated the use of the self-consistent approximation (SCA) for better porosity/velocity relationship. In this approach, he used Xu and Payne, (2009)

self-consistence model to predict the velocity response given a predominate mineral and pore aspect ratio. In the model, the pores and grains are considered inclusions in the composite. They start with a model for the solid rock that accounts for the mixed mineralogy using Reuss-Voigt-Hill (VRH) average. Then, the pores are added to the system in an iterative process that accounts for the shape, size, and fluids in the pore. Kittridge (2014) used public domain data which was done using completely empirical approach and tried to reevaluate them using the SCA approach. His approach provided more reasonable explanation to the empirically evaluated data (Figure 6-32). This study shows how accounting for mineralogy is extremely important when dealing with carbonate rocks. Without the proper evaluation of mineralogy, estimating acoustic velocity as a function of porosity will not provide conclusive results.

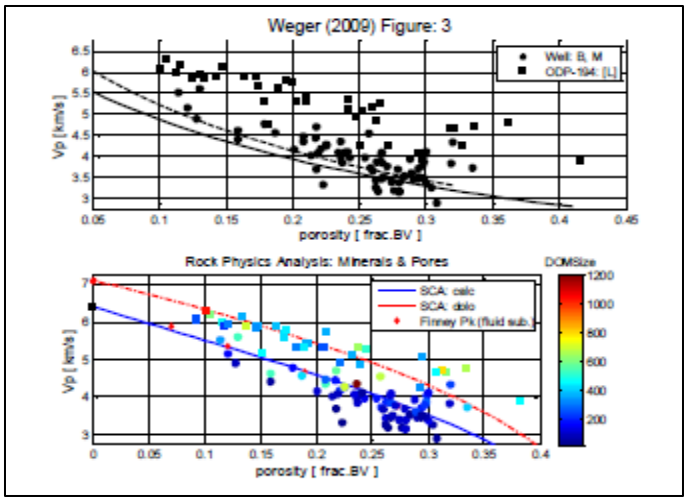

Figure 6-32: P-wave velocity vs. porosity from Weger (2009). Top figure shows empirical evaluation with no mineralogy distinction. Bottom figure shows SCA evaluation accounting for mineralogy and using single pore type.

Gomez et al., (2007) evaluated the effect of microstructure and pore fluids on carbonate samples that ranges in porosity from zero to 23%. By incorporating thin section petrographic analysis, he was able to explain the

behavior of the various velocity/porosity responses. Samples with predominant interparticle porosity shows higher pressure dependence compare to samples with predominant moldic, vuggy or intraparticle porosity (Figure 6-33). Pore compressibility in spherical pores is low, resulting in limited pressure dependence and high velocity. As the pore complexity increases, the pore compressibility increases and the velocity decreases. SEM and thin section petrographic analysis have helped in understanding the effect of pore type on acoustic velocity response.

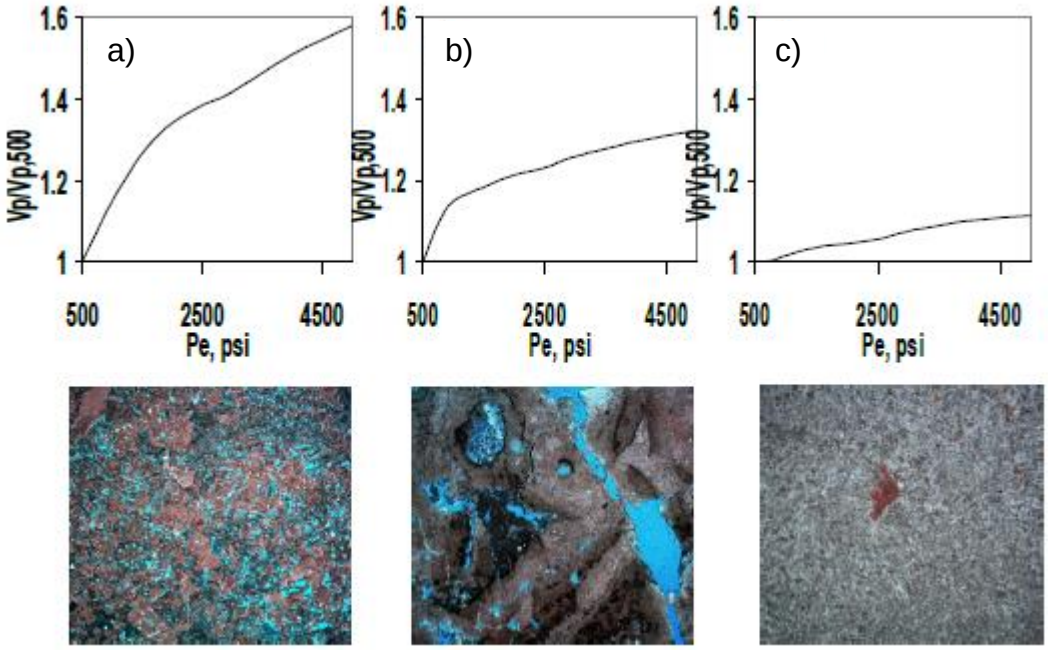

Figure 6-33: Normalized P-wave velocity vs. effective pressure for three carbonate samples, a) 8.0% interparticle, 3.6% carbonate matrix, 2.0% intrafossil, 0.7% moldic porosity, b) 3% fracture, 2.4%, carbonate matrix, 0.7% intrafossil, 0.7% vuggy, c) 6.9% intraparticle porosity.

The tight carbonate section in our study has a porosity that ranges up to 7% and it has similar mineralogy distribution. Nevertheless, the dry P-wave velocity has a wide range of values ($\Delta V_p \leq 2000$ m/s). Grain density, porosity

and petrographic analysis suggest that we are dealing with two distinctive zones (Figure 6-34). Therefore, each zone will be evaluated separately. Zone 1 has a range of mineralogy that goes from almost pure calcite to pure dolomite. Also, petrographic analysis suggests that this section is mainly finely crystalline carbonate. In Zone 1, the P-wave velocity will be investigated based on mineralogy and texture. Zone 2 has mainly dolomite mineralogy and very narrow range of porosity. This zone will help investigate the importance of thin section and petrographic analysis in addition to NMR T_2 relaxation time.

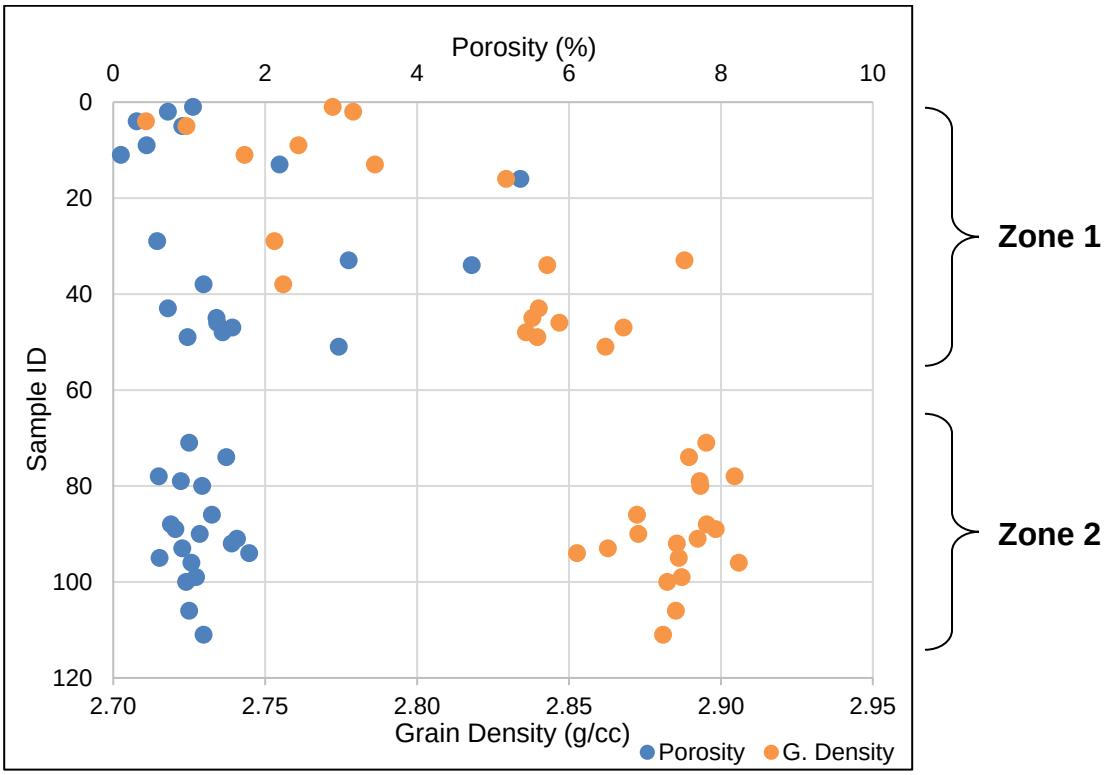

Figure 6-34: Cross plot of sample ID vs. porosity and grain density. Notice the distinctive behavior of Zone 1 and Zone 2.

Zone 1: Velocity – Porosity Relationship

Zone 1 can be divided into calcite rich and dolomite rich groups. Figure 6-35 shows a cross plot of velocity vs. porosity for this zone. Figure 6-35

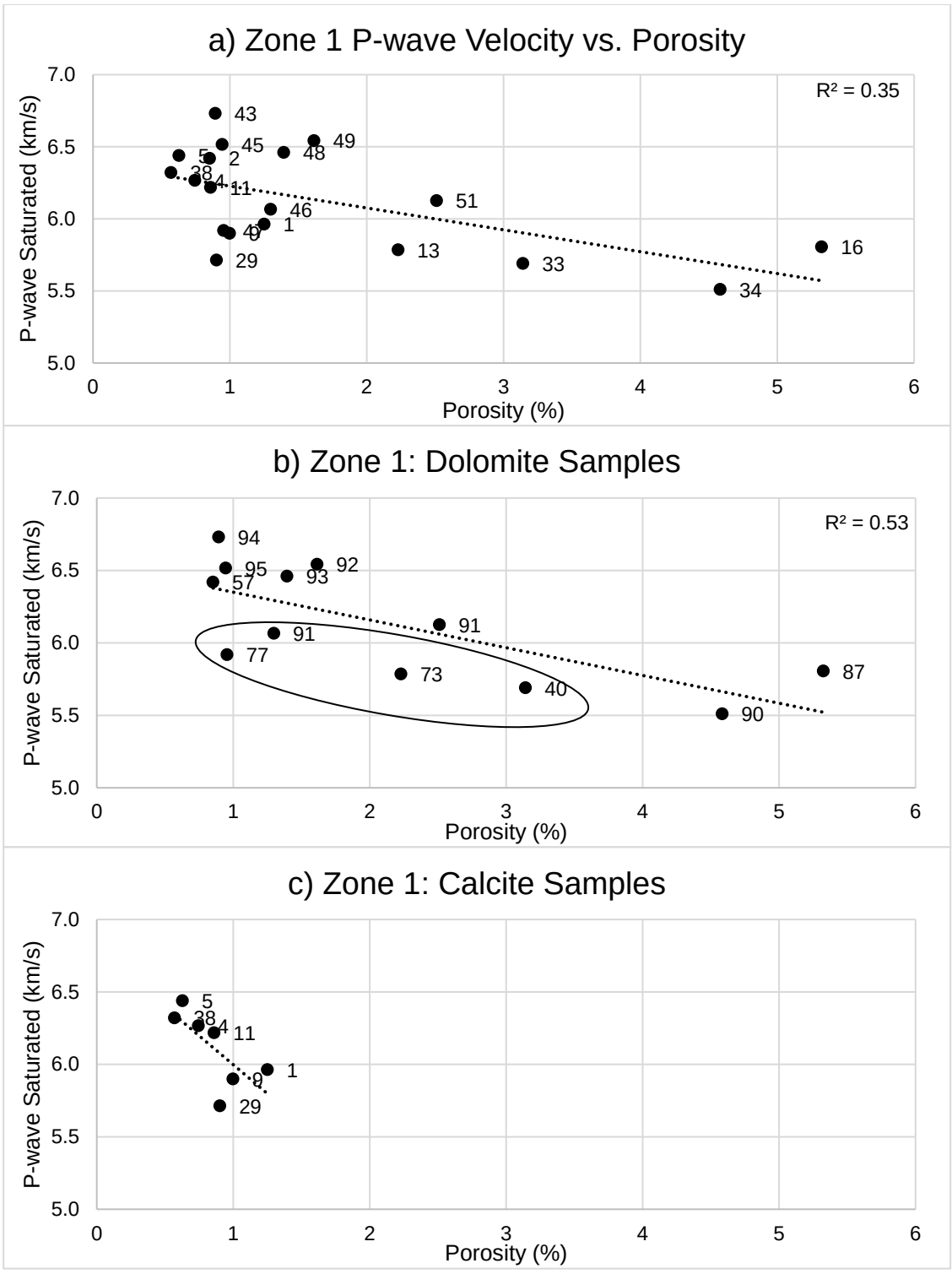

Figure 6-35: Saturated P-wave velocity vs. porosity for zone 1. (a) has no mineralogy discrimination. (b) Shows the dolomite rich samples numbered by dolomite content. (c) Shows calcite rich samples numbered by sample ID.

(a) Is a plot of all Zone 1 data points without mineralogy discrimination. The correlation in this figure is poor with R^2 of 0.35. Figure 6-35 (b) and (c) separate the data points based on their predominant mineralogy. The velocity/porosity relationship become more prominent after incorporating mineralogy.

In Figure 6-35 (B) We can notice that almost all of the dolomite rich data points are following similar trend except for the samples with low dolomite content. They show relatively lower velocity compared to the rest of the dolomite samples. Comparing these samples to the others using QEMSCAN mineralogy images shows uniform distribution of anhydrite across the samples (Figure 6-36). Anhydrite has lower velocity than dolomite. Dolomite has a velocity of 7300 m/s and anhydrite has a velocity of 5500 m/s which may explain the lower velocity in these anhydritic dolomite samples.

The calcite rich samples shown in Figure 6-35 (c) are all around 1% porosity. Yet, they show a reasonable relationship with velocity. The data points are numbered by sample ID. Figure 6-37 compares sample 4 (89% calcite) and sample 29 (53% calcite) using QEMSCAN mineralogy images. Since these two samples have similar porosity and mineralogy, velocity deviation can be explained by the difference in texture and fabric. Sample 4 appears more compacted and shows intact calcite crystals. However, sample 29 shows more separated calcite and dolomite crystals. Also, it shows possible organic lineations/fragments that was not recognized by QEMSCAN. These together could help reduces velocity compare to sample 4 fabric.

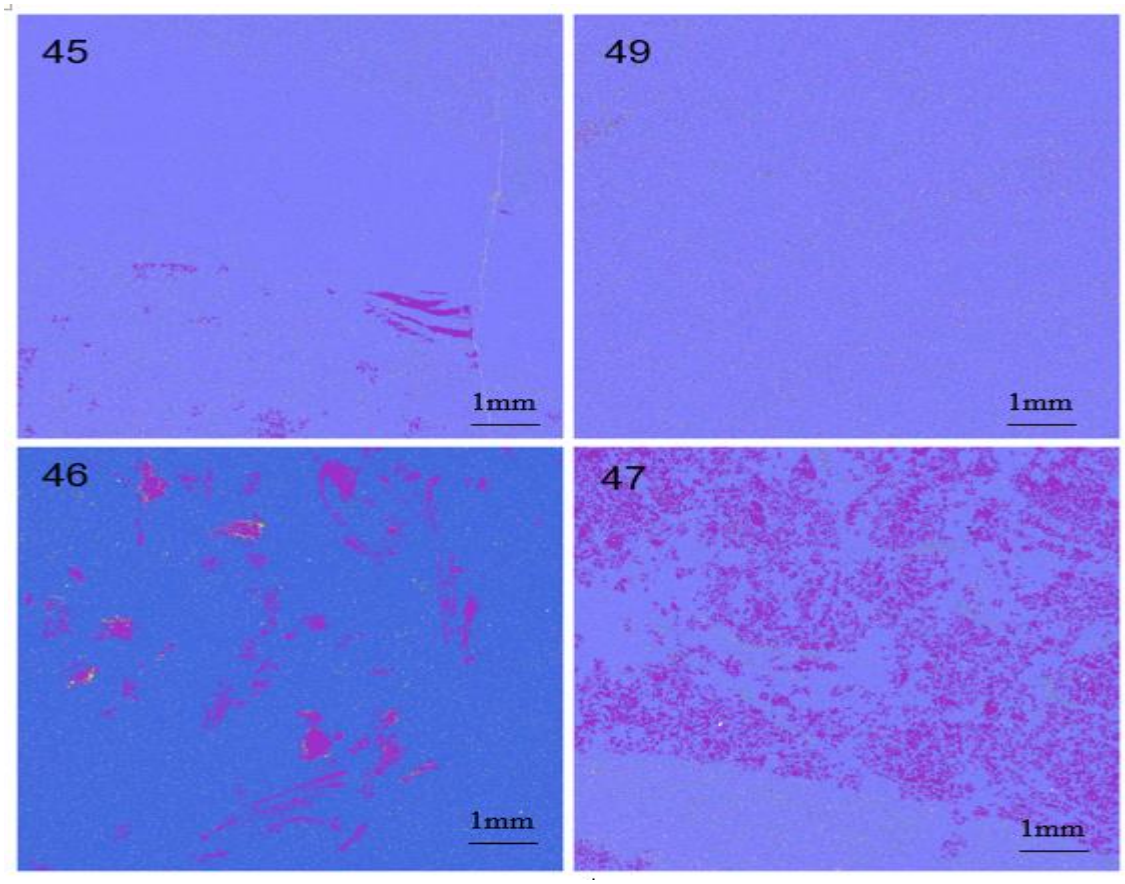

Figure 6-36: QEMSCAN mineralogy images for dolomite rich samples from Zone 1. Bottom images show uniform distribution of anhydrite. Anhydrite content: 45 (2%), 49 (4%), 46(5%), 47(20%)

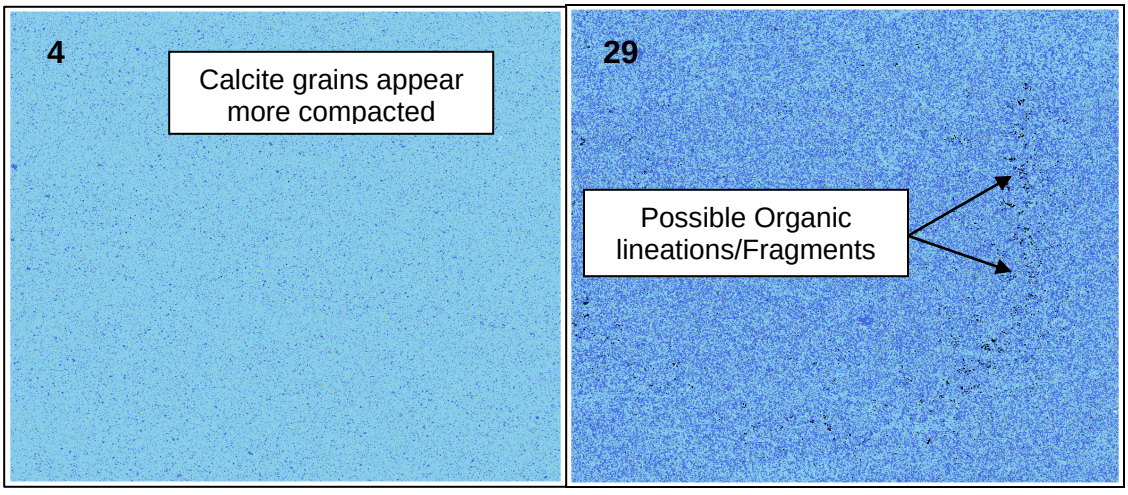

Figure 6-37: QEMSCAN mineralogy maps for two calcite rich samples. Light blue (calcite), dark blue (dolomite). Left sample has higher velocity than right sample.

Thin section petrographic analysis has been done on sample 4. This sample has a micritc finely crystalline limestone texture with minor intercrystalline pores that ranges in size between 0.5 and 2um (Figure 6-38). The calcite crystals are uniformly distributed and range in between ~10-20um. Diagenetic dolomite crystals occur as selective replacement of primary calcite background. Trace amount of pyritized organic matter can be seen within the sample. The uniform and narrow range of calcite crystals size is the main factor that increases the grain to grain contacts and, as a result, increases velocity.

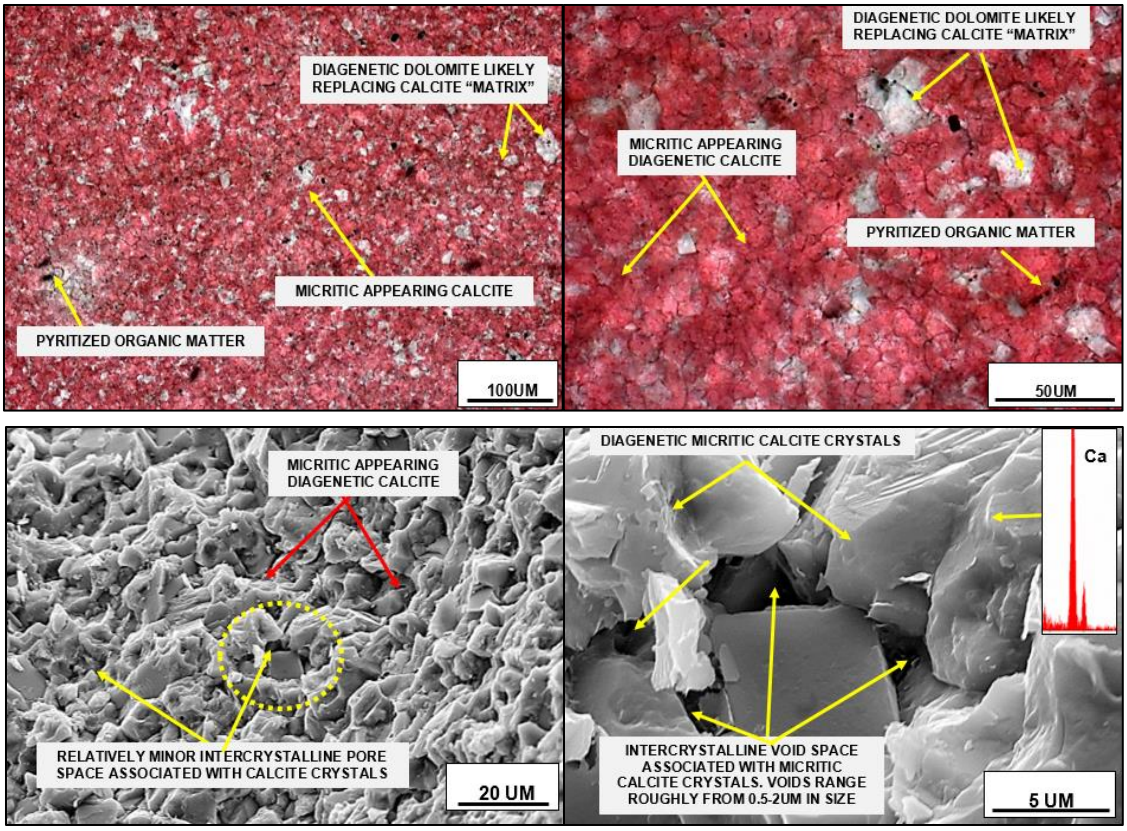

Figure 6-38: Thin section and SEM images for sample 4 showing compacted micritic calcite crystals with few intercrystalline pore space.

We have seen how incorporating mineralogy in the velocity/porosity relationship could help provide better relationship. However, if we plot velocity

as a function of mineralogy (matrix bulk modulus) alone, we do not see any significant relationship (Figure 6-39). The matrix bulk modulus was calculated using the VRH mixing law. See Table 6-4 for the standard minerals' bulk modulus that were used.

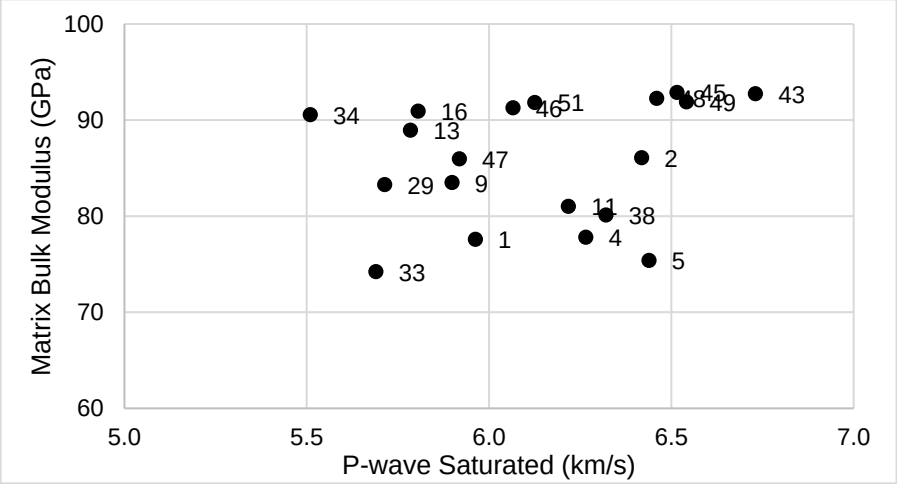

Figure 6-39: Cross plot of P-wave saturated velocity vs. matrix bulk modulus shows no significant relationship. Data points number by Sample ID.

Zone 2: Velocity – Porosity Relationship

Zone 2 has mainly dolomite and anhydrite mineralogy with narrow range of difference in composition, therefore the samples cannot be differentiated based on mineralogy. Also, the porosity of the section does not exceed 1.6%. Yet, the porosity/velocity relationship still gives a reasonable correlation with small deviation (Figure 6-40) if we exclude samples (71, 93, 85). These three samples show velocity lower than the overall trend of the samples. NMR data and petrographic analysis will be used to investigate their behavior.

Comparing samples (71, 93, 95) to the rest of the samples using their NMR T_2 responses show that they have single pore systems with similar pore size (Figure 6-41). All the remaining samples show wider range of pore sizes and sometimes with two or more pore systems. We can see how NMR T_2 relaxation response can be utilized to differentiate samples even at very narrow range of porosity and mineralogy.

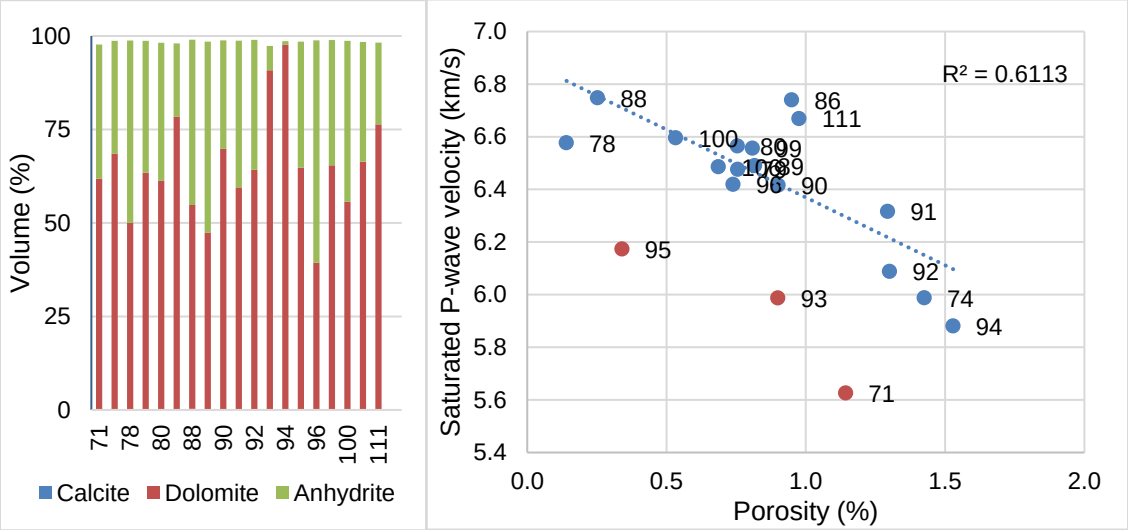

Figure 6-40: Left- Mineralogy data for Zone 2 (QEMSCAN). Right- saturated P-wave velocity vs. porosity for the same zone.

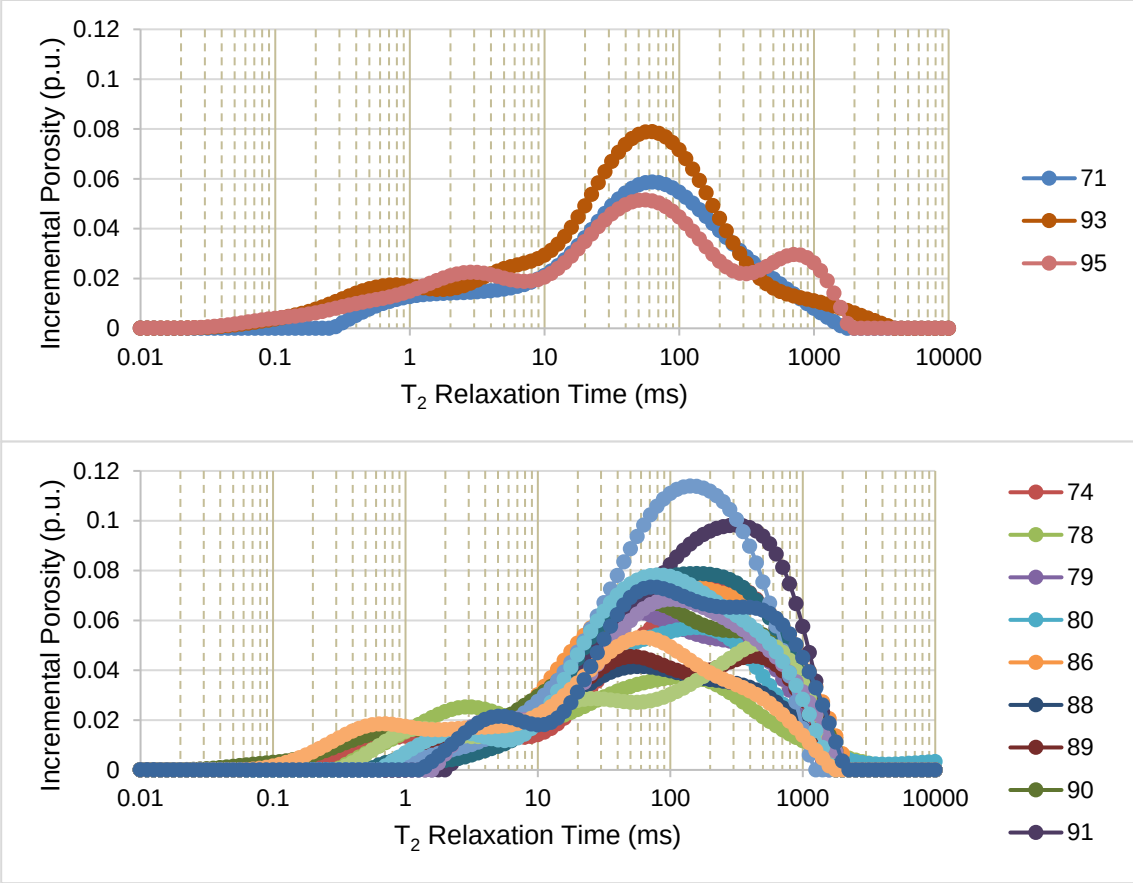

Figure 6-41: NMR T_2 relaxation time response for Zone 2 samples. Top- shows samples 71,93,95 (low velocity). Bottom- shows the rest of the samples.

The petrographic analysis of samples from Zone 2 suggests that all pores are within 1-2 micrometer in size. However, sample 71 has been analyzed with poor sorting and a wider range of grain size (0.1-4.9mm) compare to the rest of the samples. This texture reduces the grain to grain contact which will result in lower velocity response (Khazanehdari and Sothcott, 2003). In addition, possible linear porosity exists between anhydrite cleavage planes (Figure 6-42).

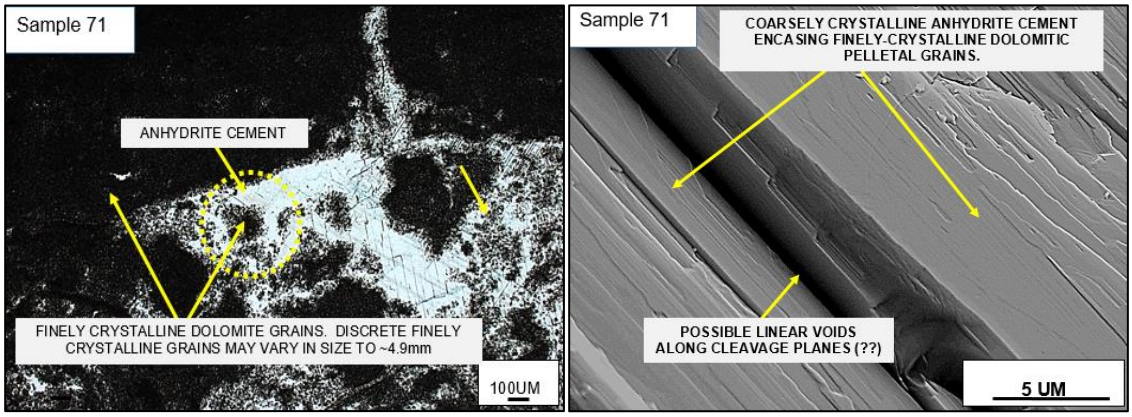

Figure 6-42: Thin section images for sample 71 (low velocity) showing wide range of grain sizes with poor sorting. Possible linear voids may exist between cleavage planes.

Sample 95 has been analyzed with moderate range of grain size (0.15-2.6mm). In addition, transgranular fractures are present and healed with anhydrite/dolomite cement and trace amount of organic material. Sorting and presence of fractures are more likely the main two reasons behind the lower velocity response in this sample (Figure 6-43).

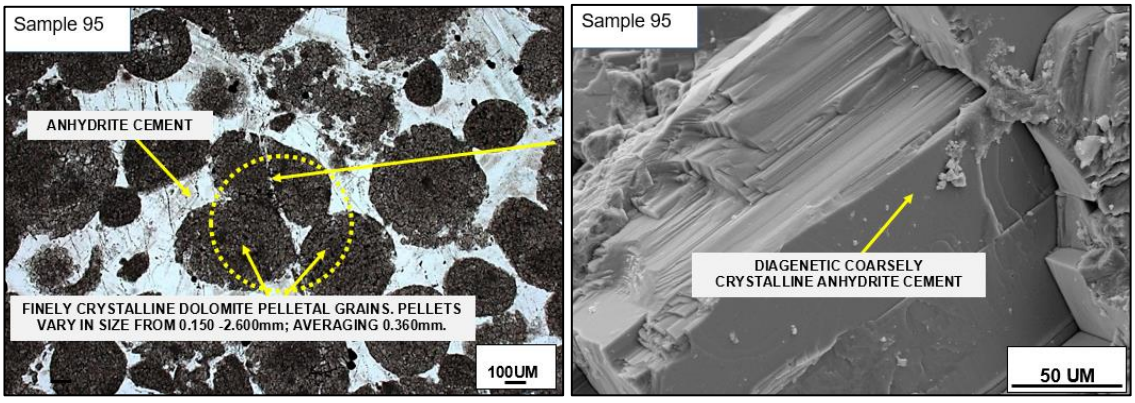

Figure 6-43: Thin section images for sample 95 (low velocity) showing moderate range of grain sizes with fractures. Possible linear voids may exist between cleavage planes.

Sample 111 shows a high velocity response compare to the rest of the samples within the zone. It has been analyzed with a narrow range of grain size (0.2-1.0mm) and good sorting in addition to significant mechanical/chemical compaction texture (Figure 6-44). Sorting and compaction increases the grain to grain contact and as a result, the velocity response increases.

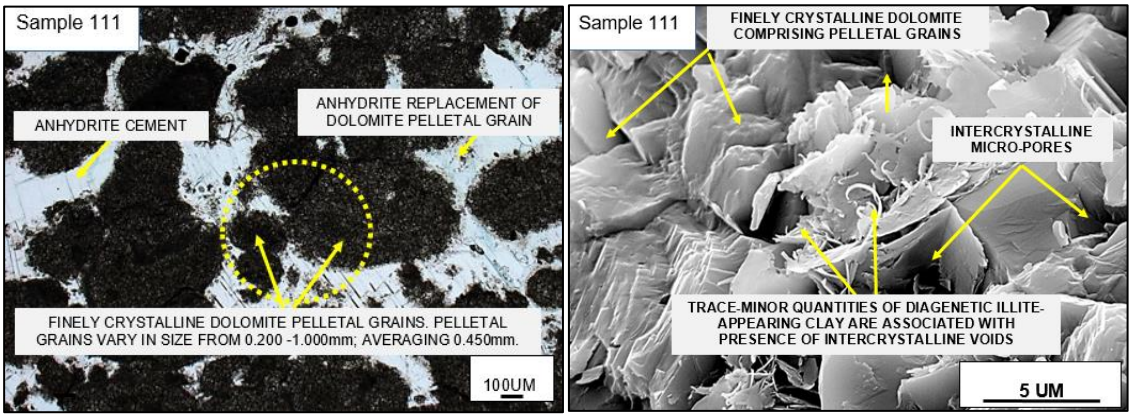

Figure 6-44: Thin section images for sample 111 (high velocity) highly compacted with narrow range of grain sizes.

We can notice how discriminating the data based on their predominant mineralogy give a better representation of the velocity/porosity relationship. In addition, NMR T_2 relaxation time can help discriminate the data based on their pore size or pore system. When dealing with tight carbonate samples that have very low porosity and limited mineralogy difference, their velocity response can be explained using petrographic analysis, and/or QEMSCAN images.

Predicting Bulk Modulus – Biot-Gassmann

Several theoretical models are available in the literature that tries to relate acoustic velocity to porosity. Wyllie et al., (1958) proposed a linear relationship between the porosity and the interval transit time (slowness) of the compressional velocity. His theory suggests that the total transit time of the formation should be equal to the sum of the transit time of the fluid filled pores and the transit time of the grains. However, such theory cannot be justified theoretically especially if we are dealing with complex heterogeneous rocks like carbonate. Individual pores and grains are usually very small which requires very small wavelength to account for them separately. In addition, these pores and grains must be arranged as layers perpendicular to the ray path (Mavko et al., 2009). Therefore, such rock physics model must be avoided since it does not realistically explain the wave propagation in the rock.

Gassmann (1951) studied the elastic waves in porous media. This is a medium of differential elasticity that consist of solid frame (matrix) and pore space filled with fluids (porosity). Velocity can be calculated based on the elasticity theory using elastic moduli. The elastic moduli are basically material properties that relate stress and strain. Based on his theory and under a set of assumptions, the elastic moduli of the porous medium can be calculated from porosity and the moduli of solid material, porous frame and fluids. This theory allowed for the calculation of the velocity of both the elastic longitudinal and transverse waves under both dry and saturated conditions.

Biot (1956) studied the propagation of waves in porous media and introduced the consolidation factor (n) that relate the dry frame bulk modulus (K_{Dry}) to the matrix or grain modulus (K_g). Combining the findings of Gassmann (1951) and Biot (1956) helped developed the Biot-Gassmann Equation that currently used in many rock models applications. It enables us to calculate the change in effective bulk modulus when porosity, fluids or mineralogy are varied.

The Biot-Gassmann equation helped model the seismic response in any porous rock. Many seismic related techniques are derived based on this equation including 4D seismic and AVO attributes. Time-labs (4D) seismic are widely used in reservoir monitoring to model dynamic changes in the reservoir properties like saturation and fluids. Amplitude versus Offset (AVO) is used mainly for exploration and reservoir delineation. It has the ability to detect fluids by relying heavily on the S-wave velocity (Kittridge, 2014).

The Biot-Gassmann theory will work as long as the assumptions behind its derivation are not violated:

1. Large enough sample to represent the parent material
2. Homogeneous rock
3. Isotropic rock
4. Rock with connected pores
5. Slow deformation to allow for pore pressure equilibration
6. No chemical interaction between the rock and the fluid

When one or more of the assumptions above are violated, the equation will more likely fail and produce inaccurate results.

$$K_e = K_{dry} + \frac{K_f n^2}{\left[\phi + \frac{K_f}{K_g}\left(n - \phi\right)\right]}$$

K_e: Effective saturated bulk modulus
K_{dry}: Dry porous frame bulk modulus
K_f: Fluids bulk modulus
K_g: Matrix bulk modulus
n: Biot constant ($1-K_{dry}/K_g$)

Biot-Gassmann Equation

In our calculations of the effective bulk modulus using the Biot-Gassmann equation we used standard mineral's and fluid bulk moduli. The matrix or grain bulk modulus (K_g) was calculated as a VRH average using the QEMSCAN mineralogy concentrations and standard mineral's bulk moduli (Table 6-4). The fluid bulk modulus was used as 1.352 GPa (dodecane). The dry porous frame modulus (K_{Dry}) was derived from the dry velocity measurements at 5000 psi and the dry bulk density. Using the connected (HPP) porosity, Figure 6-45 shows the estimated and measured effective bulk moduli. The difference between the calculated and the measured moduli has an average of 7.2 GPa. The model underestimates the values by an average of 11.4%. Similar results were found by Gomez et al., (2007). They used carbonate samples with porosity range of 0-23% and most of the samples were below 12% porosity. Using the Biot-Gassmann model with brine and mineral spirits saturation, the predicted saturated bulk modulus was underestimiated. At the same time, the saturated shear modulus was higher than the dry shear modulus (Figure 6-46).

Table 6-4: Summary of Standard Minerals Bulk Moduli (Mavko et al., 2009)

Mineral	Bulk Modulus (GPa)	Mineral	Bulk Modulus (GPa)
Calcite	76.8	**Dolomite**	94.9
Anhydrite	62.1	**Quartz**	37.9
Pyrite	147.4		

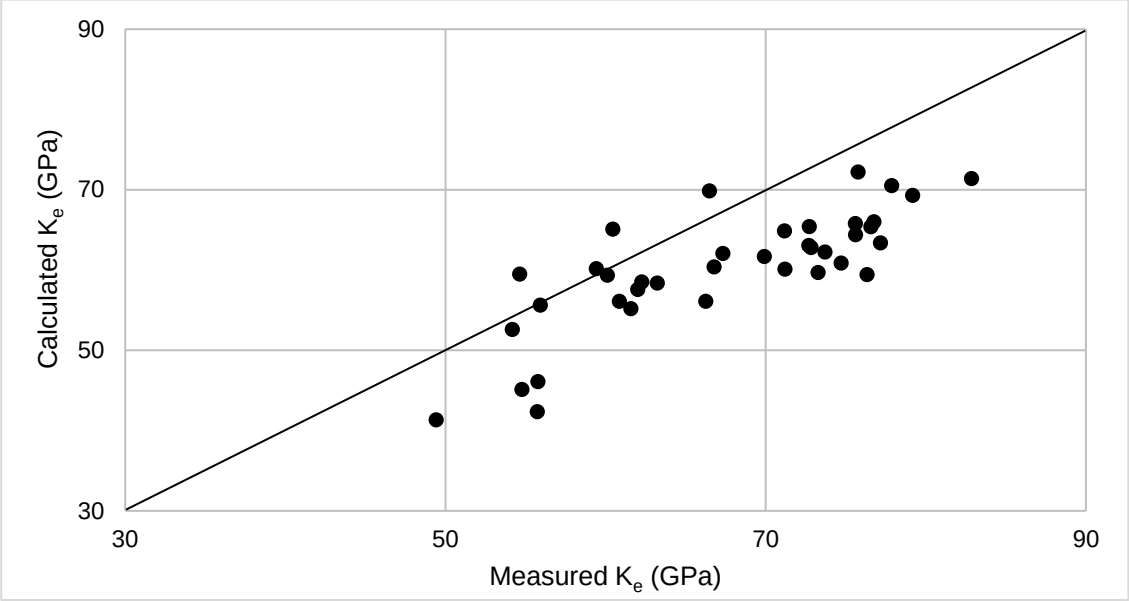

Figure 6-45: Cross plot of the measured vs. calculated K_e (Biot-Gassmann) using the connected (HPP) porosity. Black line: 1to1 line

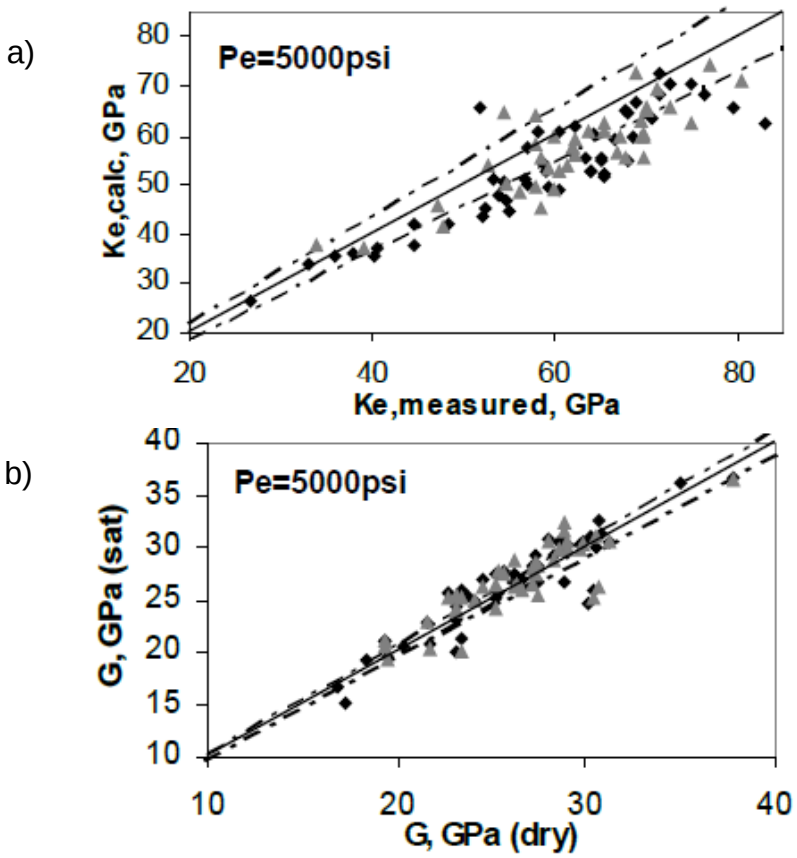

Figure 6-46: (a) Calculated bulk modulus (Biot-Gassmann) vs. measured using brine (triangles) and mineral spirits saturation (rectangles). Dashed lines are the 9% estimated error. (b) Saturated vs. dry shear modulus. Dashed lines are the 2.5% estimated error (Gomez et al., 2007).

Looking back at the assumptions behind the derivation of the Biot-Gassmann equation and our data, we find the following:

- **Isotropic:** the acquired perpendicular shear velocities (V_{s1}, V_{s2}) suggest that we are dealing with isotropic medium (Figure 6-21).
- **Connectivity of pores:** NMR and helium (HPP) porosities gave different results suggesting the presence of isolated or occluded pores in the medium (See detailed discussion in the porosity section).

- **No Interaction between rock and fluid:** Carbonates are usually sensitive to dissolution effect when saturated with water. Bhagat et al., (2012) studied three different saturation fluids in carbonates. Brine and dodecane have been found to minimize the dissolution and rock-fluid interaction. Saturating our samples with dodecane assures that there will be no rock-fluid interaction. The variables that could result in the deviation in the G_{dry} vs. $G_{saturated}$ are now reduced to pore connectivity and sufficient time for pore pressure equilibrium.

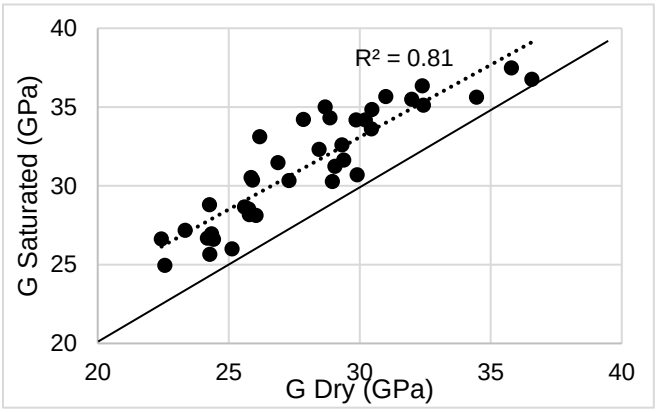

Figure 6-47: Cross plot of the dry and saturated shear moduli. Black line: 1 to 1 line

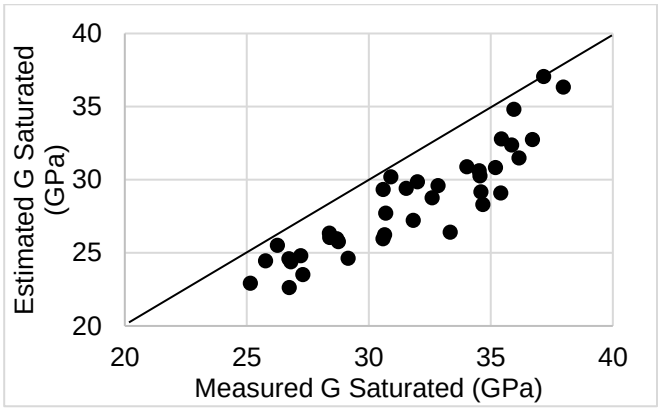

Figure 6-48: Cross plot of the estimated vs. measured saturated shear moduli. Black line: 1 to 1 line

- **Pore pressure equilibrium:** At ultrasonic velocity, complicated pores require longer time for the induced pore pressure to equilibrate. If the deformation is not slow enough, it will result in velocity dispersion. This is more likely the reason behind the deviation in the shear modulus dry vs. saturated (Figure 6-47). Under dry conditions, the pores are filled with compressible fluids (gas/air). If compressible fluids are in the pores, the measured moduli will be free of dispersion. Therefore, the estimated saturated shear modulus from the dry shear modulus is expected to be free of dispersion. Plotting of the measured vs. calculated saturated shear modulus shows that the measured values are always higher than the calculated values (Figure 6-48). This confirms the possibility of having velocity dispersion in association with the measured moduli.

Effect of Fluid Saturation on Rock Shear Modulus

Several studies suggest that rocks follow Biot-Gassmann theory where the dry and the saturated shear modulus remain constant (Krief et al., 1990; Gomez et al., 2007). However, other studies have noticed that is not always true especially in carbonates (Baechle et al., 2009; Kittridge, 2014). In general, they have found that samples with interparticle and intercrystalline porosity show shear strengthening (increase in G with saturation). While samples that are dominated by grainstone with microporosity show shear weakening.

Frequency dispersion has been related to shear stiffness. Generally, velocity dispersion is observed as an increase of velocity (elastic moduli) with

frequency. During ultrasonic velocity measurements and the presence of very small pores, the induced local pore pressure that results from the acoustic waves propagation will not have sufficient time to equilibrate. The unrelaxed fluids in these small pores cause an increase in the rock stiffness (Khazanehdari and Sothcott, 2003). The average pore size that was measured in our samples was around 2 micrometers. This very small size of pores increases the effect of velocity dispersion.

Grain to grain contact is the main factor that control rock stiffness. As we increase the grain to grain contact, the rock becomes stiffer. In sandstone, it was reported that with saturation the shear modulus tends to increase as a result of clay expansion which ultimately increases the grain to grain contact (Khazanehdari and Sothcott, 2003). At ultrasonic velocity and because of the size of the pores in the study section, the shear wave doesn't have enough time to equilibrate which results in high shear modulus.

In summary, the velocity dispersion and the type and size of pores could have a big effect on the rock stiffness and the shear modulus. It was noticed that the increase in the shear modulus with saturation causes an overall under prediction of velocity using Biot-Gassmann equation. Figure 6-49 shows the behavior of two rocks in terms of shear modulus change with saturation and the predicated Gassmann velocity. Sample A shows shear strengthening and it is characterized as recrystallized limestone with high grain to grain contacts and small pores. On the other hand, sample E shows shear weakening and it is

characterized as grainstone-packstone with bigger pores and only points contacts between grains.

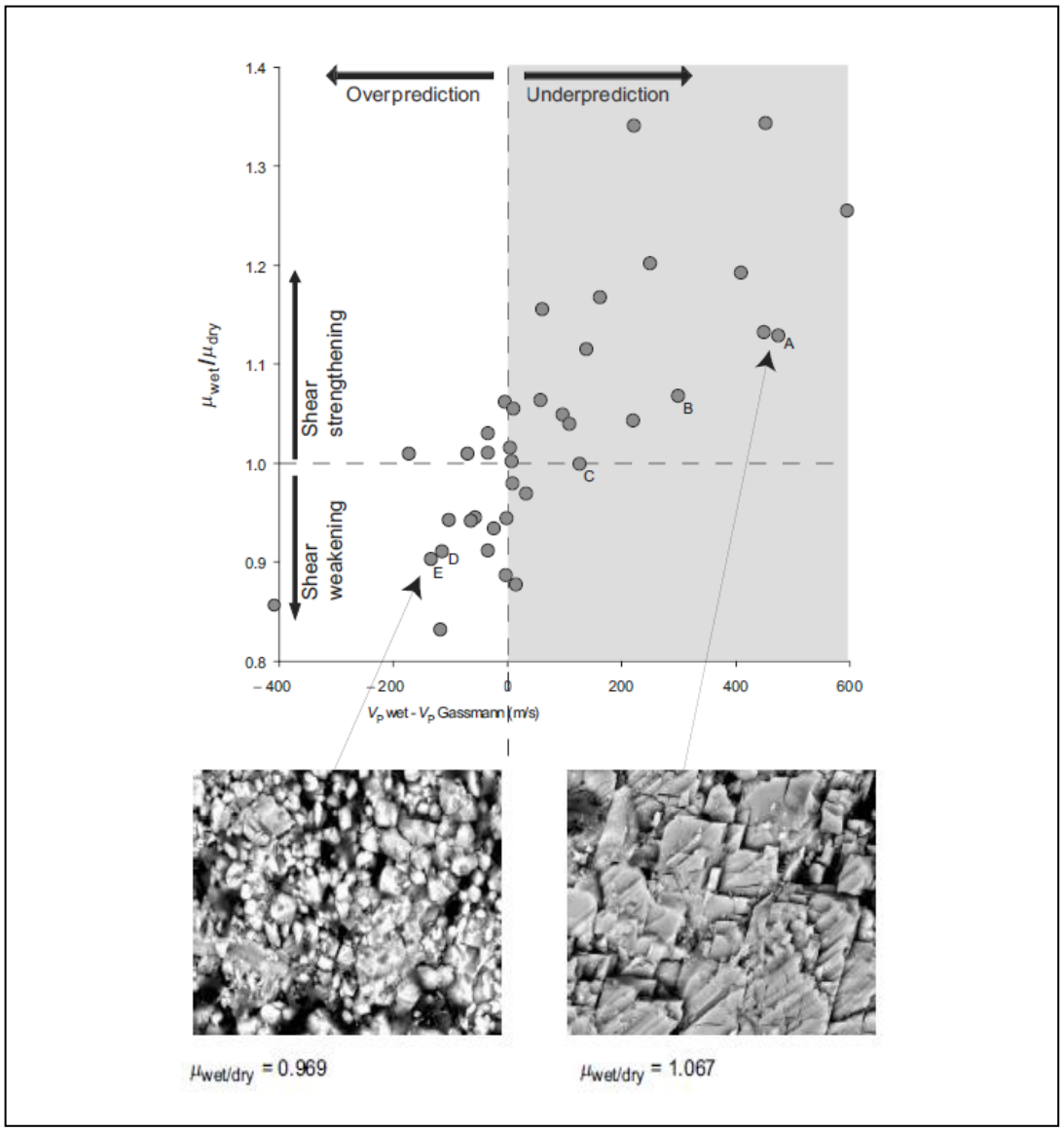

Figure 6-49: Plot of G_{sat}/G_{dry} vs. Vp_{sat}-Vp_{Cal} showing the relationship between shear weakening and strengthening on the predicted Vp by Gassmann. Below: two SEM images showing poor grain contact and big pores on left and excellent grains contacts on the right with small pores (Baechle et al., 2009).

SEM thin sections and petrographic analysis for our samples suggest that we are dealing with mainly tight recrystallized dolomite section with very small pores around 2 um in size (Figure 6-50). Therefore, velocity dispersion at ultrasonic frequency is expected to give higher shear modulus with saturation.

Baechle et al. (2009) shows that the predicted velocity of rocks with higher G_{sat} compared to G_{dry} give underestimated values using Biot-Gassmann model. While the rocks with weakening effect ($G_{sat} < G_{dry}$) give overestimated values using the model. Our samples are showing strengthening effect and it is more likely the reason behind the underestimation of the P-wave velocity using the model (Figure 6-51).

The use of Biot-Gassmann theory in such tight carbonate formation might not provide accurate prediction because of their complicated microstructure. The pores are not completely connected and the type of texture and size of pores will give dispersion effect. As a result, both the S- and P-wave measured velocities were higher than the estimated velocities (Figure 6-51 and Figure 6-52). At 5000psi differential pressure, the calculated velocity dispersion has a range of 1-12% and 0.2-12% for P- and S-wave velocities respectively (Figure 6-53). At seismic frequency, Biot-Gassmann can be used to predict the seismic velocities since the pore pressure can equilibrate. However, depending on the rock type, at ultrasonic velocity the induced pore pressure doesn't always equilibrate and it produces dispersion effect.

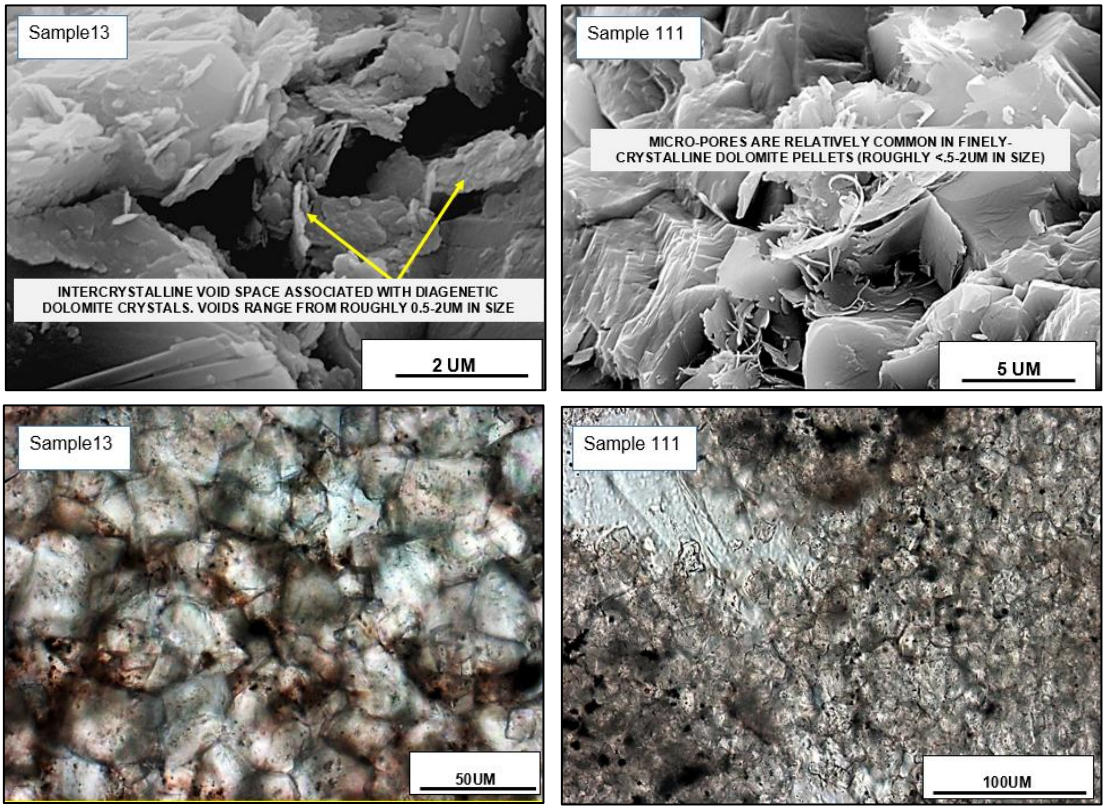

Figure 6-50: Thin section images of two samples (13 ,111) illustrating the type of grain to grain contact and the size of pores that we observe across the section

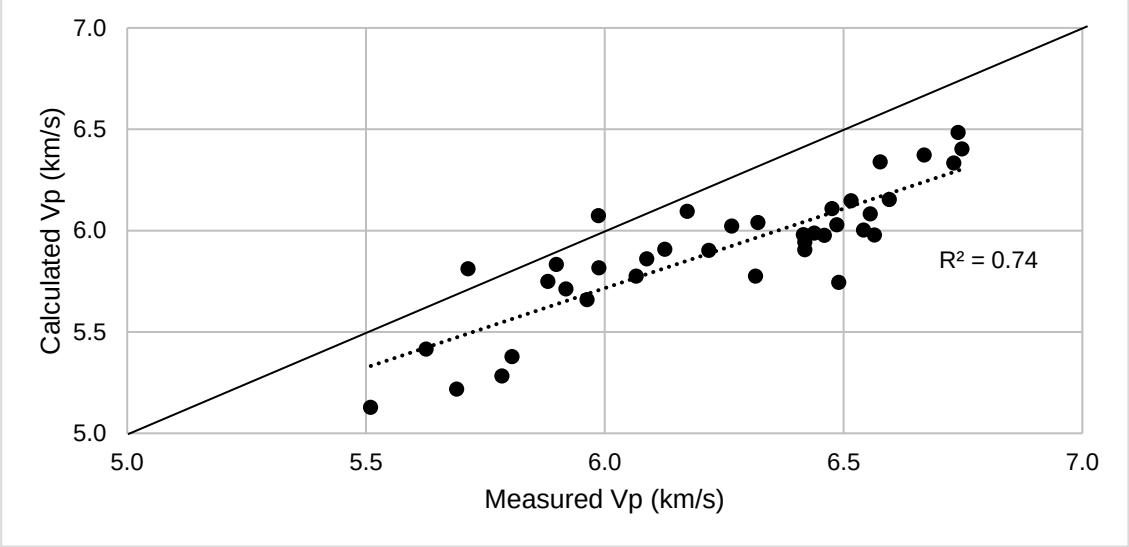

Figure 6-51: Cross plot of calculated P-wave vs. measured P-wave at 5000 psi using Biot-Gassmann. Black line: 1 to 1 line.

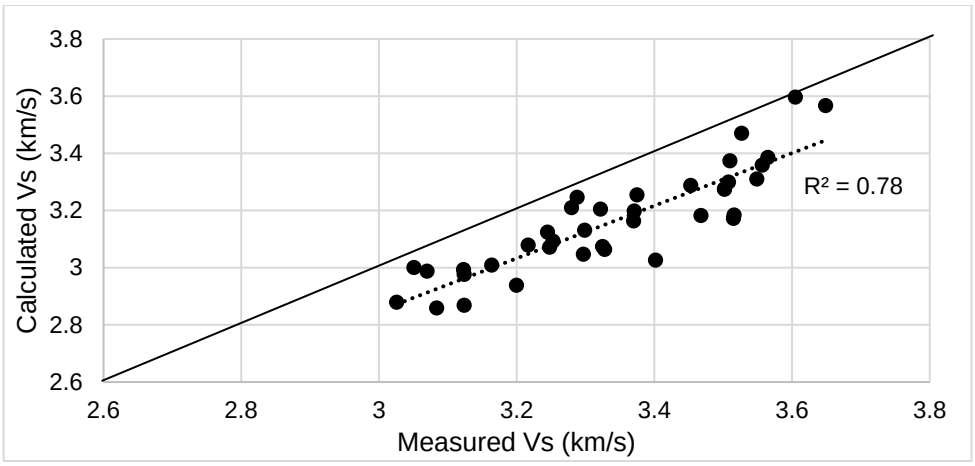

Figure 6-52: Cross plot of calculated S-wave vs. measured S-wave at 5000 psi using Biot-Gassmann. Black line: 1 to 1 line.

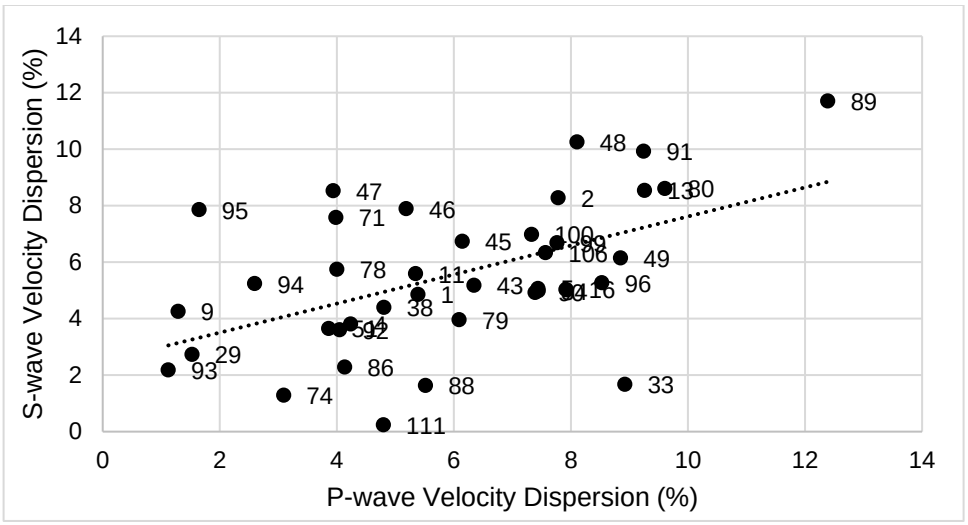

Figure 6-53: Cross plot showing the range of velocity dispersion in the P- and S-wave velocities at 5000psi.

Depending on the rock type and the microstructure, the present results indicate that velocity dispersion may occur at high frequencies in saturated rocks. Dry rocks are always dispersion free. Therefore, additional detailed analysis maybe useful in order to understand the dispersion behavior as a function of frequency.

Chapter 7: Conclusion

In this study, we have examined a low porosity section from the Khuff-C carbonates in Saudi Arabia. Several petrophysical properties have been measured in order to investigate their effect on acoustic velocity in the given narrow range of porosity. Using these various lab-based petrophysics and rock physics measurements, we developed the following results:

- The section has both connected and occluded porosities. The average connected porosity is 1.5%. NMR data provided an average porosity of 3.0% which has been considered as the total porosity. Which suggests that the average occluded porosity is about 1.5%.
- The NMR predicted pore sizes were in agreement with measured range of pore sizes using SEM images. Petrographic thin section analysis can be used to calibrate/support NMR pore size calculation.
- The LPP (crushed sample) grain density measurements were consistently higher than the HPP (whole plug) grain density. It was interpreted as the result of opening the occluded pores and drying out the fluids inside them. This difference in density support the presence of occluded pores and explained the higher porosities that were measured by NMR.
- The QEMSCAN and FTIR quantification mineralogy in this carbonate formation provided consistent results despite some minor differences. Both techniques were in good agreement for the major minerals.

However, FTIR was able to detect small fractions of illite and siderite up to 10 wt% which were missed by QEMSCAN.

- Excellent separation has been seen between the dry and the saturated V_p/V_s ratios. This ratio could be used to differentiate between dry/gas saturated rocks and fluids saturated rocks. In addition, it could be used to detect overpressure zones which usually result in reducing the reservoir overall differential pressure.
- Despite the low porosity and the limited change in mineralogy within the section, the velocity response was evaluated systematically using NMR and petrographic analysis. It revealed that the microstructure greatly controls the acoustic velocity response and it can explain the deviation in the velocity/porosity relationship.
- Due to the complicated microstructure that leads to dispersion effect at ultrasonic velocity, the Biot-Gassmann rock physics model will not provide accurate estimations. Both P- and S-wave velocities were underestimated using the model. At 5000psi differential pressure, the calculated velocity dispersion was up to 12% in both P- and S-wave velocity.

References

Al-Jallal, I.A. 1987. "Diagenetic Effects on Reservoir Properties of the Permian Khuff Formation in Eastern Saudi Arabia." *SPE-15745.* Manama, Bahrain.

Anselmetti, flavio, and Gregor Eberli. 2012. "Sonic Velocity in Carbonates-A Combined Product of Depositional Lithology and Diagenetic Alterations." Society for Sedimentary Geology.

Ardila, J., and E.A. Clerke. 2014. "Khuff C Carbonate Mineralogy Data at Multiple Sample Scales." *SPWLA 55th Annual Logging Symposium.* Abu Dhabi, UAE.

Ayling, Bridget, Peter Rose, Susan Petty, Ezra Zemach, and Peter Drakos. 2012. "QEMSCAN (Quantitative Evaluation of Minerals by Scanning Electron Microscopy): Capability and Application to Fracture Characterization in Geothermal System." *37th Workshop on Geothermal Reservoir Engineering.* Stanford, California: SGP-TR-194.

Baechle, Gregor T., Gregor P. Eberli, Ralf J. Weger, and Jose Luis Massaferro. 2009. "Changes in Dynamic Shear Moduli of Carbonate Rocks with Fluid Substitution." *GEOPHYSICS*, 135-147.

Ballard, Bryce D. 2007. "Quantitative Mineralogy of Reservoir Rocks Using Fourier Transform Infrared Spectroscopy." Anaheim, California: SPE 113023.

Bhagat, Anita, Carl H. Sondergeld, and Chandra S. Rai. 2012. "The Petrophysical Study on UAE Carbonates." Las Vegas, Nevada: SEG.

Bocangel, Wara, Carl Sondergeld, and Chandra Rai. 2013. "Acoustic Mapping and Characterization of Organic Matter in Shales." New Orleans, Louisiana: Society of Petroleum Engineers.

Chang, Dahai, Harold Vinegar, Chris Morriss, and Charis Straley. 1994. "Effective Porosity, Prodcuible Fluid and Permeability in Carbonates from NMR logging." SPWLA.

Clerke, E. A. 2009. "Electrofacies and Geological Facies for Petrphysical Rock Typing: Khuff C." Alkhoobar, Saudi Arabia: SPE Technical Symposium and Exhibition.

Dang, Son Thai. 2013. "Study of Kerogen Maturity using Transmission Fourier Transform Infrared Spectroscopy (FTIR) ." *SPE Annual Technical Conference and Exhibition.* New Orleans, Louisiana.

Eberli, G., G. Baechle, F. Anselmetti, and M. IncZe. 2003. "Factors Controlling Elastic Properties in Carbonate Sediments and Rocks." *The Leading Edge*, 22.7 ed.

Ehrenberg, S. N., P. H. Nadeau, and A. A. Aqrawi. 2007. "A Comparison of Khuff and Arab Reservoir Potential Throughout the Middle East." *AAPG Bulletin* 91 (3): 275-286.

Fathalla, M. 1985. "Khuff Development: Overview." Bahrain: SPE 13677.

Fuller, Brian N., William Iverson, and Scott B. Smithso. 1989. "AVO for Thin Sand Bed Detection ." SEG.

Goergen, E. T., M. E. Curtis, J. Jernigen, C. Sondergeld, and C. Rai. 2014. "Integrated Petrophysical Properties and Multi-Scaled SEM Microstructural Characterization." *Society of Petroleum Engineers.* Denver, Colorado.

Gomez, Juan P., Chandra S. Rai, and Carl H. Sondergeld. 2007. "Effect of Microstructure and Pore Fluid on the Elastic Properties of Carbonates." San Antonio: SEG Annual Meeting.

Gottlieb, P., G. Wilkie, D. Sutherland, E. Ho-Tun, S. Suthers, K. Perera, B. Jenkins, S. Spencer, A. Butcher, and J. Rayner. 2000. "Using Quantitative Electron Microscopy for Process Mineralogy Applications." (JOM, Journal of Minerals, Metals and Materials Society) 52, Number 4, Page 24.

Gunter, G., D. Spain, E. Viro, J. Thomas, G. Potter, and J. Williams. 2014. "Winland Pore Throat Prediction Method - A proper Retrospect: New Examples from Carbonates and Complex Systems." Abu Dhabi, UAE: SPWLA.

Kenyon, W. E. 1992. "Nuclear Magnetic Resonance as a Petrophysical Measurement." *Nucl. Geophys.* 6: 153-171.

Khazanehdari, J, and Jeremy Sothcott. 2003. "Variation in Dynamic Elastic Shear Modulus of Sandstone upon Fluid Saturation and Substitution." *GEOPHYSICS* 68 (2): 472-481.

Kittridge, Mark G. 2014. "Investigating the Influence of Mineralogy and Pore Shape on the Velocity of Carbonate Rocks: Insights from Extant Global Data Sets." *SPWLA 55th Annual Logging Symposium.* Abu Dhabi.

Krief, M., J. Garat, J. Stellingwertff, and J. Ventre. 1990. "A Petrophysical Interpretation Using the Velocities of P and S waves (Full-Waveform Sonic)." Paris, France: SPWLA.

MacDonald, Robin, David Kersey, Tianhua Zhang, Mahmood Akbar, and Wail Mousa. 2009. "Effect of Carbonate Hetrogeneity on Core - Log Intergration." Kuwait, Kuwait: SPE 127290.

Mavko, Gary, Tapan Mukerji, and Jack Dvorkin. 2009. *The Rock Physics Handbook.* 2nd. Cambridge University.

Powers, R. W., L. F. Ramirez, C. D. Redmond, and E. L. Elberg. 1963. *Geology of the Arabian Peninsula: Sedimentary Geology of Saudi Arabia.* Washington: U.S. Geological Survey.

Rafavich, F., C. Kendall, and T. Todd. 1984. "The Relationship between Acoustic Properties and the Petrographic Character of Carbonate Rocks." *Geophysics* 49 (10): 1622-1636.

Raymer, L., E. Hunt, and J. Gardner. 1980. "An Improved Sonic Transit Time-To-Porosity Transform." *SPWLA 21st Annual Logging Symposium.*

Rojas, E., T. Davis, M. Batzle, Manika Prasad, and Reinaldo Michelena. 2005. "Vp-Vs Ratio Sensitivity to Pressure, Fluid, and Lithology Changes in Tight Gas Sandstones." Houston, Tx: SEG.

Ruessink, B. H., and D. G. Harville. 1992. "Quantitative Analysis of Bulk Mineralogy: The Applicability and Performance of XRD and FTIR." *Society of Petroleum Engineers.* Lafayette, Louisiana.

Sayers, Colin M. 2008. "Th Elastic Properties of Carbonates." *The Leading Edge*, August: 1020-1024.

Siggins, A. F., and D. N. Dewhurst. 2003. "Saturation, Pore Pressure and Effective Stress from Sandstone Acoustic Properties." *Geophysical Research Letters* 30 (2).

Sondergeld, C., and C. Rai. 1993. "A New Concept in Quantitative Core Characterization." Tulsa, Ok: SEG.

Sulucarnain, Ismail, Carl Sondergel, and Chandra Rai. 2012. "An NMR Study of Shale Wettability and Effective Surface Relaxivity." Calgary, Alberta: SPE 162236.

Vanorio, Tiziana. 2006. "Vp/Vs Ratio in Gas-pressured Saturated Sandstones." New Orleans: SEG Annual Meeting.

Wampler, J., C. Sondergeld, C. Rai, and O. Abdelghany. 2010. "Estimating Permeability in UAE Carbonates using NMR." Denver, Co: SEG Annual Meeting.

Weger, Ralf J., Gregor P. Eberli, Gregor T. Baechle, Jose L. Massaferro, and Yue-Feng Sun. 2009. "Quantification of Pore Structure and its Effect on Sonic Velocity and Permeability in Carbonates." *AAPG Bulletin, V. 93 No. 10* 1297-1317.

Wood, Paul. 2013. "From Core to Pore." *GEO ExPro.*

Xu, S, and M.A. Payne. 2009. "Modeling Elastic Properties in Carbonate Rocks." *The Leading Edge* 28 (1): 66-74.

Xu, Shiyu, Ganglin Chen, Yaping Zhu, Jie Zhang, Mike Payne, Max Deffenbaugh, Limin Song, and John Dunsmuir. 2007. "Carbonate Rock Physics: Analytical Models and Validations Using Computational Approaches and Lab/Log Measurements." Dubai, UAE: International Petroleum Technology Conference.

Appendix A: Thin Section Petrographic Analysis

Eight plug samples have been evaluated using thin section and SEM images. Extensive details can be seen within these samples about the lithology, texture, pore structure and organic fragments. Below we will highlight some of the important features in each samples:

Sample 4: mainly micritic limestone with minor intercrystalline micro pores measuring roughly 0.5-2um in size. The porosity occurs mainly between individual calcite crystals. Trace amount of detrital clay material was seen attached to the pore walls. Individual calcite crystals are in the range of ~10-20um with uniform distribution. Diagenetic dolomite crystals occur as selective replacement of the original calcite matrix. Organic lineations occur and generally have been replaced by authigenic pyrite (Figure A-1).

Sample 13: Mainly finely crystalline calcareous dolostone with moderate quantities of intercrystalline micro pores measuring roughly 0.5-2um in size. The porosity occurs mainly between individual dolomite crystals. Trace amount of detrital clay material was seen attached to the pore walls in addition to trace amount of non-descriptive calcite fossil fragments. Diagenetic dolomite crystals occur as selective replacement of the original calcite matrix and range in size between ~10-40um. Subtle parallel alignment was seen accentuated by orientation of pyritized organic lineations (Figure A-2).

Sample 16: Mainly finely crystalline argillaceous dolostone with moderate quantities of intercrystalline micro pores measuring roughly 0.5-2um in size. The porosity occurs mainly between individual dolomite crystals. Detrital clay material is commonly distributed and contains absorbed organic druse on its surface. Diagenetic dolomite crystals occur as selective replacement of the original calcite matrix and range in size between ~20-40um. Subtle parallel alignment was seen accentuated by orientation of pyritized organic lineations (Figure A-3).

Sample 51: Moderately anhydritic pelletal dolostone with moderate quantities of intercrystalline micro pores measuring roughly 2-5um in size. Dolomite crystals have a size range of 10-20um. Pellet-like dolomite grains have a size range of 0.2-0.44mm. The porosity is associated with dolomite crystals within pellet-like dolomite grains. Diagenetic illite material was seen attached to the pore walls. Diagenetic anhydrite has more likely postdated that of dolomite authigenesis occurring as pore-fill cement, selective replacements of dolomite and as fracture filling. Several calcite fossil fragments appear to be dolomitized (Figure A-4).

Sample 71: Anhydritic pelletal dolostone with moderate quantities of intercrystalline micro pores measuring roughly <1-2um in size. Dolomite crystals have a size range of 10-20um. Pellet-like dolomite grains are poorly sorted with a wide range of size (0.1-4.9mm). Trace amount of diagenetic illite material was

seen attached to the pore walls. Possible linear porosity exists between anhydrite cleavage planes. Diagenetic anhydrite has more likely postdated that of dolomite authigenesis occurring as pore-fill cement, selective replacements of dolomite and as fracture filling. In several larger load-bearing pelletal grins, diagenetic anhydrite has infilled stress/tension related fractures (Figure A-5).

Sample 95: Anhydritic pelletal dolostone with moderate quantities of intercrystalline micro pores measuring roughly ~1um in size. Dolomite crystals have a size range of 20-40um. Pellet-like dolomite grains have a size range of 0.15-2.6mm. The porosity is associated with dolomite crystals within pellet-like dolomite grains. Several pelletal grains have been extensively replaced by diagenetic anhydrite. Transgranular fractures are present and healed with anhydrite/dolomite cement and trace amount of organic material. These fractures cut several of the pellets and they have more likely postdated the major pulse of anhydrite pore-filling. Pyritized organic matter have been seen within several pelletal grains. In addition, discrete pyrite cement occurs within the anhydrite pore fill-cement (Figure A-6).

Sample 96: Anhydritic pelletal dolostone with minor quantities of intercrystalline micro pores measuring roughly ~1um in size. Dolomite crystals have a size of about ~10um. Pellet-like dolomite grains range upwards to 1.2mm. The porosity is associated with dolomite crystals within pellet-like dolomite grains. Possible linear porosity exists between anhydrite cleavage

planes. Several large/small fractures exist and have been interpreted as artifacts of the coring process. The original peloidal grainstone structure has been altered by diagenetic dolomite/sulfate replacement to anhydritic pelletal dolostone. Several argillaceous laminae appear stylolitic and partially/extensively replaced by diagenetic pyrite (Figure A-7).

Sample 111: Anhydritic pelletal dolostone with moderate quantities of intercrystalline micro pores measuring roughly ~1-2um in size. Dolomite crystals have a size range of 10-20um. Pellet-like dolomite grains have a size range of 0.2-1mm. Grains are moderately sorted and exhibit significant mechanical/chemical compaction texture. The porosity is associated with dolomite crystals within pellet-like dolomite grains. Diagenetic illite material is commonly seen attached to the pore walls. Diagenetic anhydrite occurs as pervasive pore/fill cement and selective replacement of pelletal grains. Minor quantities of diagenetic pyrite occur associated to anhydrite cement and as selective replacement of pelletal grains (Figure A-8).

Figure A-1: Thin section and SEM images for sample 4.

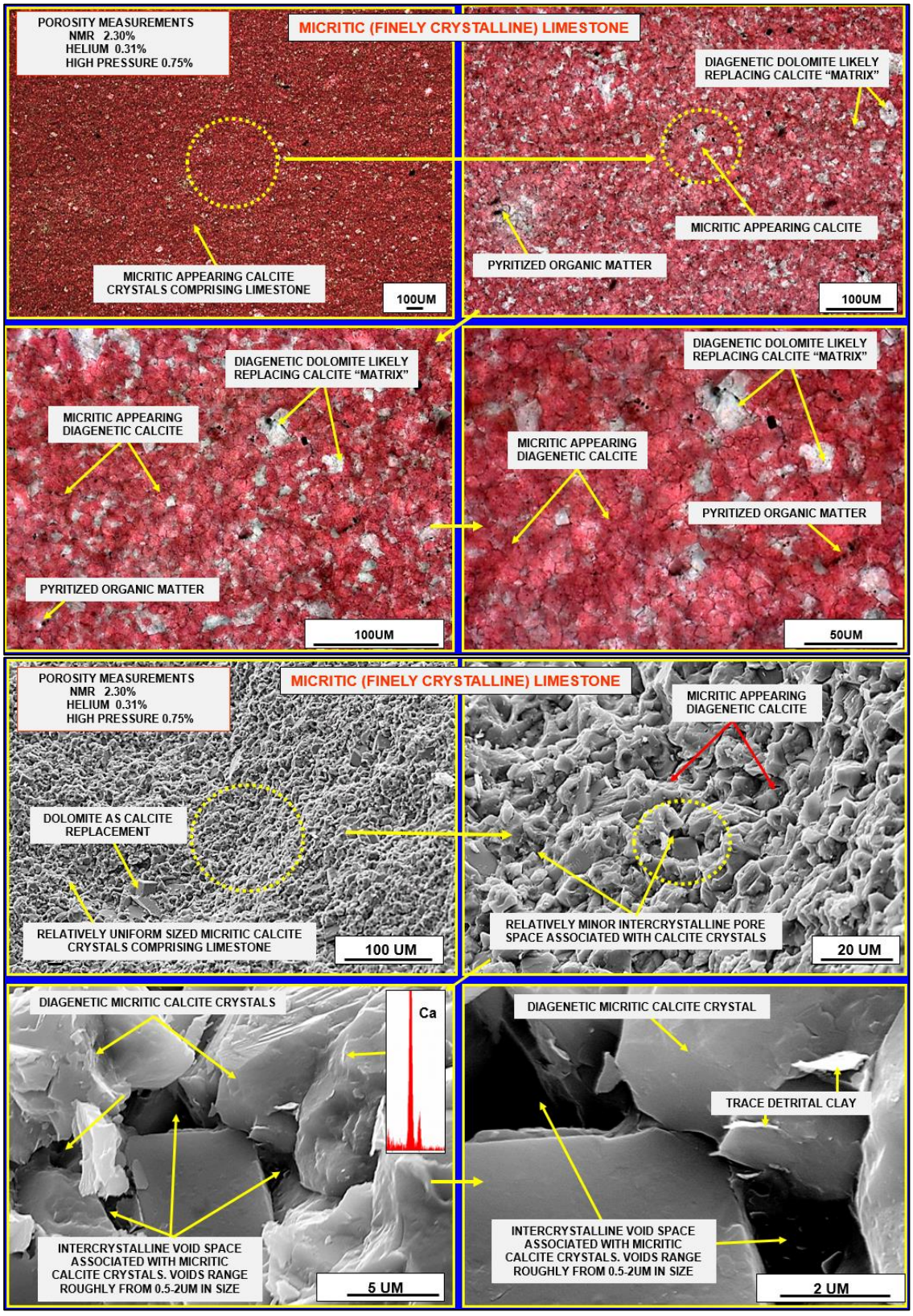

Figure A-2: Thin section and SEM images for sample 13.

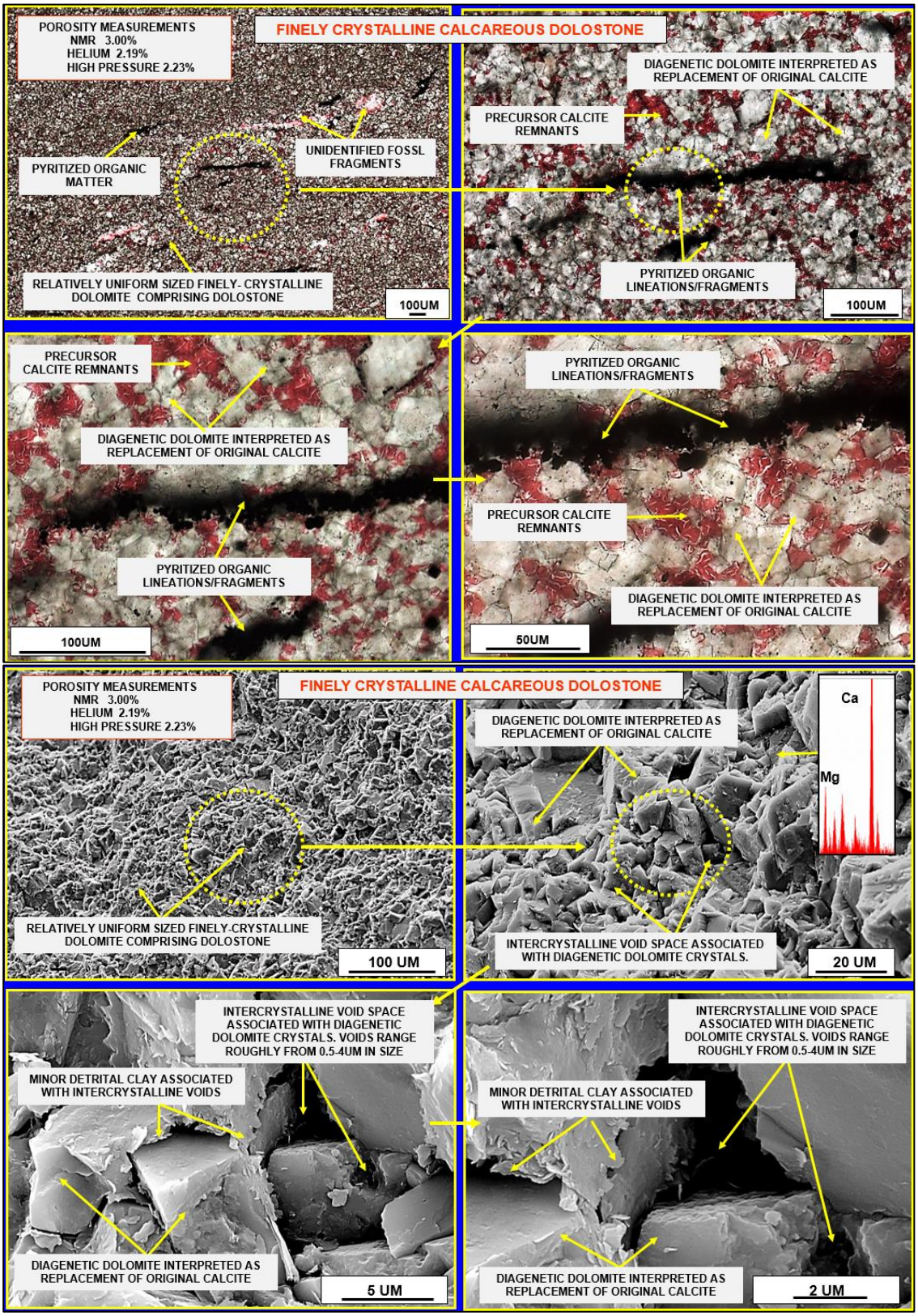

Figure A-3: Thin section and SEM images for sample 16.

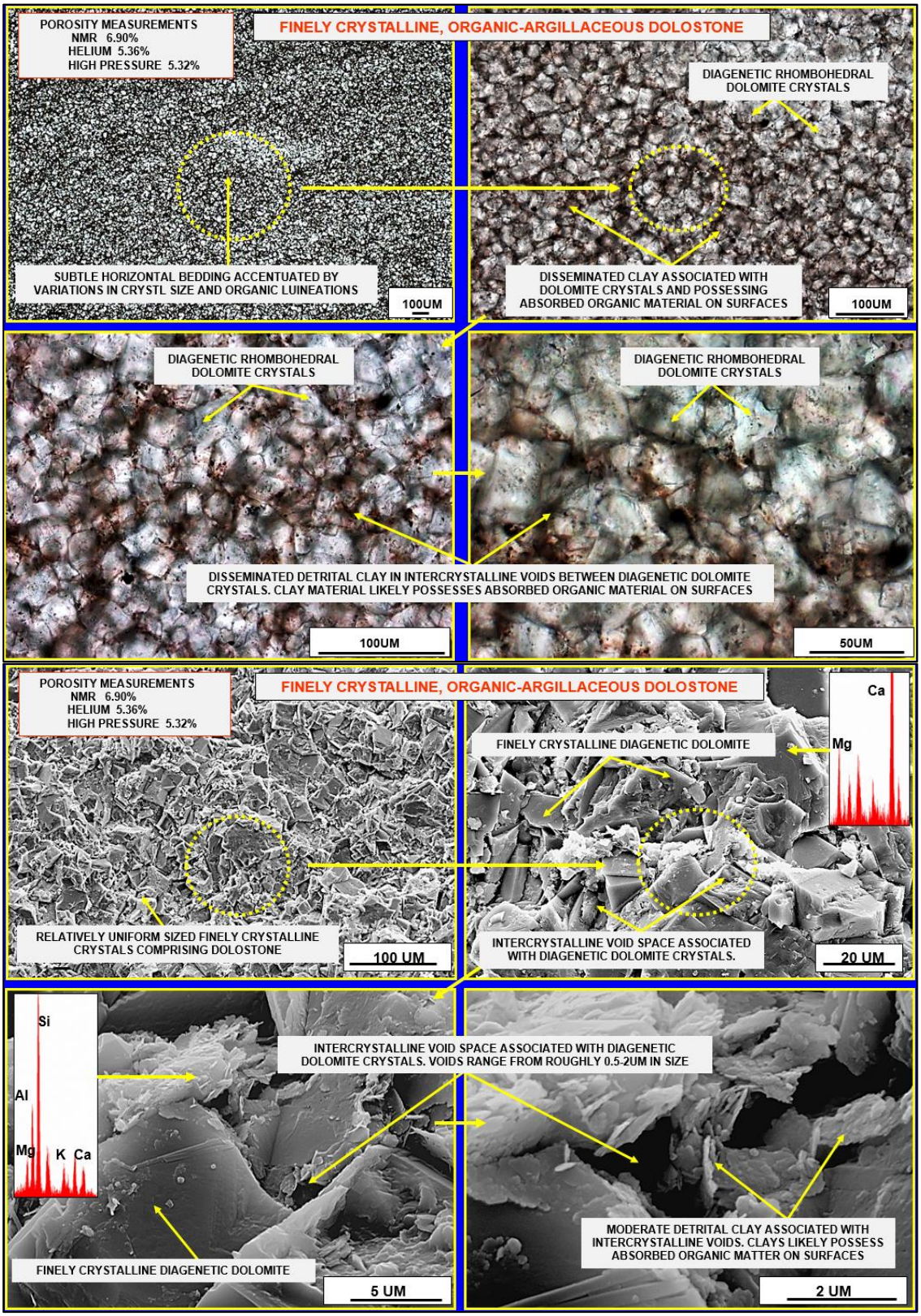

Figure A-4: Thin section and SEM images for sample 51.

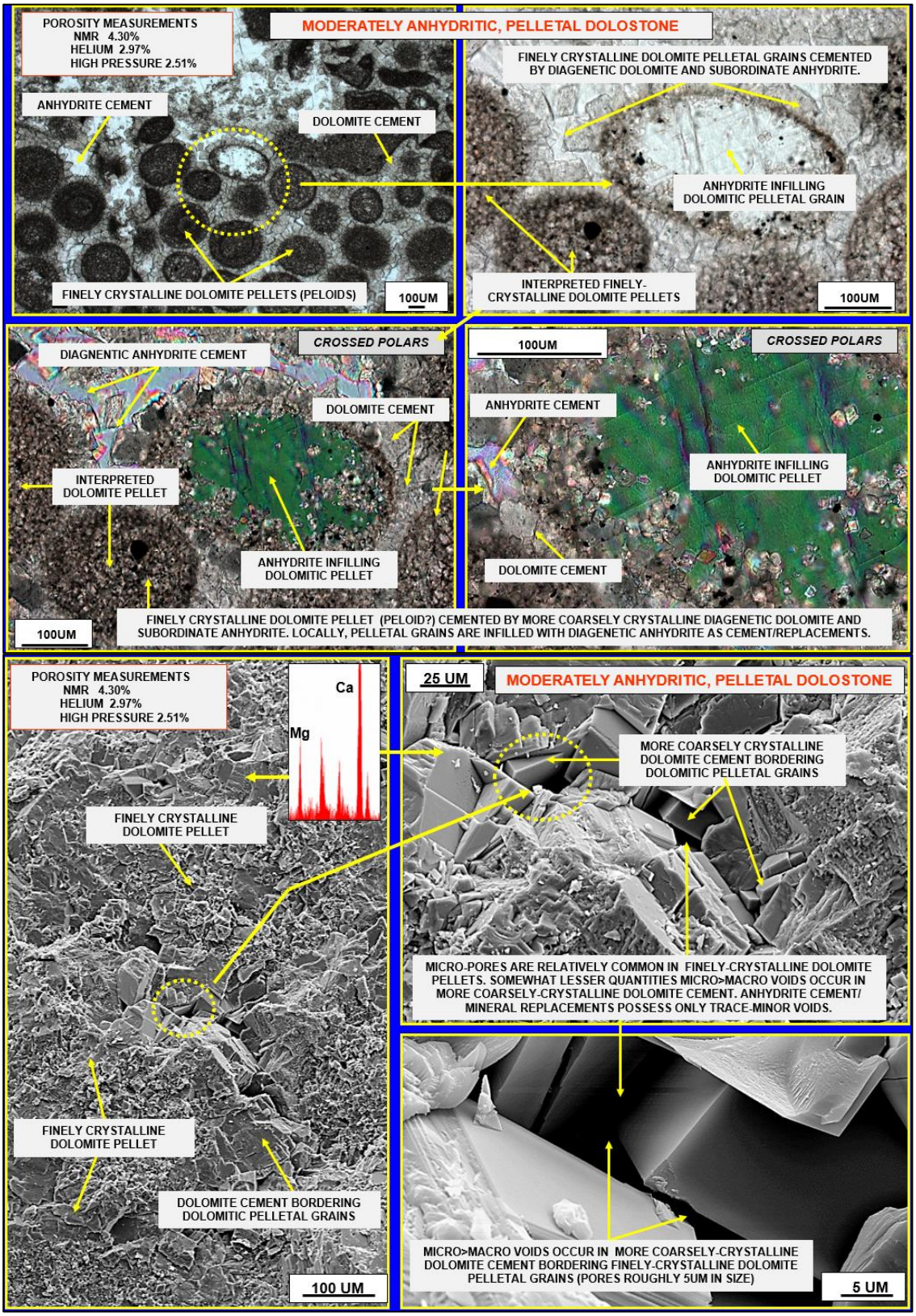

Figure A-5: Thin section and SEM images for sample 71.

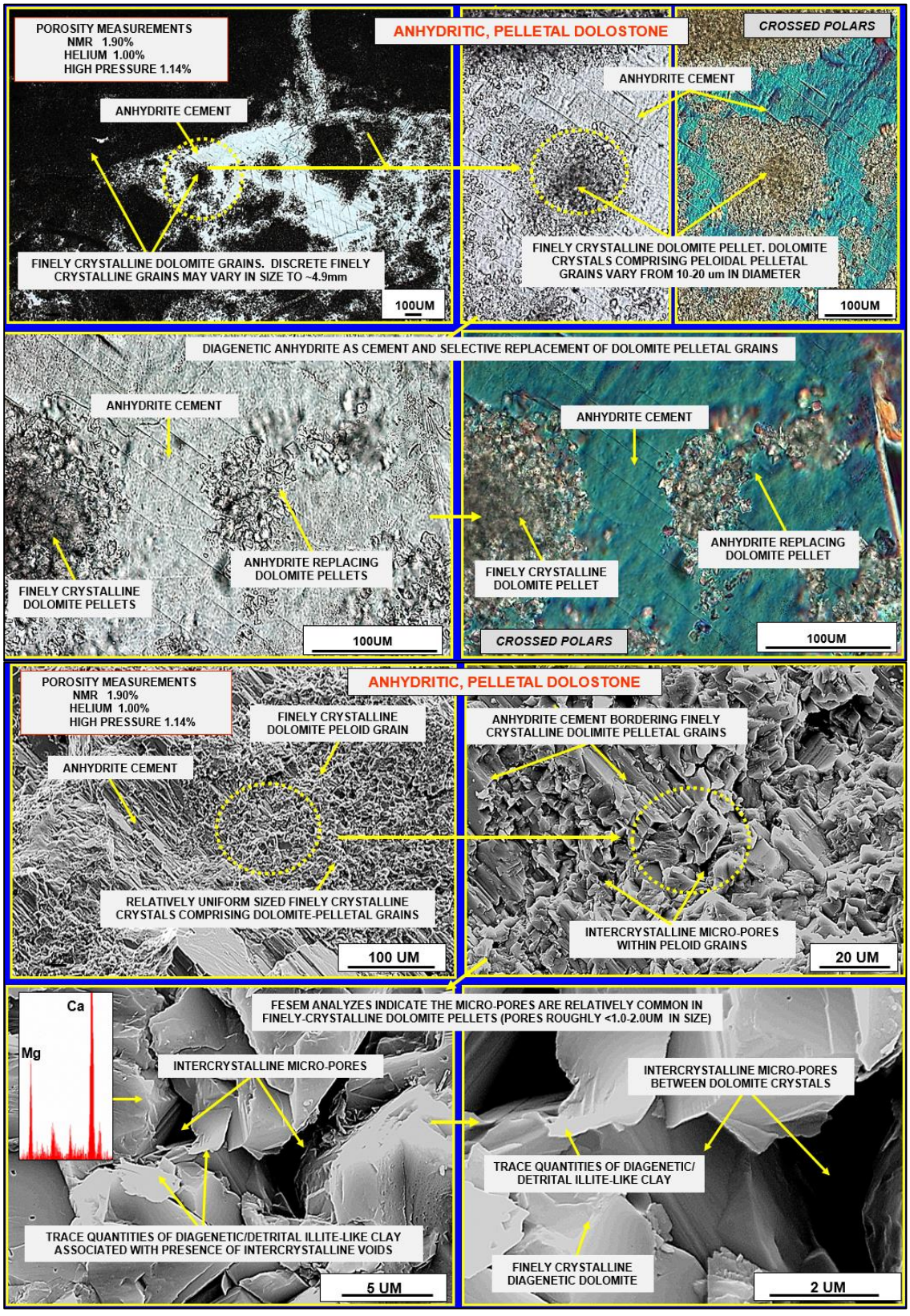

Figure A-6: Thin section and SEM images for sample 95.

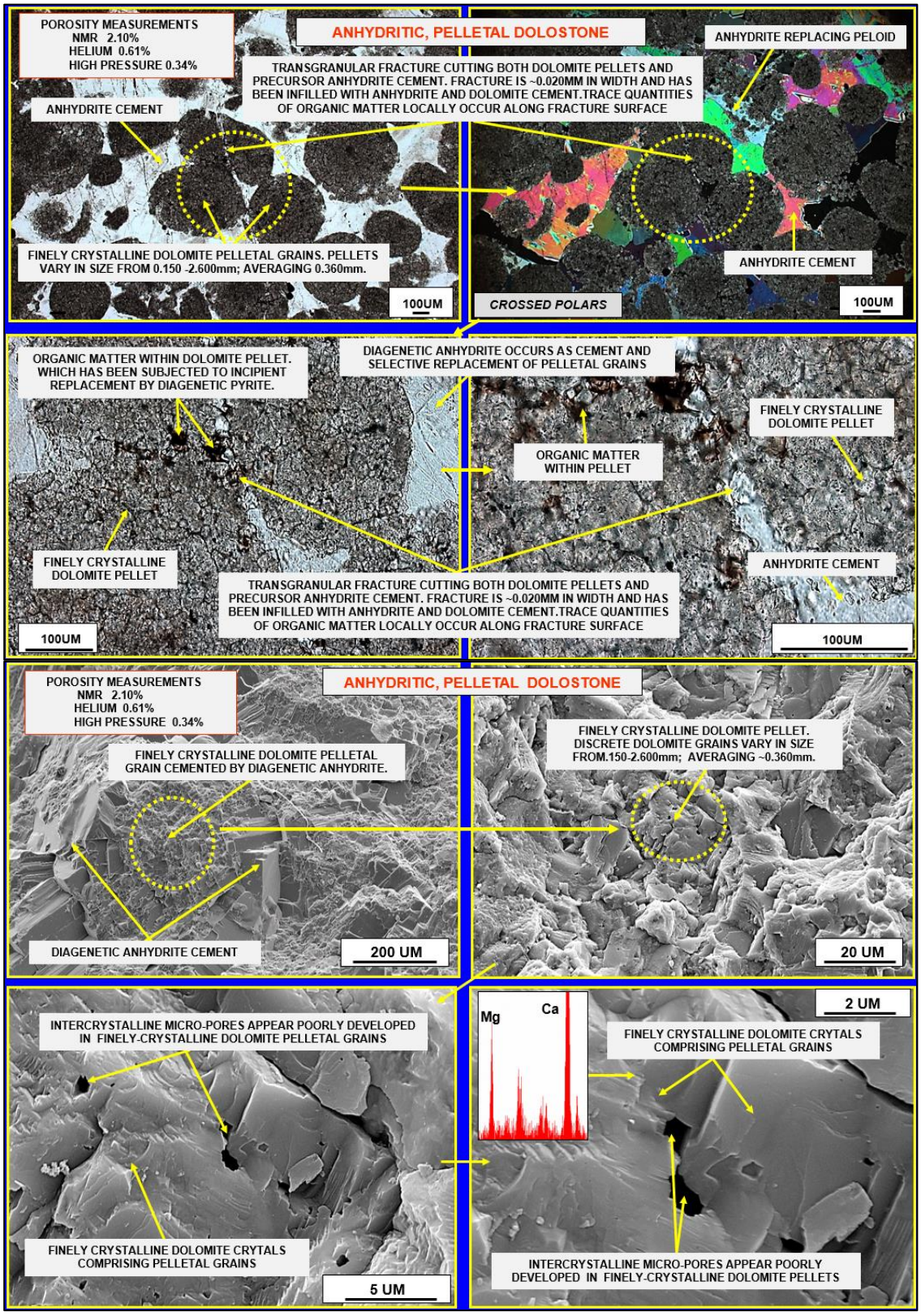

Figure A-7: Thin section and SEM images for sample 96.

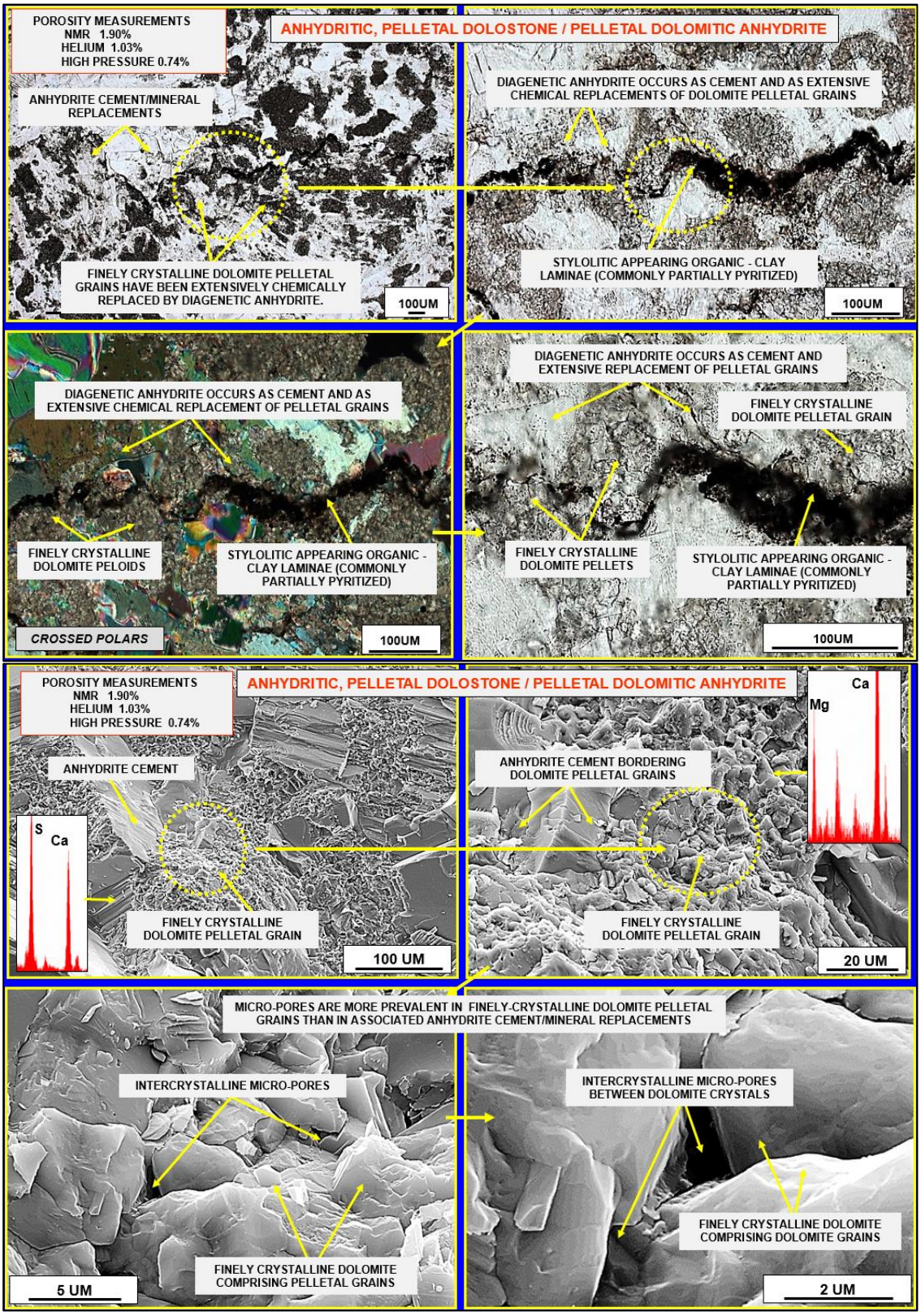

Figure A-8: Thin section and SEM images for sample 111.